FIELD SIMULATION OF WASTE IMPOUNDMENT SEEPAGE IN THE VADOSE ZONE: EXPERIMENT DESIGN AND TWO-DIMENSIONAL MODELING

by

Earl D. Mattson

Submitted in Partial Fulfillment of
the Requirements for the Degree of
Master of Science in Hydrology

New Mexico Institute of Mining and Technology
Soccoro, New Mexico

April, 1989

ABSTRACT

A field experiment was conducted to simulate uniform seepag from a lined 10.5 m x 10.5 m impoundment into a stratified soi in the vadose zone. Water was applied through a drip irrigatio system at a discharge rate of approximately $2x10^{-3}$ m^3/d pe emitter representing a flux of approximately $8x10^{-3}$ m/d. Th flux was approximately 100 times less than the mean saturate hydraulic conductivity of the soil profile.

The soil profile is stratified, consisting of two majo facies. The piedmont slope facies, comprised of red brown silt sand and pebbles, is the upper unit which extends to a depth o about 5.5 meters below datum. The lower unit is a fluvial san facies derived from the ancestral Rio Grande River. Soil cor samples (100 cc) and split spoon samples were analyzed in th laboratory to determine the saturated and unsaturated hydrauli properties of the field site.

Moisture movement was monitored using neutron loggin techniques. A mass balance analysis was conducted to compare th known amount of injected water to the water increase measured b neutron logging in the soil profile. The results of the mas balance indicate that the neutron probe only account fo approximately 70% of the injected water.

Warrick's (1974) time-dependent linearized surface poin source solution was used to predict the moisture conten distribution beneath the irrigation system in the upper piedmon slope facies. The analytical model was modified to account fo anisotropy by scaling the input parameters and coordinates. Th time-dependent solution results in an unrealistic moistur content profile which bears little resemblance to field observe moisture contents because of uncertainty of the calibration o the model input parameters, the model's appropriateness to th field conditions and the requirement of a constant diffusivity.

TABLE OF CONTENTS

Table of Contents--Continued

LIST OF ILLUSTRATIONS

List of Illustrations---Continued

List of Illustrations---Continued

Figure Page

LIST OF TABLES

ACKNOWLEDGEMENTS

This research was funded by the U.S. Bureau of Mines Generic Waste and Recovery Center. The research project has continued to receive support from this source as well as other sources to further the understanding of unsaturated flow from simulated impoundments.

Much thanks is due to my advisor and current employer, Dr. Daniel B. Stephens. His support and guidance since 1985 is appreciated.

Student workers helped with the setup and monitoring of this research project. Thank you to Robert Mace, Bob Friesen, Todd Stein, and Tracy McFarland. I hope they found the experience useful in their future carriers. Warren Cox, Jeff Havlena, and Bob Knowlton assisted with ideas to solve the many field problems encountered during this research. I would have not survived Soccoro without the unique social events created by Swen, Bruce, Marcy, Barb, Cindy, Gary, Greg, Ken, and my other hydrology and geology fiends.

My parents and family have always been supportive of educational and learning endeavors. A special thanks is owed to my field partner, Alva Parsons, for her patience, support, and joyful outlook on live. She helped me maintain a balance between work and play.

1. INTRODUCTION

Federal regulations require operators of waste mill sites to demonstrate there will be no seepage discharge from the mill tailings impoundments which will impact the underlying water resources. Mill operators have responded to the federal regulations by installing synthetic and clay liners beneath the tailings or cap materials over the tailings to inhibit seepage from impoundments. Seepage into the underlying porous media through unexpected breaks in the liners or slow release of moisture through the liners will not likely saturate the underlying porous media.

Prediction of the pathways and travel time of unsaturated seepage flux is difficult due to a number of factors. First, there are difficulties in characterizing the hydraulic properties of unsaturated material, as discussed by Larson and Stephens (1985). Secondly, proper characterization is complicated by the inherent spatial variability of hydraulic properties in unsaturated soil. The spatial heterogeneity of soil hydraulic properties causes infiltration to spread over a large area. Mualem (1984) develop a conceptual model which indicated that anisotropy is enhanced in a dry anisotropic medium. Stephens and Heerman (1988) demonstrated lateral spreading occurs due to anisotropy and dry initial conditions in a sand box infiltration

experiment.

Stratification greatly amplifies the lateral flow components as infiltration occurs. The sharp contrast of textural changes in a stratified soil inhibits downward movement of seepage. Miller and Gardner (1962) conducted laboratory experiments demonstrating that downward moisture movement is inhibited at the interface of a fine over a coarse layer. The wetting front stopped at the interface until the soil water tensions are reduced enough to allow seepage into the underlying coarser material. Through laboratory experiments, Palmquist and Johnson (1962) found that when downward moisture movement is halted at a textural interface, lateral spreading occurred.

Lateral spreading in a stratified soil has also been documented in the field. Miller (1963) observed lateral spreading beneath a 3m x 3m irrigated plot which contained a fine layer over a coarse layered media. Greater horizontal than vertical movement of seepage from a radioactive storage tank was observed by Routson and others (1979) in a stratified glacial fluvial environment. Johnson and others (1981) observed lateral spreading in a silty sand to coarse sand river deposit due to leachate from a landfill.

In this present investigation, a large scale field experiment was conducted in the vadose zone. The purpose of the field experiment is to compare field results with single and multi-dimensional analytical and numerical models. Field results should prove useful for calibrating and validating the predictive

capabilities of multi-dimensional flow and transport codes. The objectives of my study are to:

* Describe in detail the water application system experimental design,

* Provide information on equipment testing and calibration, and

* Compare the moisture content profile predicted by time dependent and steady state linearized analytical multi-dimensional models (Warrick, 1974) to the field observations.

In a companion report, Parsons (1988a) provides a detailed description of the geologic and hydraulic properties of the experimental field site and compares the observed moisture movement to the one-dimensional analytical solution of McWhorter and Nelson (1979).

In the field, water was applied to the native undisturbed soil through a 10m x 10m drip irrigation system which irrigates a 10.5m x 10.5m area. The seepage flux rate was approximately 100-fold less than the average saturated hydraulic conductivity of the soil profile. The moisture movement in the soil was monitored with tensiometers and neutron logging equipment.

The experimental field site is located west of the New Mexico Tech campus in Socorro, New Mexico, approximately 120 km south of Albuquerque in a semi-arid environment (Figure 1.1). Due to the low annual precipitation of about 20 cm annually, vegetation is very sparse at the field site. The site is

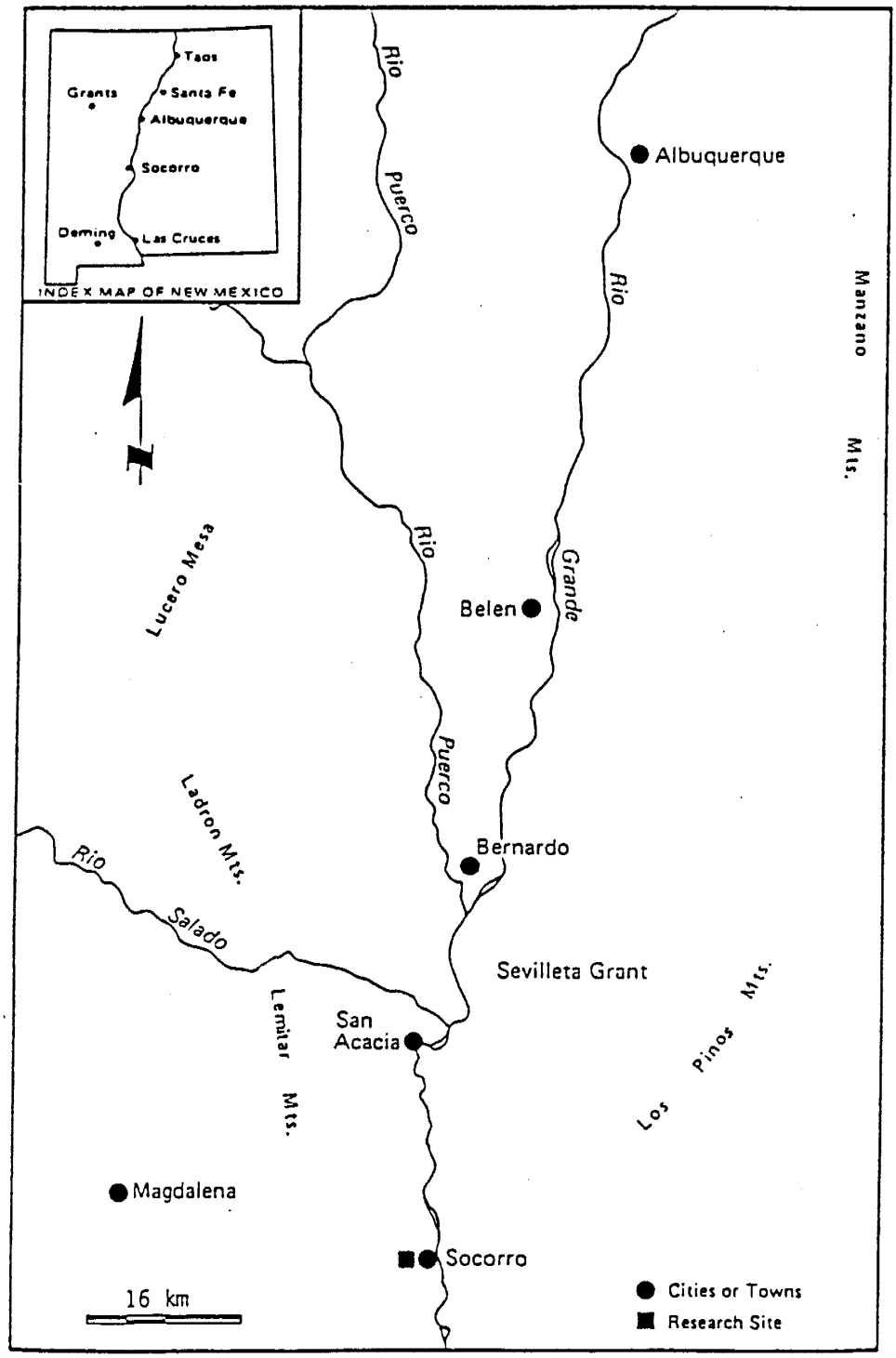

Figure 1.1. Index map.

situated in an abandoned east-west trending arroyo. The arroyo is traversed by a flood control dike just west of the field site, so that there is no major runoff near the plot. The New Mexico Tech golf course, located to the east adjacent to our field site, is irrigated for most of the year, however the site itself has never been previously irrigated. Depth to the water table is approximately 24 meters.

2. METHOD OF ANALYSIS

Two-dimensional cross-sections of moisture movement observed in the field for the first 153 days of infiltration are compared to results predicted by a computer program using Warrick's (1974) time dependent and steady state linearized point source analytical solutions. Warrick's linearized point source solution predicts moisture content profiles in a homogeneous isotropic media. The computer program solution, TRANS.FOR, uses superposition of point source solutions to effectively simulate a large impoundment with uniform leakage. Anisotropy is incorporated by transforming the coordinate system and coefficients of the governing PDE. Comparison of the moisture content distributions predicted by the computer model to the observed moisture contents in the field may determine to what degree the layered soil beneath the field site may be treated as an equivalent homogeneous anisotropic media. The following sections present the development and previous work with multi-dimensional linearized analytical models, discuss the linear point source solutions (Warrick, 1974), and describe modifications to the model input which allow for transformation of the anisotropic media to an equivalent isotropic media.

2.1. THEORY OF LINEARIZED MOISTURE FLOW

Description of soil water flow from a trickle irrigation system is based on a form of Richard's equation:

$$\partial\theta/\partial t = - \nabla\cdot(K\nabla H) \qquad (2.1)$$

where θ is the volumetric water content (L^3L^{-3}), t is time (T), ∇ is the vector gradient operator (1/L), K is unsaturated hydraulic conductivity (LT), and H is the hydraulic head (L). The hydraulic head for unsaturated flow is composed of two terms:

$$H = \psi - z \qquad (2.2)$$

where ψ is the soil water potential (cm of water) and z is the depth below the ground surface (positive downward). Rewriting Richard's equation using equations 2.1 and 2.2, the flow equation becomes:

$$\partial\theta/\partial t = - \nabla\cdot(K\nabla\psi) + \partial K/\partial z \qquad (2.3)$$

Equation 2.3 is non-linear due to the interrelationship of K, θ, and ψ. Linearization of equation 2.3 is accomplished by defining a new variable, the matric flux potential (ϕ), used by Gardner (1958):

$$\phi = \int_{\infty}^{\psi} K(h)\,dh = K(\psi)/\alpha \qquad (2.4)$$

where

$$K(\psi) = K_0\exp(\alpha\psi) \qquad (2.5)$$

and α (1/L) is a coefficient which represents the slope of the natural logarithm (ln) of the $K(\psi)$ versus ψ relationship in the range of interest. K_0 (L/T) is a coefficient that represents the intercept of the $K(\psi)$ versus ψ relationship at $\psi = 0$. Depending

on the range of interest of ψ, K_0 may be near the saturated hydraulic conductivity or orders of magnitude smaller. α is commonly in the range of $2x10^{-3}$ to $2x10^{-1}$ cm^{-1} (Philip, 1969; Braester, 1973). Equations 2.4 and 2.5 are required to simplify equation 2.3, making analytical solutions for certain steady flows possible.

Using equations 2.4 and 2.5 in equation 2.3, the moisture flow equation becomes:

$$\partial\theta/\partial t = \nabla^2\phi - \alpha(\partial\phi/\partial z) \qquad (2.6)$$

For steady state flow, $\partial\theta/\partial t$ equals zero, simplifying equation 2.6 to:

$$\nabla^2\phi = \alpha(\partial\phi/\partial z) \qquad (2.7)$$

Equation 2.7 was studied by Philip (1968, 1969, 1971), Wooding (1968), and Raats (1970, 1971 1972).

For the time dependent case (Warrick, 1974), the linearization of equation 2.6 requires a further restriction; namely, $d\theta/d\phi$ is assumed to be a constant (α/k), simplifying the left hand side of equation 2.6 to:

$$\partial\theta/\partial t = (d\theta/d\phi)(\partial\phi/\partial t) = (\alpha/k)(\partial\phi/\partial t) \qquad (2.8)$$

where $k = dK/d\theta$ (the slope of the K-θ relationship). Incorporation of equation 2.8 into equation 2.6 results in the time dependant linearized equation:

$$\partial\phi/\partial t = (k/\alpha)\nabla^2\phi - k(\partial\phi/\partial z) \qquad (2.9)$$

The linearized solution of equation 2.9 is useful for small variations of moisture content. Such conditions exist in high-frequency trickle irrigation systems.

2.2. PREVIOUS WORK

The transform presented in equation 2.4 was introduced by Kirchoff in the late 1800's. For this reason, many investigators call the matric flux potential the Kirchoff potential. The matric flux potential was proposed by Klute (1952) to analyze horizontal moisture movement in a partially saturated soil. Gardner (1958) presented a partial differential equation for moisture movement in unsaturated soil which included the effect of gravity. Gardner further introduced the exponential relationship for K-ψ. The exponential K-ψ relationship fits the measured K-ψ relationship well, for small ranges of pressure head.

The first detailed analysis of steady state infiltration was presented by Philip (1968), who studied infiltration from a buried sphere with a small radius. Wooding (1968) developed a solution for steady infiltration from a circular pond. Philip (1969) discussed the solution for infiltration from a buried single horizontal line source. Raats (1970) developed a line solution for a source of an array of equally spaced surface line or furrow sources. Raats (1971) and Philip (1971) independently expanded the linearized point and line analytical solutions to include sources at the surface. Raats (1971) also compared buried and surface point source solutions. He concluded that for

the radius, R, equal to zero and at large depth, z, the two solutions are equivalent. Along the surface (z = 0) and when the radius was relatively large, the effect of gravity was greater for the surface source than the buried source. However, near the point source the surface matric flux potential was approximately twice the magnitude of the buried matric flux potential.

Philip (1971) confirmed Raats' conclusions of the comparison between buried and surface point source solutions. Philip generalized the steady state point, line, and areal surface solutions to be calculated from the mathematically simpler buried source.

The following year, Philip (1972) applied the theory of steady state buried and surface point and line sources to a heterogeneous isotropic soil. The heterogeneous soil was chosen such that the hydraulic conductivity was an exponential function of both the moisture potential and depth. The results of the heterogeneous solutions were presented in a later publication (Philip, 1975).

Warrick (1974) derived the time dependent case (equation 2.9) for a point source buried or at the surface by assuming $d\theta/d\phi$ is constant (equation 2.8). The assumption that $d\theta/d\phi$, or equivalently $dK/d\theta$, is a constant implies the diffusivity is a constant (Ben-Asher and others, 1978). As discussed later, invoking the assumption of a constant diffusivity implies that realistic shapes of the wetting front cannot be predicted (Clothier and Scotter, 1982). Warrick and Lomen (1976) extended

the time dependent analysis to include strip and disc source geometries. Lomen and Warrick (1978) incorporated moisture loss by evaporative flux at the soil surface to their 1976 analysis. The evaporative flux was assumed to be proportional to the matric flux potential at the soil surface. Warrick and others (1980) accounted for plant extraction of water, where the sink was radially symmetric. Later the solutions were expanded to include rectangular source and sink geometries (Warrick and Lomen, 1983).

Ben-Asher and others (1978) compared a non-linear finite difference numerical solution to the linear time dependent analytical solution (Warrick, 1974). Their first comparison involved a cyclic infiltration case with infiltration durations set according to a one hour on/off cycle. Ben-Asher and others concluded that the numerical solution reacted more quickly than the analytical solution to the change in infiltration rate. Both solutions dampened the effect of cyclic infiltration with distance from the source, and approached the same matric flux potential. The two models were also compared to moisture content profiles observed in the field (Ben-Asher and others, 1975). Figure 2.1 presents the predicted and experimental data at four selected times. Ben-Asher and others (1978) concluded that the non-linear numerical solution best describes the wetted area near the source, while the linear analytical solution predicts the moisture content more accurately in the drier soil further from the source.

Clothier and Scotter (1982) compared Warrick's (1974) time

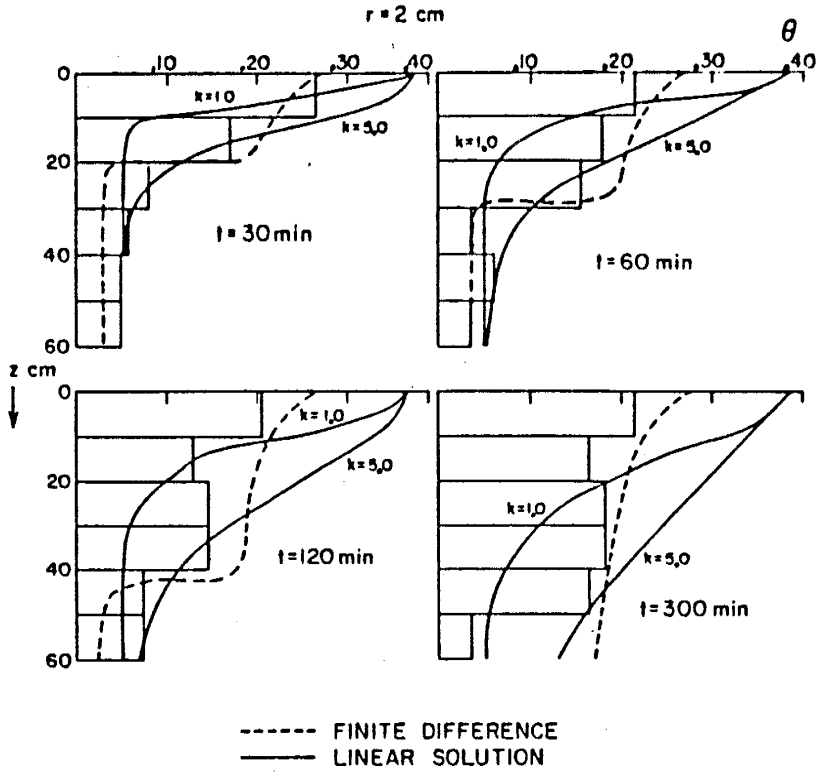

Figure 2.1. Comparison of finite difference and linearized moisture flow equation predictions with observed water content profiles for trickle irrigation on Sinai sand (after Ben-Asher and others, 1978).

dependent and Raats' (1971) steady state point source solutions to a laboratory infiltration experiment. The laboratory experiment consisted of a small sand tank (20cm x 20cm x 30cm) with water applied through a quarter hemisphere cavity at one corner of the tank. Measured moisture contents versus distance from the source is shown in Figure 2.2. The horizontal profile of Raats' steady state surface point source solution predicts quite well the moisture content behind the wetting front (Figure 2.2). Even during this short time period, the water content predicted by Raats' solution (1971) agrees favorably with the observed experimental moisture content behind the wetting front. Conversely, Warrick's linearized time-dependent point source solution is a poor predictor of the observed moisture content. Recall that the time-dependent case requires the restrictive assumption that $dK/d\theta$ is a constant. The assumption implies that diffusivity is independent of moisture content. The predicted steep drop near the source and the flat water content distribution further away from the source is a result of the assumption of constant diffusivity (Clothier and Scotter, 1982).

2.3. TRANSIENT POINT-SOURCE SOLUTION

Although the time dependent solution (Warrick, 1974) was incapable of predicting the shape of the wetting front in the Clothier and Scotter experiment (1981), Warrick's solution was chosen to be the most appropriate two-dimensional model to apply

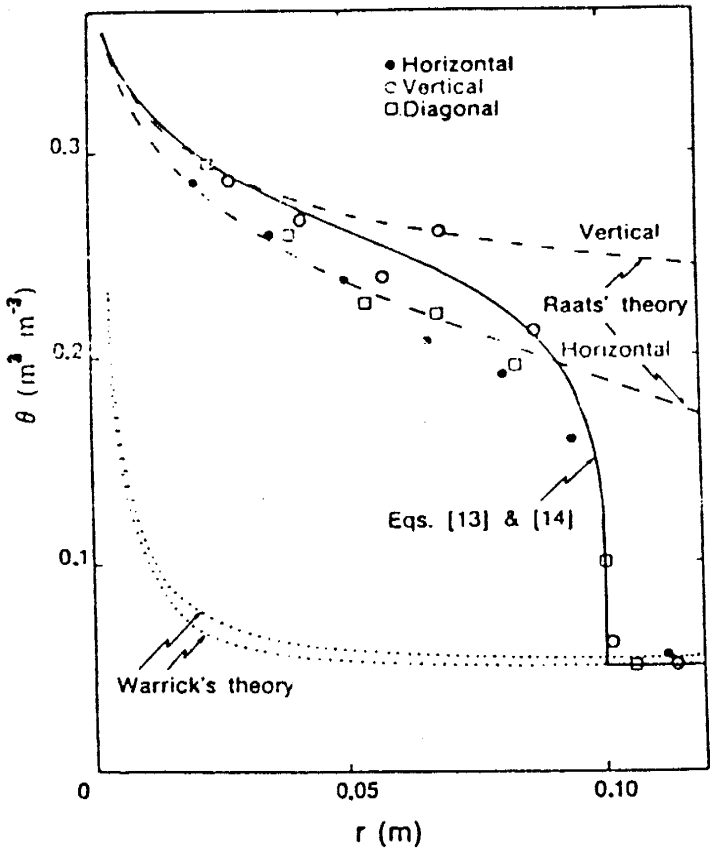

Figure 2.2. Predicted and measured water contents after 60 minutes of constant flux infiltration (after Clothier and Scotter, 1981). The solid line shows Clothier and Scotter's numerical results (1981), the dashed line is Raats (1971) steady state solution, and the dotted line is Warrick's (1974) time dependent solution.

to our field experiment for several reasons. First, the time dependent linearized solution is acceptable for small changes in moisture content (Warrick, 1974). The expected change in moisture content is expected to be approximately 5% from Parsons (1988a) one-dimensional, two-layer analysis. Clothier and Scotter's experiment had a large increase in moisture content (over 20%) behind the wetting front which contributed to the poor fit of Warrick's solution. In my field experiment, the 5% expected change in moisture content for this field experiment is expected to permit the assumption of constant diffusivity in the time dependent linearized solution (Warrick, 1974).

A second reason to use Warrick's time dependent case is due to the major facies change from the piedmont slope facies to the fluvial sand facies located approximately 5.5 meters below datum. A steady state analysis would have to include both the piedmont and fluvial sand facies, so that the assumption of a homogeneous soil profile could not be met. Conversely, the time dependent analysis can predict moisture content at early times, before the wetting front reaches the underlying fluvial facies.

Lastly, although several source geometries could be used to represent our field site, superimposing the point source solution was chosen to best represent the actual source geometry. The point source has the added advantages of being time dependent with the ability to vary the flux among the emitters, although varying point source discharge is not within the scope of this study. The point source solution is relatively simple to solve,

while the disk and strip source geometries can pose numerical difficulties (A.W. Warrick, Univ. of Arizona, personal communication, 1988). The upper boundary condition of the surface point source is accurately represented at our site due to the impermeable plastic layer over the drip irrigation system (see Section 4.2 for detailed description of the system layout). It is assumed that no injected water evaporates from the soil surface. No soil moisture sinks (ie. plant roots) are assumed to be present at the site.

To obtain a unique solution to equation 2.9, an initial condition and two boundary conditions are necessary. The initial condition requires the soil to be initially dry at time equal to zero:

$$\phi(r,z,0) = 0 \qquad (2.10)$$

The first boundary condition implies no flow at the soil surface except at the origin:

$$-(\partial\phi/\partial z) + \alpha\phi = 0; \quad z = 0, \; r \neq 0 \qquad (2.11)$$

where r and z are the real cylindrical coordinates. The second boundary condition states that ϕ and the derivatives of ϕ vanish at large z or r:

$$\lim(r^2 + z^2)^{1/2} \rightarrow 0 \quad \phi(r,z,t) = 0 \qquad (2.12)$$

It is convenient to define dimensionless variables. Thus the space coordinates, time, and matric flux potential become respectively (Warrick, 1974):

$$R = \alpha r/2 \qquad (2.13)$$

$$Z = \alpha z/2 \qquad (2.14)$$

$$T = \alpha kt/4 \qquad (2.15)$$

$$\Phi = 8\pi\phi/\alpha q \qquad (2.16)$$

Transient and steady state solutions for surface point sources are applied to the field experiment. The transient case with the source at the surface is represented by Warrick (1974, equation 16):

$$\Phi = 2\{\Phi_B - e^{2Z}\int_{\infty}^{Z} e^{-2Z^*}[\Phi_B]_{Z=Z^*}\, dZ^*\} \qquad (2.17)$$

where Φ_B is the dimensionless matric flux potential for a buried point source and Z^* is a dummy integration variable. Φ_B is solved by Warrick (1974, equation 13). This equation is similar to that of Philip (1969, equation 159) derived for adsorption from a small buried source. Warrick's (1974, equation 13) is:

$$\Phi_B = e^{Z}/(2\rho)\{e^{\rho}\mathrm{erfc}(\rho/(2\sqrt{T}) + \sqrt{T}) + e^{-\rho}(\rho/(2\sqrt{T}) - \sqrt{T})\} \qquad (2.18)$$

where

$$\rho^2 = R^2 + Z^2 \qquad (2.19)$$

The steady state case for a source at the surface is defined by Philip (1971, equation 30), Raats (1971, equation 43) and Warrick (1974, equation 18) as:

$$\Phi = 2[\ \exp(Z-\rho)/\rho - \exp(2Z)E_1(Z+\rho)\ ] \qquad (2.20)$$

$E_1(x)$ is the exponential integral defined by Abromowitz and Stegun (1964, equation 5.1.1):

$$E_1(x) = \int_x^{\infty}(e^{-\tau})/\tau\, d\tau \qquad (2.21)$$

Inasmuch as equations 2.7 and 2.9 are both linear, their respective solutions for single point sources (equations 2.17 and 2.20) are appropriate for superimposing multiple sources. The solution a for dimensionless matric flux potential, Φ, for each

of the point sources, are added together. For this study, the 441 emitters constitute the multiple sources. The computer program used to solve the equations incorporates nested DO loops to solve equation 2.17 or 2.20 for each of the emitters (Appendix A). The associated pressure head is calculated using equations 2.4 and 2.5. Determination of volumetric moisture content is calculated from the fitted θ-ψ relationship regressed from van Genuchten's (1980) closed form analytical solution. Section 3.4.3. explains the van Genuchten computer code in more detail.

2.4. ANISOTROPIC TO ISOTROPIC TRANSFORMATIONS

Anisotropy can be incorporated by scaling the coordinates and coefficients in Warrick's solution (1974). Coordinate and coefficient scaling implies that the anisotropic behavior is independent of moisture content and pressure head. Scaling the coordinate system results in transforming the anisotropic Richard's equation to one that has the properties of an equivalent isotropic equation. For Cartesian coordinates the following transformations are applied:

$$x = x'(K_y/K_x)^{1/4} \qquad (2.22)$$

$$y = y'(K_x/K_y)^{1/4} \qquad (2.23)$$

$$z = z'\{(K_xK_y)^{1/2} / K_z\}^{1/2} \qquad (2.24)$$

where x', y', and z' are the coordinates in the real anisotropic system. Radial symmetry (ie. $K_x = K_y = K_H$) simplifies the Cartesian transformations to:

$$r = r' \tag{2.25}$$

$$z = z'(K_H/K_Z)^{1/2} \tag{2.26}$$

where K_H is the horizontal saturated hydraulic conductivity. The transformations imply that the parameter K_0 of equation 2.5 is the horizontal saturated hydraulic conductivity when applying the anisotropic transformations. For the anisotropic case:

$$K_0 = (K_X K_Y)^{1/2} = K_{H0} \tag{2.27}$$

Due to the coordinate transformation, the coefficients of equation 2.20 also must be transformed:

$$\alpha = \alpha'(K_Z/K_H)^{1/2} \tag{2.28}$$

$$k = k'(K_Z/K_H)^{1/2} \tag{2.29}$$

where α' and k' are the real anisotropic coefficients.

The anisotropic transformation utilized in Warrick's point source solution follows the transformation described by McKee and Bumb (1983) for a linearized Richard's equation containing diffusivity . There is no transformation required for the diffusivity term (A.C. Bumb, In Situ, Inc., personal communication, 1988), however the diffusivity is implicitly transformed due to the its functional dependance on α. In this derivation the term α/k is mathematically equivalent to the diffusivity term used in McKee and Bumb's analysis. Therefore the k term must also be transformed to nullify the effect of the transformed α (equations 2.27 and 2.28). Appendix B contains the verification of the anisotropic transforms. The steady state and Warrick's time dependent solutions are solved by the computer program TRANPT.FOR (Appendix A).

3. HYDROGEOLOGIC SITE CHARACTERIZATION

The hydrogeologic site characterization includes details on the geologic and hydraulic properties of the soil profile. The following sections provide a summary of the general geology, subsurface features of the field site, soil sampling procedures, and laboratory analyses. These topics are described in more detail by Parsons (1988a). The last section describes the hydrogeologic data input to a linearized point source analytical model.

3.1. GEOLOGY

The experimental field site is located in the eastern-most part of the Basin and Range Province within the Rio Grande Depression (Figure 3.1). The field site is underlain by alluvial sediments of the Sierra Ladrones Formation, the upper subdivision within the Santa Fe Group in central New Mexico.

Geologic cross-sections were developed using sample descriptions from boreholes at selected monitoring stations (Figure 3.2). Borehole logs for each station, included in Appendix C, show sampling intervals and provide geologic visual descriptions. Sampling depths have been adjusted to a common datum elevation for ease in geologic correlation between

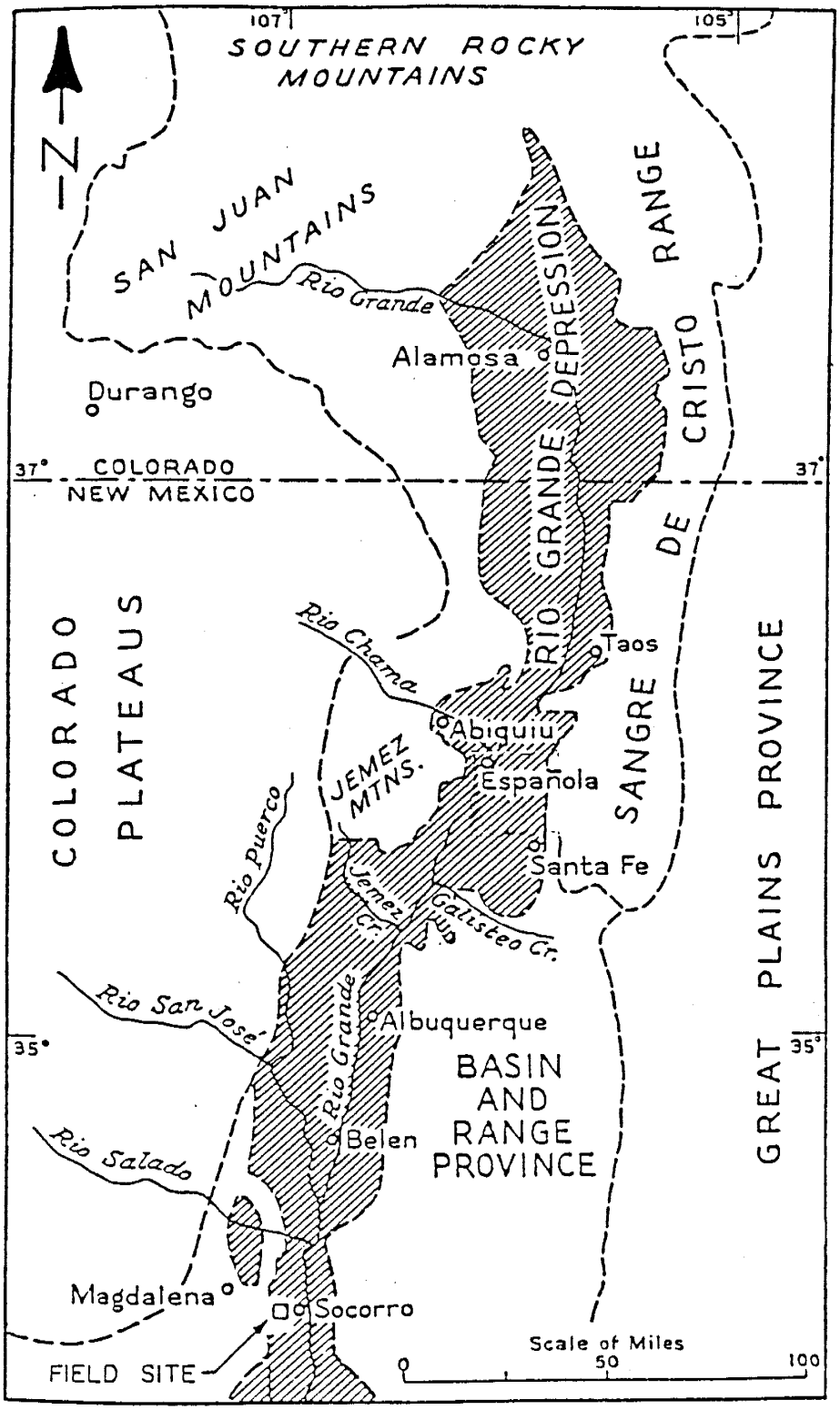

Figure 3.1. Northern Rio Grande Depression (after Denny, 1940).

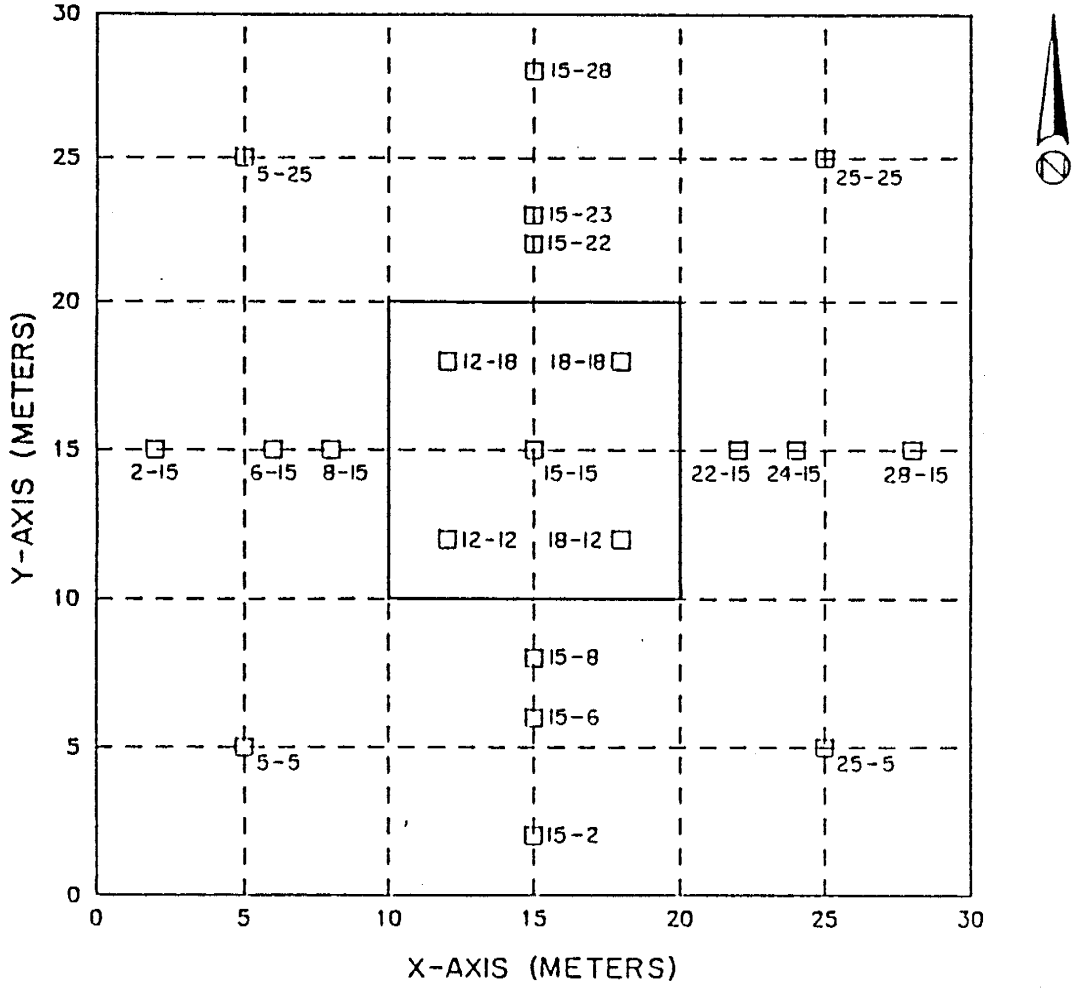

Figure 3.2. Monitoring station location numbers based on an X-Y grid with the ordinate in the southwest corner of the site. Heavy line in interior outlines the wetted area.

boreholes. The datum is a horizontal plane located approximated 0.86 m above the drip irrigation system. Geologic cross-sections of the east-west and north-south transects were developed by correlation of visual geologic characteristics between appropriate boreholes.

Two distinct facies of the Sierra Ladrones Formation are found beneath the field site: an upper facies consisting of red-brown silty sands and pebbles interbedded with cobbles and a lower facies of clean, tan sand and fine to coarse sands and pebbles. Both facies contain clay lenses of undetermined lateral extent. The upper red-brown silty sands and pebbles represent Chamberlain's (1980) piedmont slope facies derived from the Socorro Range to the west. The underlying tan sands are designated by Chamberlain as fluvial sand facies deposited by the ancestral Rio Grande River.

Figures 3.3 and 3.4 show the geologic profile beneath the field site. These figures are exaggerated twice vertically to more clearly show the layering of the soil. The profile is stratified, and consists of piedmont slope facies overlying fluvial sand facies. Discontinuous clay lenses are found throughout the profile. There are two major cobble zones approximately one half meter thick located at approximately 3 and 5 meters below the datum. Based on the drilling characteristics and cuttings, the cobbles range from 10 to 30 cm in diameter.

The piedmont slope facies are present in the soil profile to a depth of 3 to 4 meters below datum where the first major cobble

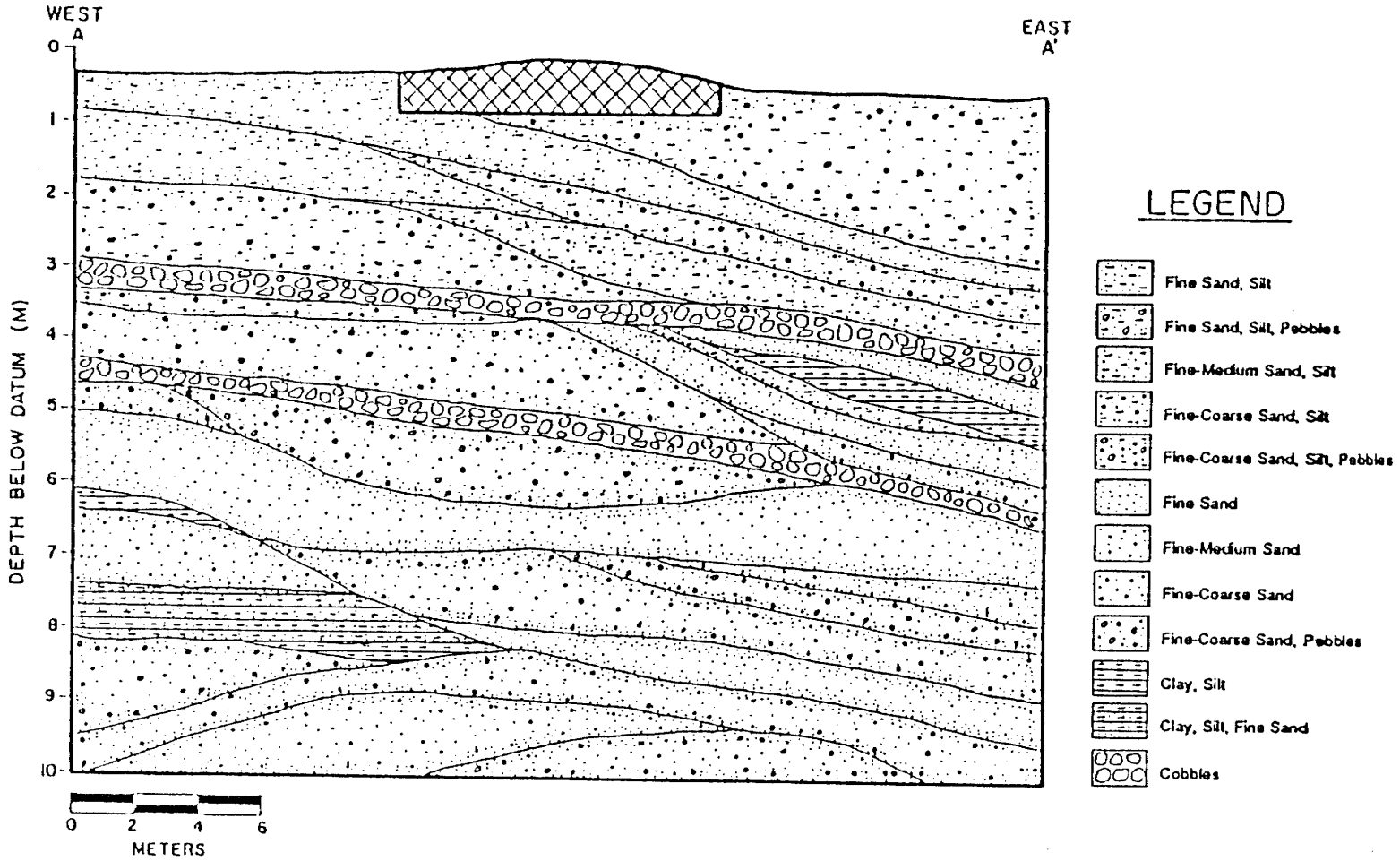

Figure 3.3. Geologic cross-section of the east-west transect (after Parsons, 1988a).

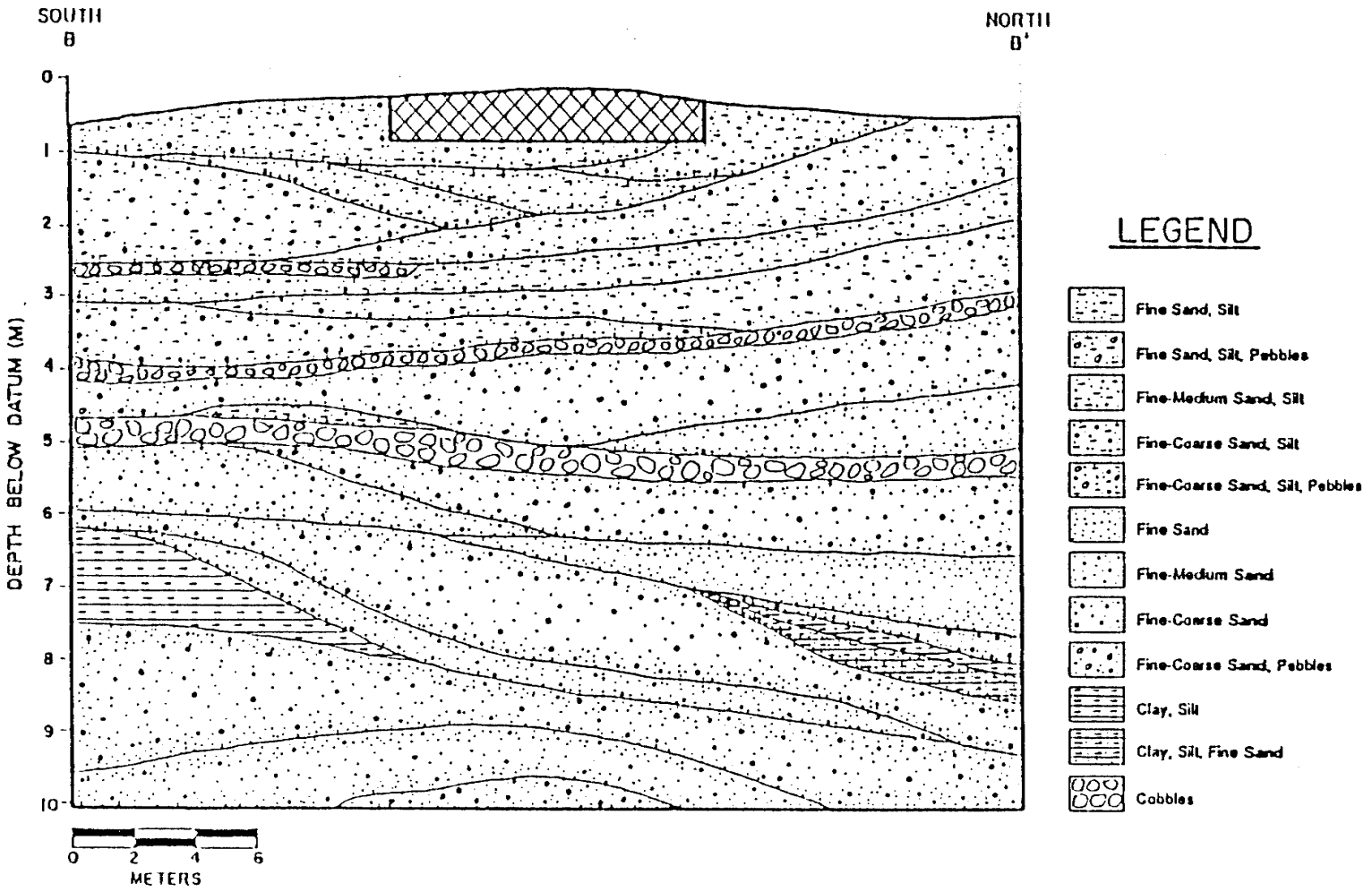

Figure 3.4. Geologic cross-section of the north-south transect (after Parsons, 1988a).

zone is located (Figures 3.3 and 3.4). There appears to be a transition zone from the piedmont slope facies to the fluvial sand facies between the two major cobble zones. The fluvial sand facies is found below the lower cobble zone at about 5 meters depth to at least 24 meters below datum. The base of the fluvial sand facies is not known at this location. Chamberlain (1980) estimates that the fluvial sand facies may be up to 250 meters thick east of Socorro Peak.

Piedmont slope facies stratification on the east-west transect (Figure 3.3) shows a general slope to the east. This inclination presumably reflects the source area to the west. The fluvial sands facies do not exhibit similar trends in either direction (Figures 3.3 and 3.4), and were probably deposited in a north-south trending fluvial system. The meandering fluvial channels consist of well-sorted, fine sands alternating with fine to coarse sands and pebbles and overbank deposits of silts and clays (Parsons, 1988a).

3.2. SOIL SAMPLING

During installation of the monitoring stations, soil samples were collected for determination of the hydraulic properties of the soil profile beneath the field site. Due to the cobble layers and collapsing nature of the soil beneath our field site, it was necessary to use a Mobil B-52 auger rig to drill the boreholes for installation of neutron access tubes and nests of

tensiometers. Split spoon samples and soil cores samples (100 cc) were collected to ten meters below the datum. For ease in referencing, each monitoring station is labeled to the nearest meter, based on the X-Y grid system. The exact location of each station was determined by surveying techniques (Table 3.1). Figure 3.5 shows the actual location of the monitoring stations.

3.2.1. Split Spoon Samples

Two hundred and forty seven (247) split spoon (disturbed) samples were collected to a depth of 10 meters below land surface. The split spoon samples were visually logged, and analyzed for gravimetric moisture content and particle size distribution.

The split spoon samples were collected using 20.3 cm (8 inch) hollow stem augers. While drilling, a star bit was attached to the cable hammer to prevent soil from entering the hollow stem. For soil sampling, the star bit was replaced with a 5.08 cm (2 inch) outside diameter split spoon sampler at selected sampling depths. The split spoon was pounded into undisturbed soil for 30 to 60 cm, in front of the auger head.

3.2.2. Soil Core Samples

A total of 76 relatively undisturbed soil core samples (100 cc) were collected for laboratory analysis of field moisture content, porosity, saturated hydraulic conductivity, moisture retention curves, and particle size distribution. Four methods of core sample collection were employed: hand augering; hand augering through the hollow stem 20.3 cm auger; hand augering in

Table 3.1.

PLAN VIEW STATION LOCATIONS

STATION		X-LOC (m)	Y-LOC (m)
2-15	NT	2.00	14.05
	A	2.00	13.30
	B	2.00	12.40
5-5	NT	5.00	4.95
	A	5.70	4.50
	B	6.50	4.00
5-25	NT	4.95	25.05
	A	4.35	24.45
	B	3.90	23.70
6-15	NT	5.93	14.77
	A	5.93	13.70
8-15	NT	8.01	15.00
	A	8.00	14.30
	B	8.00	13.30
8-16	NT	8.01	15.57
11-15	NT	10.85	15.00
	A	10.85	14.55
	SWS	11.05	15.35
12-12	NT	11.63	11.20
	A	12.10	11.00
	B	12.50	11.40
12-18	NT	11.90	18.75
	A	11.90	17.60
	B	11.70	17.35
15-2	NT	15.00	1.35
	A	14.20	1.60
	B	13.60	1.70
	T	15.00	1.35
15-6	NT	15.10	7.40
	A	14.15	7.40
15-8	NT	15.05	9.14
	A	14.10	9.14
	B	13.60	9.14
	T	15.60	9.14
15-11	NT	15.28	10.90
	A	15.00	10.90
	SWS	15.50	10.90
15-15	NT	15.00	14.59
	E	15.40	14.59
	S	14.75	14.10
	T	5.00	13.93
15-19	NT	15.29	19.40
	A	15.00	14.35
	SWS	15.60	19.25
15-22	NT	15.13	22.05
	A	14.45	22.10
	B	13.90	22.10
15-23	NT	15.14	23.25
	A	14.25	23.30
15-28	NT	15.00	28.27
	A	14.10	28.30
	B	13.30	28.30
16-23	NT	16.00	23.39
18-12	NT	18.44	10.90
	A	18.44	11.20
	B	18.44	11.90
18-18	NT	18.73	18.87
	A	18.00	18.90
	B	17.20	19.00
19-15	NT	19.00	15.22
	A	18.95	15.75
	SWS	19.00	14.72
22-15	NT	22.21	15.17
	A	22.21	15.80
	B	22.21	17.00
24-15	NT	24.05	15.12
	A	24.05	15.85
25-5	NT	24.30	4.75
	A	23.60	4.40
	B	22.80	3.75
25-25	NT	25.16	24.86
	A	24.25	25.60
	B	23.70	26.10
28-15	NT	28.20	14.94
	A	28.25	14.10
	B	28.25	12.90

STATION = station descriptive location
NT = neutron access tube
A = tensimeter nest nearest NT
B = tensiometer nest furthest from NT
SWS = soil water sampler
X- and Y-LOC = station location on X-Y grid system determined by surveying techniques.
T = thermistor nest

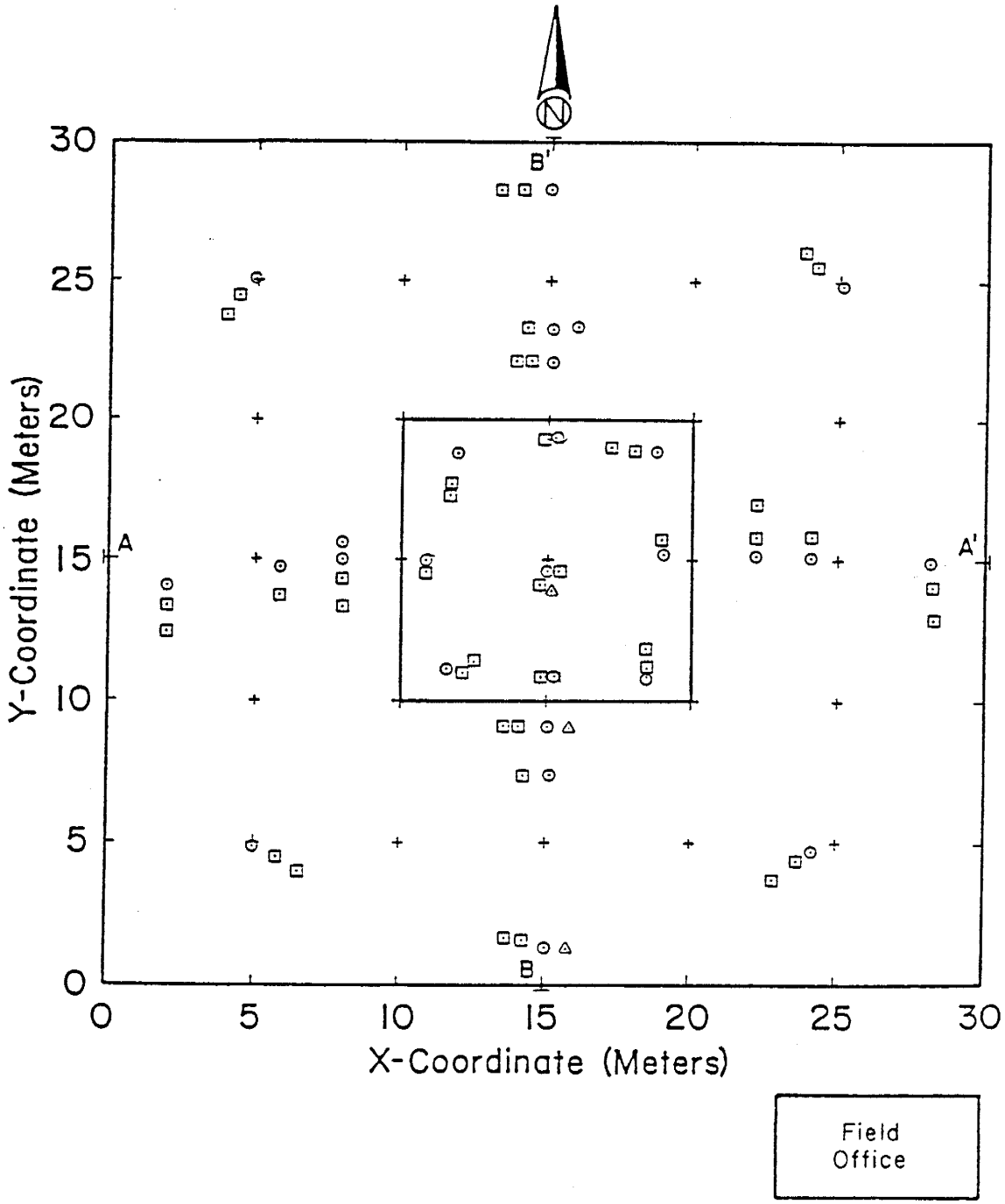

Figure 3.5. Plan view of the field site. Circles represent neutron access tubes, squares show tensiometer nests, and crosses are five meter grid locations.

conjunction with a hand power driven auger, and hand augering in conjunction with a Mobil B-30 auger rig and 5.08 cm auger. Parsons (1988a) describes each method of sample collection in detail. Table 3.2 summarizes the sampling methods utilized at each monitoring station. Figure 3.6 shows the location of soil core samples along the east-west and north-south transects.

3.3. LABORATORY ANALYSIS

Hydraulic properties of the soil samples were determined in the laboratory. Soil core samples were analyzed for the following properties: field moisture content (cc/cc), bulk density (g/cc), porosity (cc/cc), saturated hydraulic conductivity in the constant head permeameter, soil moisture retention curves determined by hanging column and 15 bar pressure plate, particle size distribution by sieve and hydrometer analysis, unsaturated hydraulic conductivity calculated from van Genuchten's closed form analytical solution (1980), and unsaturated hydraulic conductivity determined by the one-step outflow test (Kool, Parker, and van Genuchten, 1985). The split spoon samples were analyzed for gravimetric moisture content (cc/cc) and particle size distribution using sieve and hydrometer analysis. Fifteen (15) split spoon samples collected at depth were repacked into 100 cc rings at the in situ field bulk density and analyzed as soil core samples.

Table 3.2. Core Sample Collection Methods (after Parsons, 1988a)

Method	Stations
1) 0.8 cm (2") hand augering, sometimes in conjunction with Mobil B-52 rig and 0.8 cm auger to break through cobbles.	8-16, 11-15, 14-15, 15-11, 15-19, 16-6, 16-16, 19-15
2) Taken through 20.3 cm (8") boreholes, minor hand augering.	2-28, 6-15,15-6, 15-23, 24-15
3) Hand auger when possible through 20.3 cm (8") auger.	15-7.5
4) 0.8 cm (2") hand augering and hand power auger to break through cobbles.	16-23

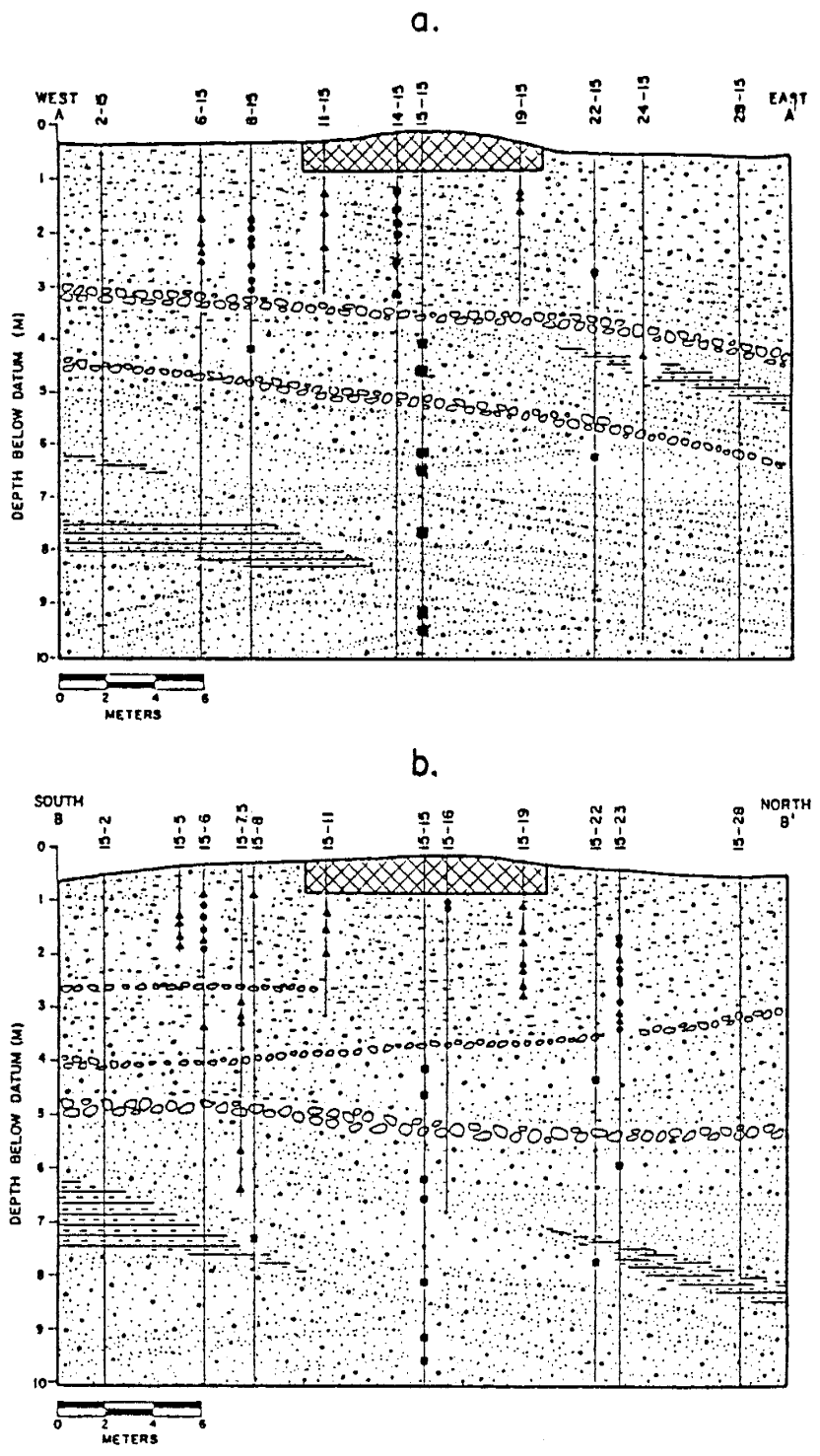

Figure 3.6. Location of soil core samples (100 cc) on the a) east-west and b) north-south transects. Circles are located directly on transect, triangles located up to a meter perpendicular to transect, and squares are repacked split spoon samples.

Raw data for laboratory tests are included in the '9I-KB' Laboratory Notebooks (Parsons, 1988b). Parsons (1988a) presents tabulated laboratory results by sample location and by facies type in her Appendices C and D respectively.

The Warrick point source analytical model used in this study requires an exponential relationship between conductivity and pressure head, or K-ψ curve. (Section 3.4.1. provides a detailed discussion of the K-ψ relationship). Three hydraulic properties are necessary to derive the K-ψ relationship: saturated hydraulic conductivity, the moisture retention curve, and unsaturated hydraulic conductivity. Therefore, the following sections will only discuss these hydraulic properties in detail. Parsons (1988a) provides an excellent discussion of the other hydrologic parameters measured.

3.3.1. Saturated Hydraulic Conductivity

Saturated hydraulic conductivity (K_S) of soil core samples was determined in the laboratory using a constant head permeameter. Several days were required for the outflow to reach equilibrium, and it was assumed that all of the entrapped air was eliminated from the sample after this time.

For samples collected at the field site, K_S ranges from $2x10^{-1}$ cm/sec (200 m/d) in coarse sand and pebbles to $8x10^{-6}$ cm/sec ($7x10^{-3}$ m/d) in clays. The geometric average K_S for the piedmont slope facies is $3.3x10^{-3}$ cm/sec (2.9 m/d). The underlying fluvial sand facies are slightly more conductive (Parsons, 1988a).

Figure 3.7 shows the logarithm of K_s along the east-west and north-south transects of the field site. The large variability of saturated hydraulic conductivity within the material at the site is apparent in the vertical direction where K_s varies by 2 orders of magnitude within a few meters.

3.3.2. Moisture Retention Characteristics

The soil moisture retention relationship (θ-ψ curve) for each soil core was measured using a hanging column apparatus and 15-bar pressure plate assembly. The hanging columns were used for determining the drainage and imbibition cycles to negative pressures of about 200 cm (Vomocil, 1965). An equilibrium period of 24 hours was allowed between moisture content determinations at varying pressure values. Although a 24 hour equilibration period is generally considered appropriate for sandy samples, it may not have been entirely adequate for the finer samples. At negative pressures less than 200 cm, a pressure plate assembly (15 Bar Ceramic Plate Extractor Cat.# 1500, Soil Moisture Equipment Co., Santa Barbara, CA) was used to apply a positive pressure to displace water from the sample at an equilibrium pressure up to 15 bars. Only the clay and silty samples were placed in the pressure plate.

3.3.3. Unsaturated Hydraulic Conductivity

The unsaturated hydraulic conductivity was calculated using a closed form analytical solution developed by van Genuchten (1980). His model calculates the relative hydraulic conductivity (K_r) from the θ-ψ relationship based on Mualem's pore structure

a.

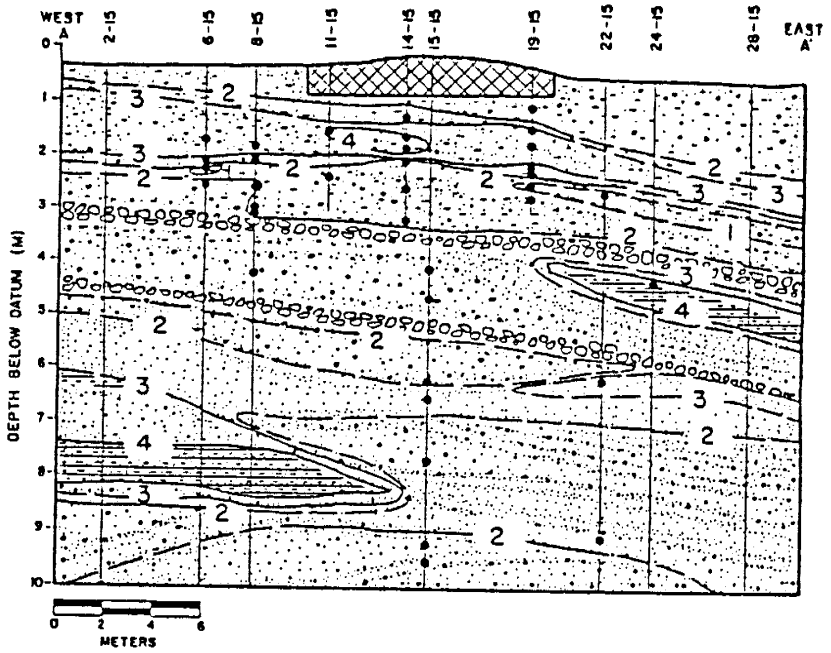

b.

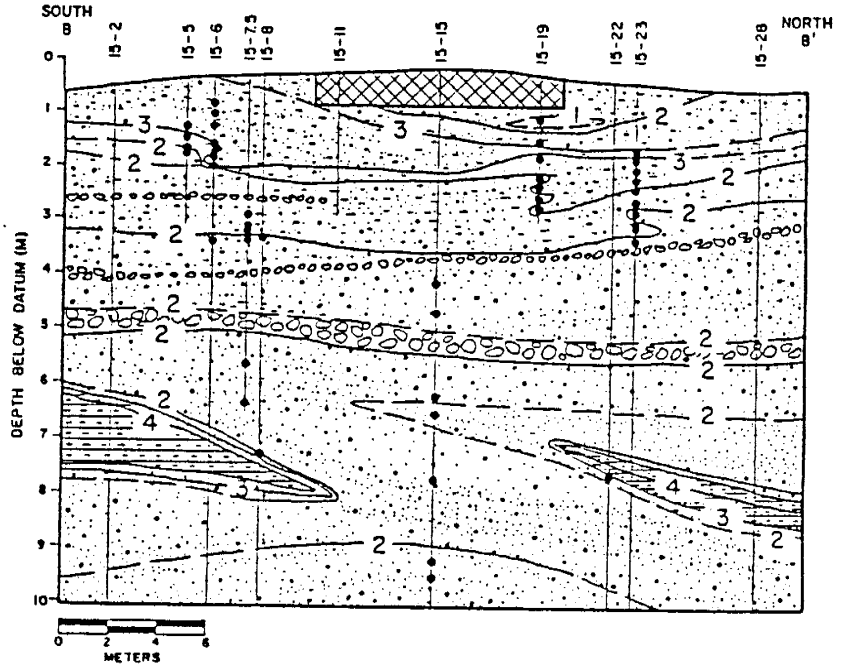

Figure 3.7. Logarithm of saturated hydraulic conductivity (cm/sec) along the a) east-west and b) north-south transects (after Parsons, 1988a). Dots show sample locations.

model (1976). Water content is expressed in a dimensionless form:

$$S_e = (\theta - \theta_r)/(\theta_s - \theta_r) \qquad (3.1)$$

where S_e is the effective saturation (dimensionless), θ is the moisture content (cc/cc), and where θ_r and θ_s refer to residual and saturated volumetric moisture contents, respectively. van Genuchten used the following relationship to represent the θ-ψ curve:

$$S_e = [1/(1 + \alpha_v h)^{n_v}]^m \qquad (3.2)$$

where h is the soil suction, while α_v, n_v, and m are parameters which depend on the shape of the ψ-θ curve. Mualem's model (1976) for relative hydraulic conductivity is based on the equation:

$$K_r(S_e) = S_e^{1/2} [\int_0^{Se} \{1/h(x)\}dx / \int_0^1 \{1/h(x)\}dx]^2 \qquad (3.3)$$

van Genuchten's closed form solution combines Mualem's theory (equation 3.3) with equation 3.2 leading to:

$$K_r(S_e) = S_e^{1/2} [1 - (1 - S_e^{1/m})^m]^2 \qquad (3.4)$$

or:

$$K_r(h) = \{1 - (\alpha_v h)^{n_v-1} [1 + (\alpha_v h)^{n_v}]^{-m}\}^2/[1+(\alpha_v h)^{n_v}]^{m/2} \qquad (3.5)$$
$$(m = 1-1/n_v)$$

van Genuchten's two-parameter model estimates α_v and n_v by a non-linear least squares regression, and calculates K_r by equation 3.3. Input data includes the laboratory parameters previously measured: the θ-ψ relationship, θ_s, θ_r, and saturated hydraulic conductivity. When using the two-parameter model, the residual moisture content was assumed to be the 15 bar moisture

content, the maximum operating pressure of the pressure plate apparatus.

The unsaturated hydraulic conductivity for each soil core sample was evaluated by van Genuchten's method. In order to more closely approximate field infiltration conditions, moisture retention data from the imbibition cycle was input to the model. Because of the possible effect of entrapped air, the saturated water content was assumed to be 90% of the measured θ_s, unless the θ-ψ curve indicated a significantly different saturation value. The two-parameter model was run for all cases where residual moisture content data (15 bar moisture content) were available.

3.4. CONCEPTUAL FRAMEWORK FOR MODEL

In order to use the Warrick (1974) analytical model selected for this study, the soil beneath the field site was assumed to be homogeneous. The soil was represented as a single, homogeneous layer of the piedmont slope facies. The geometric mean hydraulic properties of the piedmont slope facies were used. Table 3.3 lists the geometric mean hydrologic properties of the piedmont slope facies. Appendix D contains the individual sample hydrologic data.

The simplification of the stratified soil system based on piedmont slope facies hydrologic properties allows prediction of the moisture content distribution above the fluvial sand facies.

Table 3.3. Geometric Mean Hydrologic Properties used to Calculate Effective Hydrologic Relationships

Hydrologic Property	Geometric Mean	Number of Samples
K_s (m/d)	2.87	46
θ_s (cc/cc)	0.377	49
θ_r (cc/cc)	0.117	28
α_v (1/cm)	0.068	45
n_v (-)	1.61	45

a_v (1/cm), n_v (--) = van Genuchten parameters
θ_s = saturated moisture content (% vol)
θ_r = residual moisture content (15 bar moisture, % vol)
K_s = saturated hydraulic conductivity (m/d)

* satiated moisture content for imbibition considered as 90% of the measured mean value of the saturated moisture content.

The depth of the contact of the piedmont and fluvial facies varies from about 3.6 to 6.5 meters below datum. However, the interface location was a subjective division based primarily on texture and color (Parsons, 1988a). For this study, it was assumed that the interface was located at 5.5 meters below datum, below the second major cobbles zone (Figures 3.3 and 3.4).

Variability of the hydraulic properties within the piedmont slope facies required development of an averaged, or effective, θ-ψ curve. This study used the geometric mean of K_s, θ_s, θ_r, and van Genuchten parameters α_v and n_v, of 46 piedmont slope facies soil samples to generate the effective unsaturated conductivity relationship (Figure 3.8). When considering flow both parallel and perpendicular to layers of varying hydraulic conductivity, the effective saturated hydraulic conductivity calculated by the geometric mean is considered the most appropriate. Calculating the effective unsaturated hydraulic parameters using a geometric mean analysis seems to be a logical extension. Parsons (1988a) arithmetically averaged α_v and n_v van Genuchten fitted parameters from piedmont slope facies soil samples to determine the effective θ-ψ curve. However, there are no known studies which verify either approach, the arithmetic or geometric mean determination of an effective θ-ψ curve.

The linearized analytical model requires an exponential relationship between K and ψ in the form of equation 2.5. The K-ψ relationship (Figure 3.9) was calculated using equation 3.5 and the geometric mean hydraulic data listed in Table 3.3. The

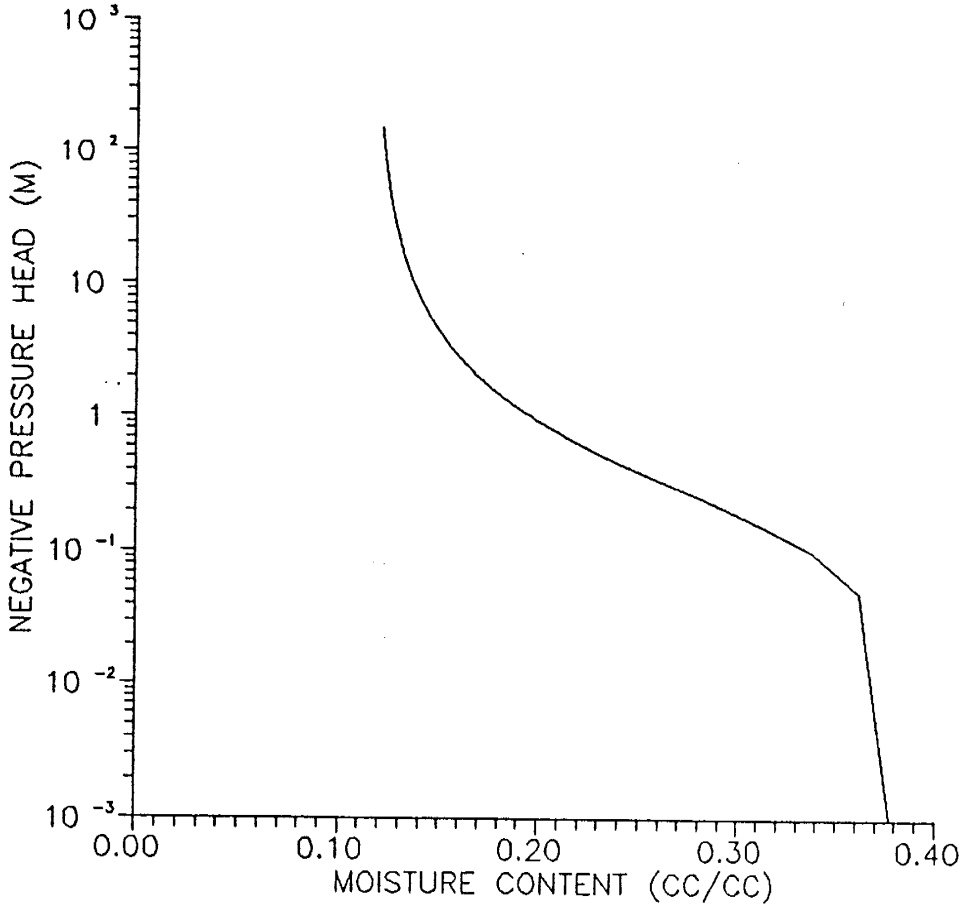

Figure 3.8. Effective θ-ψ curve from the piedmont slope facies.

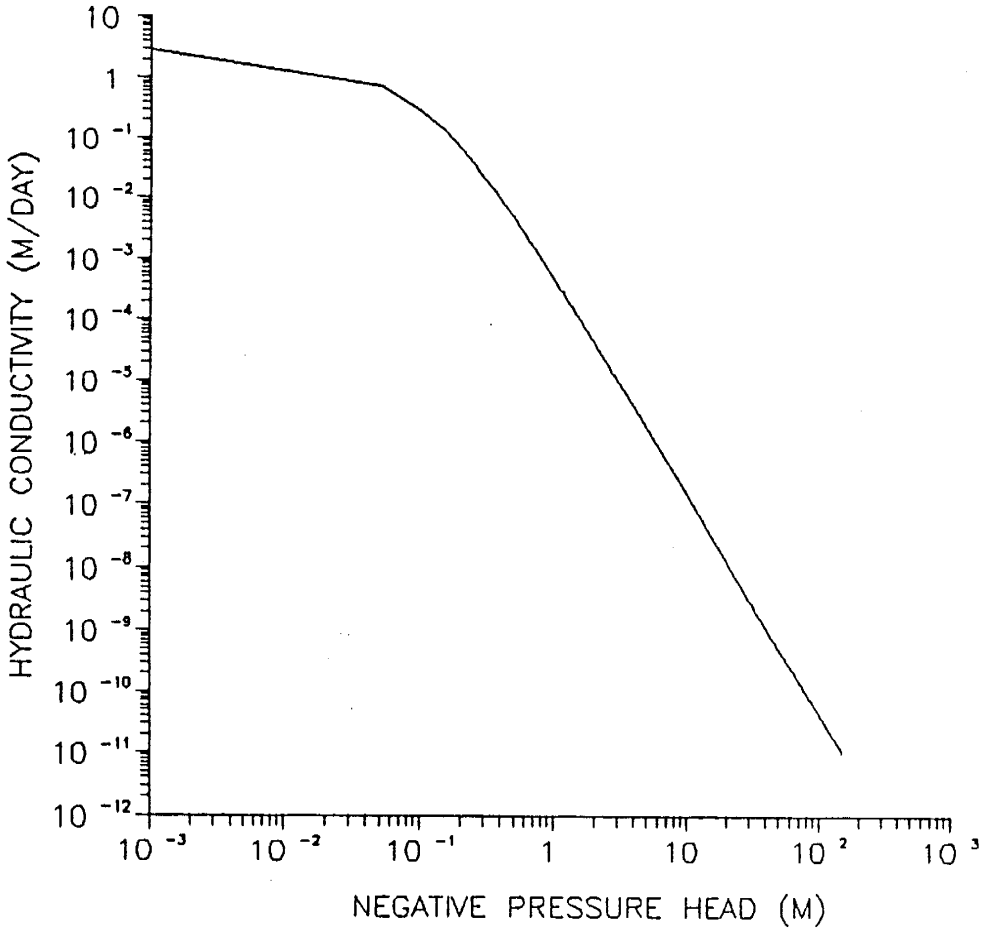

Figure 3.9. Effective K-ψ curve from the piedmont slope facies.

piedmont slope effective K-ψ curve was linearly regressed in the form:

$$\ln(K) = \alpha\psi + \ln(K_0) \qquad (3.6)$$

where α is the slope of the linear regressed line and $\ln(K_0)$ is the intercept. Table 3.4 summarizes a_L and K_0 regressions of the effective K-ψ curve. Several regressions were conducted to observe different ranges of ψ to help bracket model input parameters. The upper limit of ψ was always equal to zero. It was assumed that the area immediately adjacent to the emitters will become saturated. The lower ψ limit varied from 250 to 15000 cm negative pressure head to demonstrate the range of α and K_0. α varied from a maximum of 3.7 1/m to near 0.1 1/m in the dry range. K_0 varied from 2×10^{-2} to 8×10^{-8} m/d for the respective ranges of ψ. Appendix E contains the van Genuchten fitted K-ψ relationship.

Table 3.5 lists the slopes, α, and intercepts, K_0, of various soils determined by previous investigators. The α and K_0 determined for this study (Table 3.4) compare reasonably well with the results of similar soil types (Table 3.5). Note that comparisons should only be made for parameters computed for similar ranges of ψ.

For the time dependent model, the slope (k) of the K-θ curve is a constant (equation 2.8). The methods for determining k are less certain compared to those for determining K_0 and α (Ben-Asher and others, 1978). Ben-Asher and others recommended three

Table 3.4. Model Input Parameters Calculated from Effective K-ψ Relationship

Pressure Head Range ψ (-m)	Linear Regressed Slope α (1/m)	Intercept K_o (m/day)	Correlation Coefficient r^2 (-)	Number of Data pts. (-)
0-0.5	12.23	1×10^{-0}	0.96	11
0-1.0	7.78	4×10^{-1}	0.92	21
0-1.5	5.70	2×10^{-1}	0.90	31
0-2.0	4.50	9×10^{-2}	0.88	41
0-2.5	3.71	5×10^{-2}	0.86	51
0-5.0	1.98	7×10^{-3}	0.83	101
0-10.0	1.02	1×10^{-3}	0.80	201
0-50.0	0.27	6×10^{-6}	0.68	51
0-100.0	0.11	4×10^{-7}	0.69	101
0-150.0	0.07	8×10^{-8}	0.70	151

Table 3.5. The hydraulic conductivity parameters of several soils (after Warrick, Lomen, and Tonellato, 1981).

Soil	Range of -h [cm H_2O]		α [cm^{-1}]	K [cm/sec]	r
×Chino clay	1.02	1.79×10^{4}	6.85×10^{-4}	9.17×10^{-4}	0.75
	1.02	255	2.05×10^{-2}	3.77×10^{-5}	0.92
×Lamberg clay	1.45	33.6	3.27×10^{-1}	1.45×10^{-2}	0.98
×Bet netofa clay soil	1.25	980	6.62×10^{-2}	4.62×10^{-7}	0.99
×Lakish clay	40	700	1.38×10^{-2}	2.34×10^{-4}	0.99
×Yolo clay	37.2	147	3.67×10^{-2}	2.69×10^{-5}	0.99
×Sticky clay	1	10^{4}	8.64×10^{-4}	2.02×10^{-7}	0.72
	1	170	2.91×10^{-2}	1.63×10^{-6}	0.94
×Fragmented Lamberg clay	9	139	4.1×10^{-2}	3.78×10^{-3}	0.99
×Peat	1	10^{4}	1.04×10^{-3}	1.17×10^{-6}	0.65
	1	130	5.38×10^{-2}	2.84×10^{-5}	0.94
×Sheluhot silty clay	1.3	890	7.26×10^{-3}	4.51×10^{-7}	0.95
×Touched silt loam	12.2	298.8	1.56×10^{-2}	9.03×10^{-4}	0.93
	1.57	104.6	1.03×10^{-1}	2.61×10^{-3}	0.98
×Silt loam	0	339	1.39×10^{-2}	6.87×10^{-5}	0.99
×Indio loam	.0	10	1.69	2.82×10^{-6}	0.73
×Yolo fine sandy loam	43.3	300	2.5×10^{-2}	4.68×10^{-5}	0.79
×Plainfield sand fractions					
210-250μ	0	31	2.62×10^{-2}	3.29×10^{-3}	0.21
177-210μ	30	37	0.28	1.86×10^{-2}	0.69
149-177μ	41.5	46	0.64	8.57×10^{9}	0.92
125-149μ	45	53	0.33	9.42×10^{4}	0.74
104-125μ	55	65	0.371	2.37×10^{7}	0.73
×Dackley sand	38.7	49.8	0.513	2.16×10^{4}	0.89
×Oso flasco fine sand	0	50	7.2×10^{-2}	3.87×10^{-2}	0.96
×G.C. # 2 sand	13.2	31.6	0.17	1.73×10^{-2}	0.94
×Crab creek sand	4.17	15.4	0.466	7.16×10^{-2}	0.98
×G.E. # 2 sand	43.8	121	5.75×10^{-2}	8.52×10^{-2}	0.94
×Sand (USSL + 3445)	58.4	147.2	6.5×10^{-2}	1.32×10^{-1}	0.97

Table 3.5. continued.

Soil	α [cm-1]	K_o [cm/sec]	r
Clay loam (Thomas et al.,1976)	0.1258	1.12×10^{-3}	--
Sandy loam (Thomas et al.,1976)	0.1112	1.00×10^{-3}	--
Plainfield sand (Black et al.,1969)	0.126	3.44×10^{-3}	0.948
Columbia sandy loam (Liliberte et al.,1966)	0.100	1.39×10^{-3}	0.932
Guelph loam (Elrick & Bowerman, 1964)	0.030	3.67×10^{-4}	0.979
Ida silt loam (Green, 1962)	0.026	2.92×10^{-5}	0.873
Yolo light clay (Moore, 1939)	0.019	1.23×10^{-5}	0.883
Gila sandy loam (Morin, 1977)	0.0443	21.0	--
Lateen clay loam (Morin, 1977)	0.0386	4.5	--
Pima clay loam (Ferreira, 1977)	0.0117	1.5	--
Panoche loam (Warrick, 1975)	0.04	95.0	--
Pima clay loam (Warrick, 1975)	0.014	9.9	--

r = regression coefficient

*Data from Bresler (1978).

methods for obtaining k. The first method evaluates diffusivity at an average θ using the following relationship:

$$k = \alpha D(\theta_{av}) \tag{3.7}$$

where

$$D(\theta_{av}) = K(\psi)[d\psi/d\theta] \tag{3.8}$$

and $K(\psi)$ is calculated from equation 2.5. The second method for determining the value of k according to Ben-Asher and others (1978) utilized experimental data from a separate field or laboratory experiment. The third technique selected a k from the range of $dK/d\theta$ data.

A modification to the third method of choosing k was applied in this study. Ben-Asher and others (1978) found that k approached a constant at large K (or large θ). They used this asymptotic value as their constant k. However, the slope of the k versus K relationship for the piedmont slope facies approaches infinity as $K(\theta)$ approaches K_s. Therefore, a linear regression, similar to those performed to determine α, was applied to determine the average slope of the effective K-θ curve (Figure 3.10). k ranges from 4.17 m/d in the 0.16 to 0.38 volumetric moisture content range (0.0 to -2.5 m ψ) to 3.10 m/d in the 0.12 to 0.38 volumetric moisture content range (0.0 to -10.0 m ψ). Results of the linear regression of the piedmont slope facies effective K-θ curve are presented in Table 3.6. The linear regression was performed on evenly spaced θ data which corresponded to ψ ranges used in determining α and K_0. Due to the uncertainty of determining k, the k values calculated in

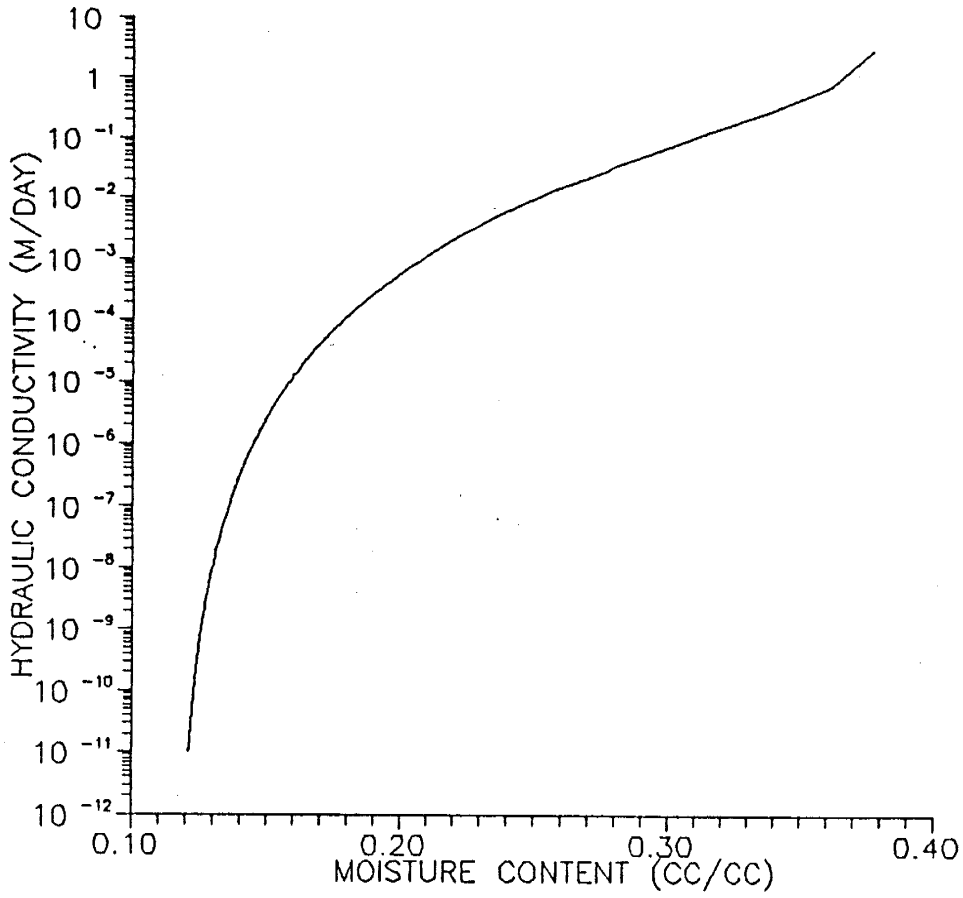

Figure 3.10. Effective K-θ curve from the piedmont slope facies.

Table 3.6. Model Input Parameters Calculated from Effective K-θ Relationship

Pressure Head Range ψ (-m)	Moisture Content Range θ (cc/cc)	Linear Regressed Slope k (m/day)	Correlation Coefficient r^2 (-)	Number of Data pts. (-)
0-2.5	.377-.163	4.17	0.40	101
0-5.0	.377-.147	3.72	0.38	101
0-7.5	.377-.141	3.54	0.37	101
0-10.0	.377-.137	3.45	0.37	101
0-20.0	.377-.130	3.30	0.36	101
0-50.0	.377-.125	3.17	0.35	101
0-100.0	.377-.122	3.13	0.35	101
0-150.0	.377-.121	3.10	0.35	101

Table 3.6 will be used as an initial guess for model input. A trial and error adjustment of k was used in the model to determine an appropriate input value of k. Appendix E contains θ and K data pairs calculated by van Genuchten's model.

4. FIELD EXPERIMENT DESIGN

The field experiment was designed to simulate uniform leakage from a lined impoundment. The following section describes the site selection and preparation; water application system including the drip irrigation system, pump system, electrical system, and water flow monitoring system; and the water pre-treatment system.

4.1. SITE SELECTION AND PREPARATION

Four criteria were used to determine the field site selection: a water table exceeding a few tens of meters, a stratified soil profile, relatively high soil permeability, and fairly level topography with good drainage. Less important criteria included: convenient access for vehicles, availability of a water supply and electrical source, and security from vandalism.

Three potential sites west of the New Mexico Tech campus were initially selected. Considerable test drilling at the three sites was conducted. The area in the northeast corner of the Physical Plant bone yard just west of the golf course was chosen as the most suitable field site (Figure 4.1). The site is fairly level, runoff from Socorro Peak has been diverted by a large

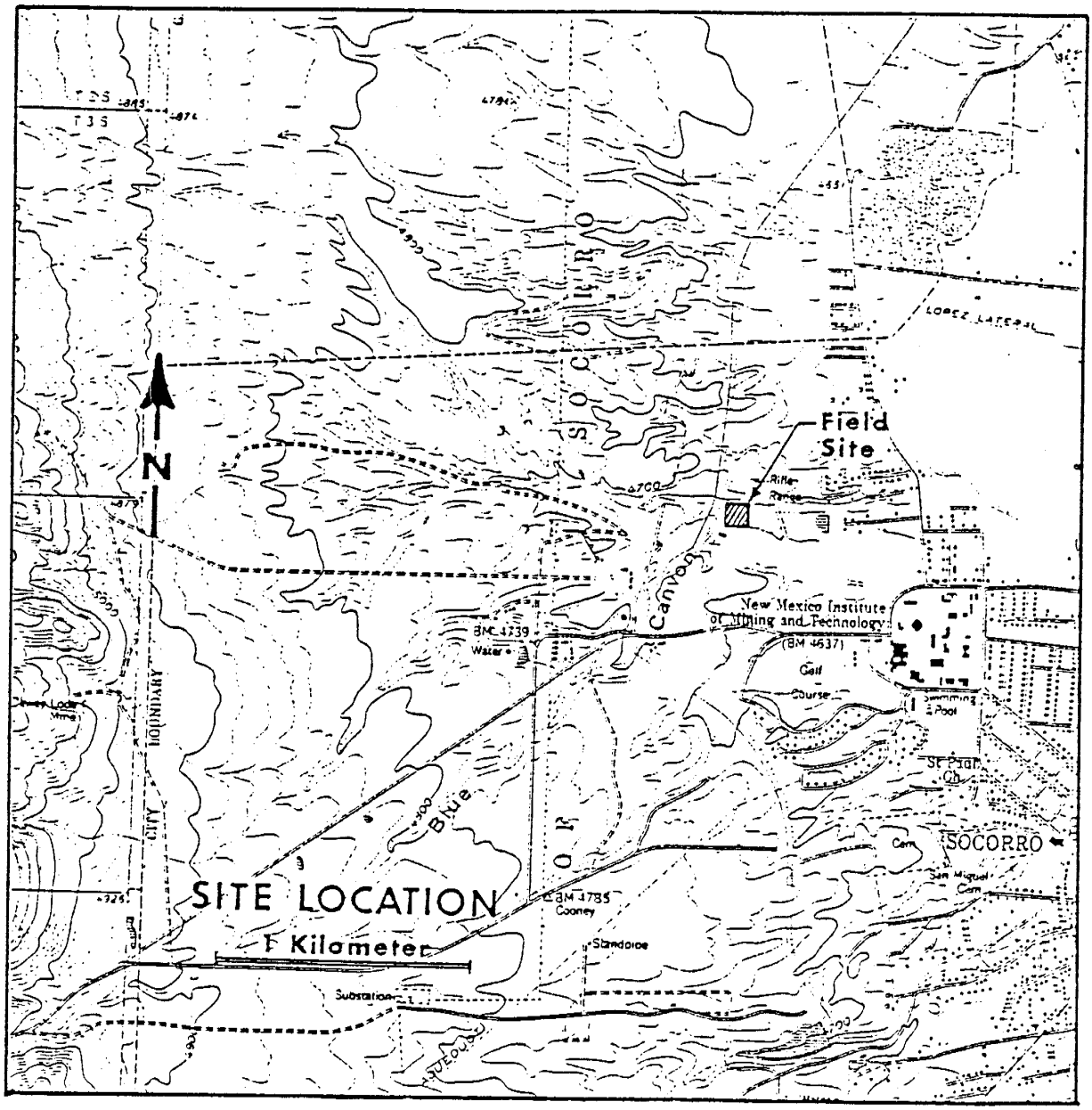

Figure 4.1. Site location map.

flood control dike to the east since 1963, the site has never been previously irrigated, and depth to water is about 24 meters.

After permission to use the site west of the golf course was granted, a 30m x 30m area was cleared of debris and vegetation. The southern and western edges of the field site were bermed to deter local runon. A five meter interval grid was surveyed across the site. The grid origin was set at the southwest corner of the field site with X in the eastern direction, and Y in the northern direction (Figure 3.2). This grid system was used to locate instrumentation nests on the field plot. A trailer was placed adjacent to the site for use as a field office and to house equipment.

4.2. WATER APPLICATION SYSTEM

This section describes the overall operation of the application system. The following subsections describe the four major components in more detail; the driplines, pump system, electrical system, and the water flow monitoring system.

4.2.1. Pump System

Water flow to the emitters was controlled by a positive displacement pump which delivered a prescribed volume of water to the driplines from the water supply tank. The pump system consists of a water storage tank, float switches, gear pump, and throttle valves (Figure 4.2). The storage tank was a 250 gallon

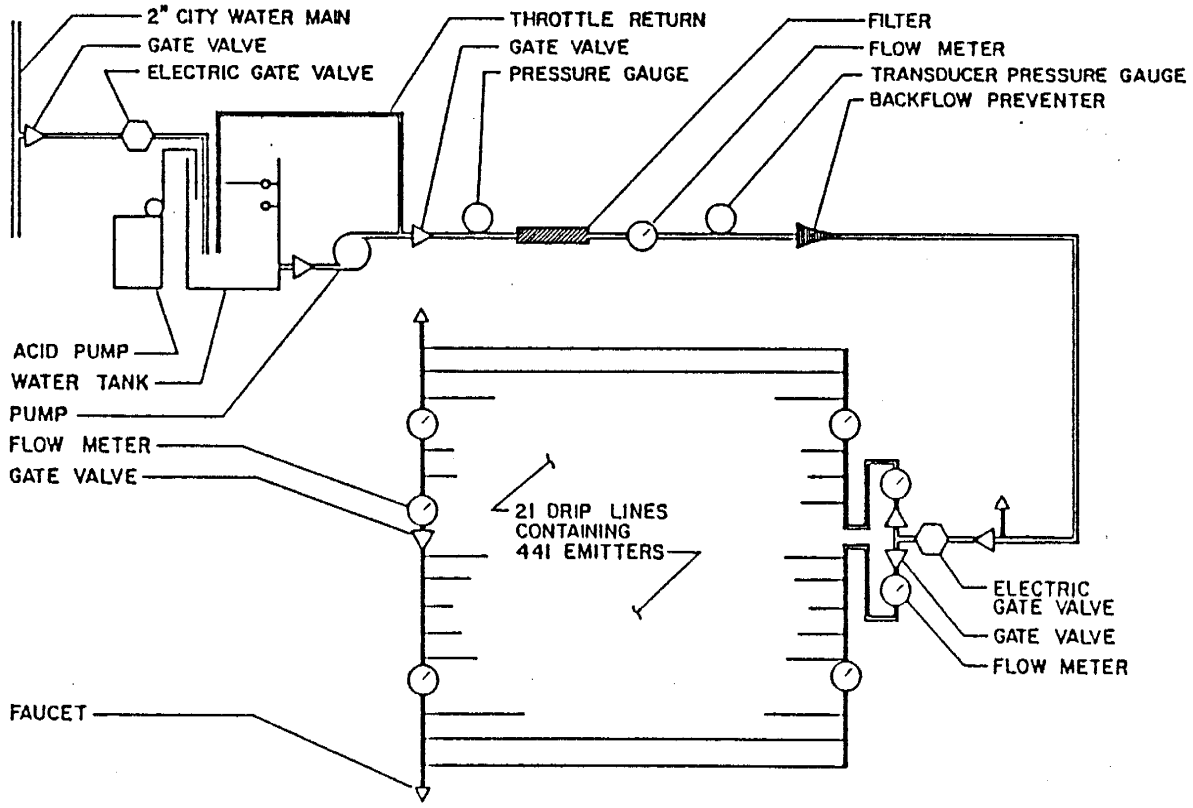

Figure 4.2. Schematic of water application system.

aluminum fuel tank standing on end. The tank was approximately 100 cm in diameter by 200 cm in length. The amount of water pumped per cycle was regulated by two float switches. The distance between the two switches determined the volume of water pumped. The switches were constructed from styrofoam-filled aluminum cans connected to micro switches. Water was withdrawn through a flexible hose to the pump unit. Due to the low volume and high pressures required, a rotary gear pump (Model 5-BBV, Sherwood, Detroit, Michigan) connected to a one horsepower electric motor was selected as the most appropriate pump for this system.

The gear pump delivered a prescribed amount of water in proportion to the number of RPMs. Regulation of the pressure in the drip system was accomplished by manually adjusting a throttle valve in series with a 0.2 cm (0.75 inch) PVC water return line placed downstream of the pump unit (Figure 4.2). The throttle valve restricts the amount of flow, hence the pressure to the drip irrigation system was regulated.

The pump was turned on for approximately one minute each hour by an electric timer, and was set to turn off when the water level in the water tank reached the bottom float switch. After the pump was off, the storage tank was refilled to an upper float switch (Figure 4.2). Total volume of water pumped per run was controlled by the distance between the upper and lower float switches. A data logger (CR7, Campbell Scientific, Logan, Utah) located in the field office records the pump operation time and

in-line water pressure.

During each pumping cycle, about 36.0 liters (9.5 gal) of water was delivered to the plot, generating a constant flux rate of about $1x10^{-5}$ cm/s ($9x10^{-3}$ m/d). The flux rate was chosen based on preliminary laboratory results for saturated hydraulic conductivity. The geometric mean K_s found in the soil profile is roughly 100-fold greater than the flux rate.

4.2.2. Electrical System

The electrical system consists of a constant power supply source, an electronic timer(BB-4, Sherwood, Shreveport, LA), and a custom made control box. The electrical system activates the gear pump and the chemical feed pump (Ecodyne 2500C Barracuda Series, MEC-O-MATIC Co., St. Paul, MN) and opens solenoid valves at a specified time. Electrical power was obtained from a power pole at the golf course maintenance shop, approximately 150 meters south of the field trailer. An underground cable supplies electricity from the power pole to the field trailer. The electricity is routed through a fuse box and a surge protector to guard against lightening strikes. A constant voltage supply device was installed to help maintain the voltage and eliminate switching the pump on and off. Due to the large demand for power when the gear pump is activated, a decrease in line voltage for a few milliseconds occurred. The voltage drop resulted in switching the pump off prematurely. When the voltage recovered, the pump was turned back on, and the cycle was repeated many times per second. The constant voltage supply eliminated this

problem.

The electronic timer controls the timing of the sequence of events for each period of pumping. It is set to Standard Daylight Time and has a 9-volt battery back-up to maintain the time program in case of power failure. The program turns circuits in the rear of the timer on and off. The circuits are joined to the control box.

The control box contains the switches and controls the operation of the water application system. The switching control circuit was modified by Charlie Rhodes, electronic technician consultant. The relays were set so that if the circuit was broken once, the circuit would remain disconnected until a signal was sent to activate it again. The one time circuit breaker prevented the gear pump from cycling on and off due to oscillations of the lower float switch. The second modification in the control box involved sending a one second current pulse to activate the gear pump switch, thereby preventing the pump from running for more than one second if the city water pressure failed to fill the water supply tank to the upper float switch.

4.2.3. Drip Irrigation System

A drip irrigation system was used to apply a uniform flux of water over a 10.5m x 10.5m area in the center of the field site. The method used to obtain a constant flux is similar to the sprinkler infiltration method described by Young (1964). Sprinklers can be used to apply a constant supply of water to a soil surface at a rate less than the saturated hydraulic

conductivity of the soil. The difficulty of Young's method in a field situation is the requirement of elaborate equipment which must be maintained to insure a uniform flux is applied to the soil. Moreover, the sprinkler infiltration method has problems with the raindrop impact effect on the soil surface, thus reducing surface infiltrability.

The water application system used in this experiment eliminates some of the problems of the sprinkler infiltration method. A drip irrigation system was used to apply water to the soil, thus eliminating the raindrop impact effect on the application surface. The application surface is below the ground surface and a layer of plastic was placed over the driplines to eliminate evaporation from the soil application area.

The drip irrigation system consists of twenty-one (21) driplines (model 164, Agrafem, Fresno, CA) and two manifold headers on the east and west side of the center 10.5m x 10.5m area of the field site (Figure 4.3). Each dripline contains twenty-one (21) one gallon per hour (3.75 l/hr) emitters spaced at 50 cm intervals. Water enters the eastern manifold header between driplines 10 and 11. The water flow is divided to the northern and southern portions of the dripline system. The western manifold head ensures even distribution of pressure to the driplines.

Application of the water below the land surface has many advantages. The drip irrigation system was placed about 60 cm below the land surface. In this manner the irrigation system

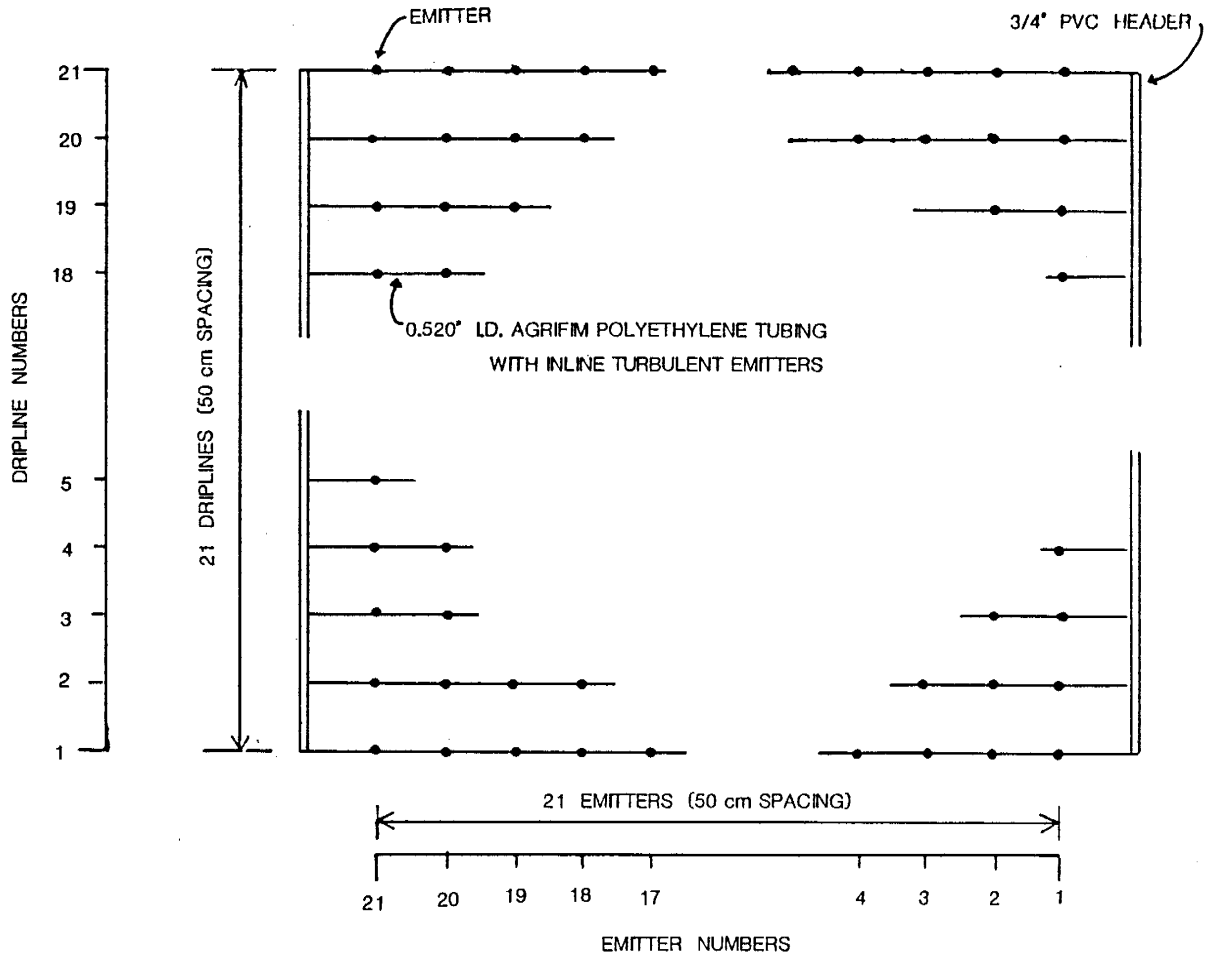

Figure 4.3. Schematic of drip irrigation system showing the dripline and emitter numbering system.

more accurately simulates slow seepage from an impoundment. Other benefits include: diminished evaporation, protection against surface temperature effects, and insurance that the irrigation system is lying on native soil.

The drip irrigation system was installed in the following manner. A rectangle approximately 10.5m x 11.5m was excavated by backhoe to a depth of 60 cm in the center of the field site. The 11.5 meter length was in the east-west direction to accommodate the manifold headers. The base of the excavated pit was surveyed and leveled by pick and shovel to ± 0.01 feet. Manifold protection boxes (Figure 4.4) were installed to facilitate repair and replacement of the irrigation lines. A layer of clean river sand was spread on the level surface between the east and west header protection boxes. The sand was leveled using board and batten techniques (similar to spreading concrete); then it was tamped by hand for stabilization. The final thickness of the sand layer was about 2 cm.

Twenty-one (21) driplines were placed on the level sand surface spaced at 50 cm intervals in an east-west direction. Each dripline had 21 emitters at 50 cm spacings, creating a 21 x 21 emitter grid of 441 total emitters. Each emitter supplies water to a 50 x 50 cm area (Figure 4.5). Thus the total area of water application is 10.5m x 10.5m.

Each dripline was covered with half shells of 6.4 cm (2.5 inch) PVC tubing supported on 1.3 cm (0.5 inch) scrap PVC tubing. The split PVC tubing was designed to create a tunnel over each

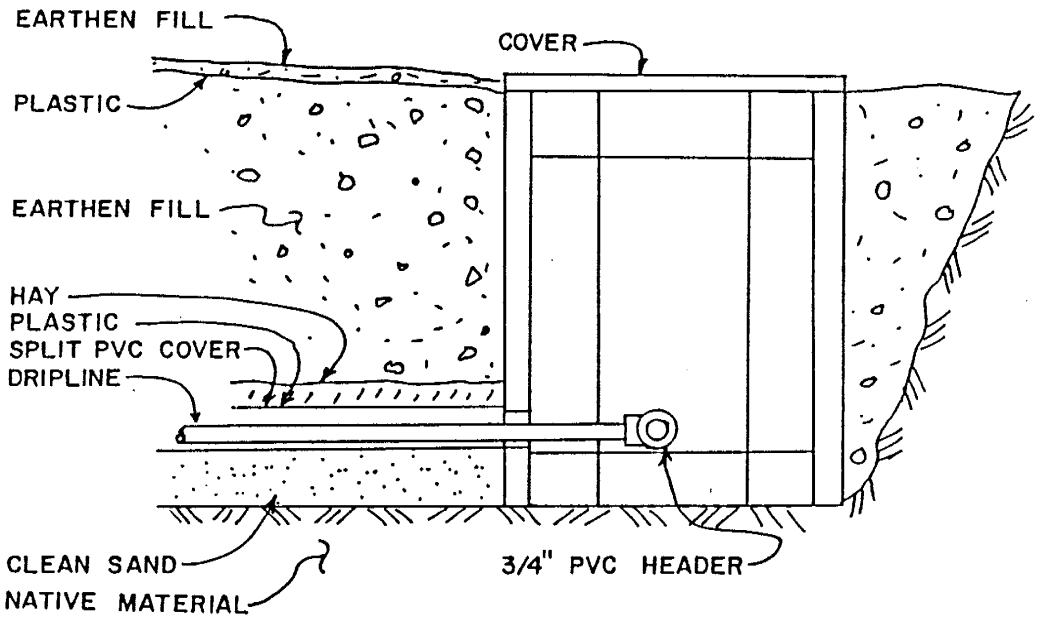

Figure 4.4. Cross-section of manifold protection boxes.

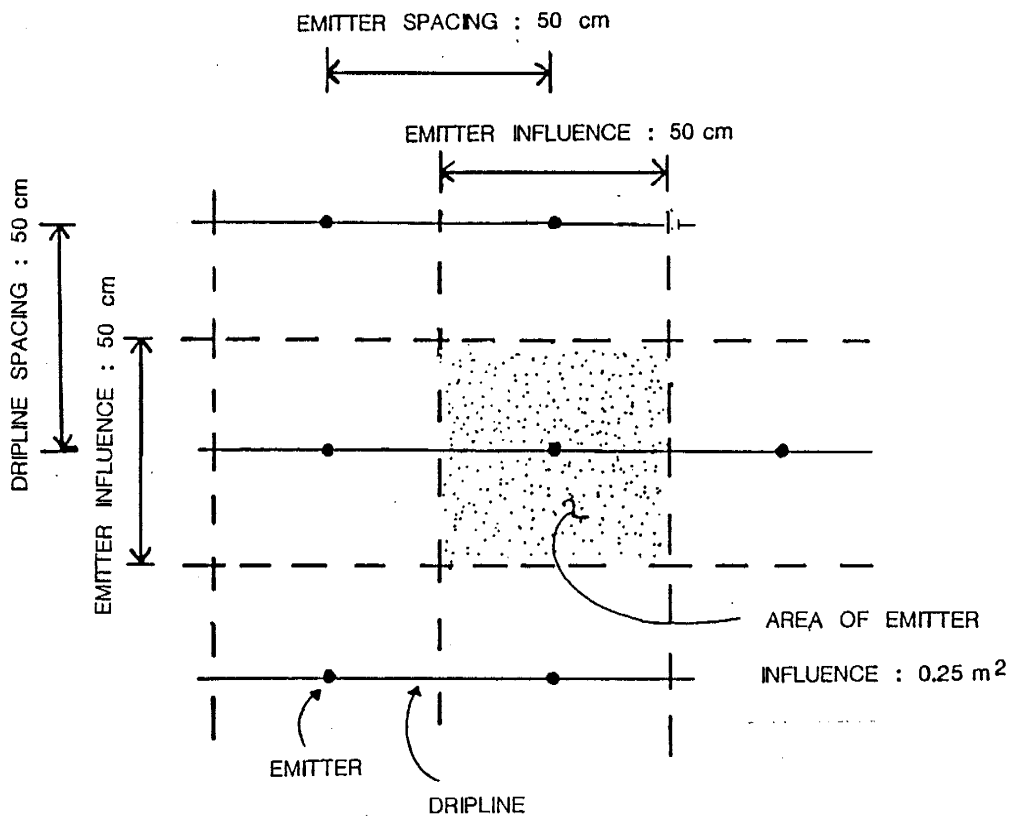

Figure 4.5. Zone of influence for an individual emitter.

dripline between the header protection boxes to facilitate dripline replacement. However, the split PVC tubing was forced into the underlying sand during subsequent fill material placement. The compression was not expected to affect the drip irrigation system performance.

A layer of 4 mil plastic was placed over the sand and split PVC tubing. The plastic acts as an impermeable layer to the upward flow of water, ensuring the infiltrated water will move only downward and laterally. A layer of hay was used as an inexpensive insulation on top of the plastic. Earthen fill was placed in the excavation to bring the level above grade. The surface was smoothed and a second layer of sealed 4 mil plastic was positioned on top to prevent infiltration of precipitation. The plastic layer was protected from the weather and traffic by approximately 2 cm of soil (Figure 4.6).

The drip irrigation system testing was conducted at the New Mexico Tech hydrology laboratory before installation in the field. Laboratory testing results indicated the irrigation system flowed uniformly. Later field tests on used driplines suggest that flow through the driplines was uniform with the exception of one emitter out of 21 plugged by a grain of sand. It was assumed that plugging of other emitters occurred randomly. Appendix F contains a detailed description of the irrigation system testing procedure.

4.2.4. Water Flow Monitoring System

The water application monitoring system is designed to check

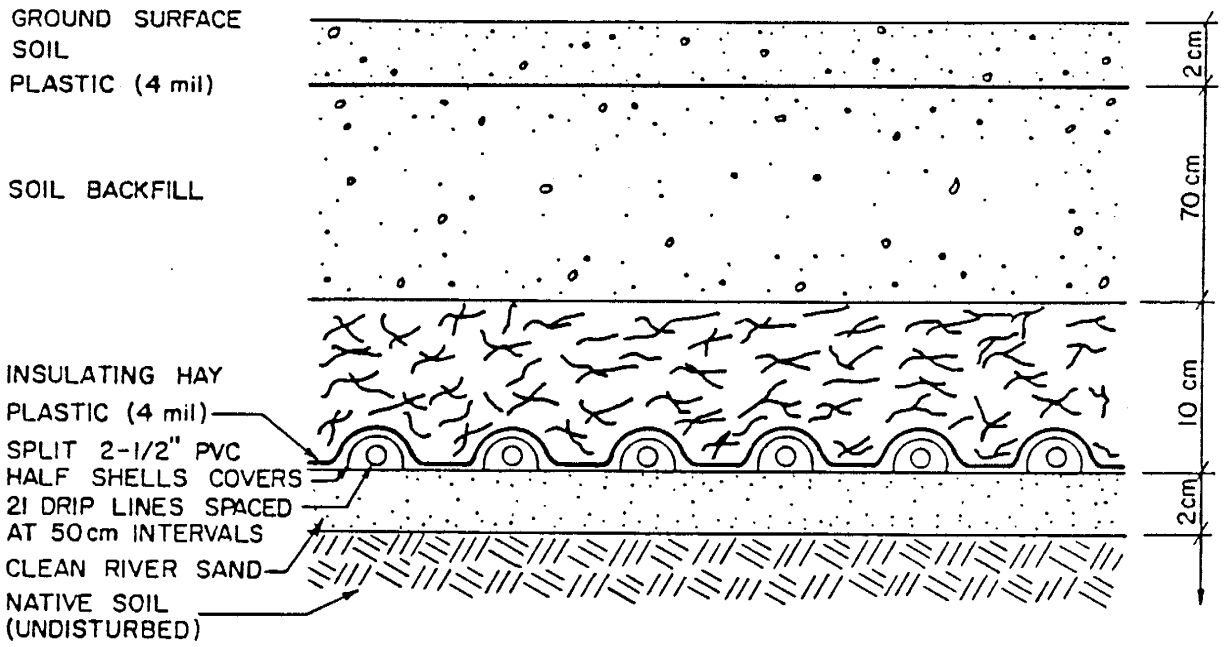

Figure 4.6. Cross-section through the irrigation plot.

the operating status of the system. The water flow monitoring system consists of a pressure transducer, data logger, a dial pressure gauge and 8 totalizing flow meters.

The pressure transducer (PDCR 10/D, Druck, Inc., Danbury, CN) measures the in-line water pressure to the driplines in conjunction with the data logger (CR7, Campbell Scientific, Logan, Utah). The CR7 records the length of time during which the in-line pressure exceeds 35 KPa (5 psi). This provides an estimate of the duration of water application. The CR7 is programmed to read the pressure transducer every second. The pressure traducer program checks the in-line pressure to determine if it is necessary to activate the timer (pressure greater than 35 KPa (5 psi)). After the timer is activated and the in-line pressure falls below 35 KPa (5 psi), the timer is stopped. On the half hour, the average in-line pressure and pump activation time is dumped to a tape in the data logger. The tape is brought to the laboratory, connected to a data down-loading device (C20 cassette interface, Campbell Scientific, Logan, UT), and the data is transferred to floppy diskettes (5.25 inch). The computer program C20DUMP.BAS will strip the data from the floppy diskette to create a pressure and pump activation time ASCII file. The pressure and pump information can be reviewed to monitor the consistency and determine when a system failure occurred.

A dial pressure gauge is located downstream of the pump throttle valve. The purpose of this gauge is to give the

operator an immediate check on the in-line pressure. The faucets located on each end of the water manifold headers are equipped with stem valve adapters, and the pressure at each stem valve can be measured with a standard automobile tire pressure gauge to survey the pressure in the irrigation system. During the system operation, the in-line pressure was maintained at 35 psi, corresponding to pressure at the emitters equal to 16 psi. Adjustment of the in-line pressure is described in section 4.2.2.

Eight totalizing flow meters measure the quantity of water flowing through the water application system. Originally only one totalizing meter was located in the field trailer to measure total volume of water pumped to the driplines. After the experiment had run for 22 days, three more flow meters were installed in the field site to measure the amount of water flow to the north and south half of the irrigation system (Figure 4.7). The water flow in the drip irrigation system was later divided into four sections with the addition of four more totalizing flow meters on experimental day 168 (Figure 4.8). The totalizing flow meters are read at regular intervals. Section 6.2 discusses the water flow results. See Appendix G for a list of flow meter data.

4.3. WATER PRE-TREATMENT SYSTEM

City water was used in this infiltration field experiment. A 5.1 cm (2 inch) PVC city water line that feeds the golf course

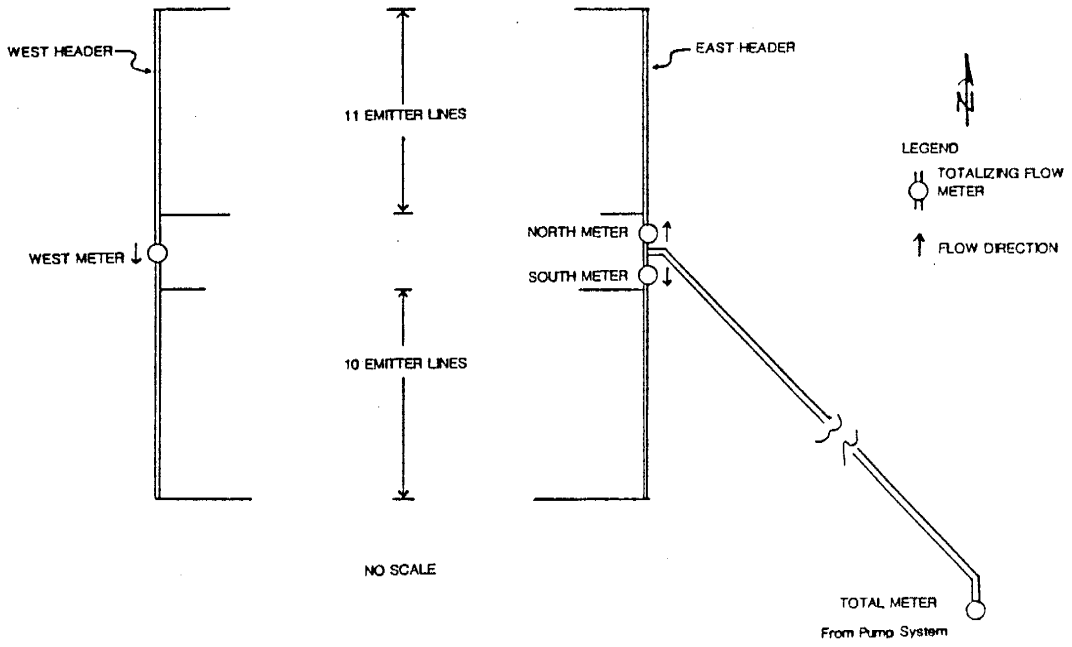

Figure 4.7. Flow meter layout for experimental days 22 to 168.

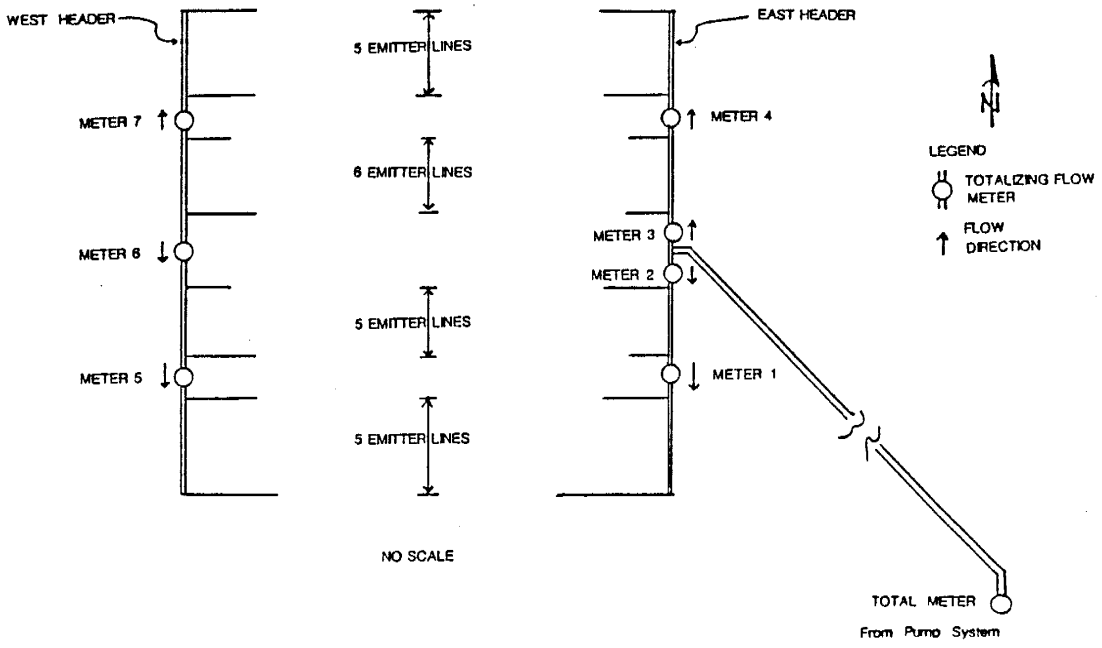

Figure 4.8. Flow meter layout from experimental day 168 through the present.

maintenance shop was tapped with a 2.5 cm (1 inch) PVC tee. A trench was dug to accommodate the water supply pipe and the underground cable to the field trailer.

The tap water has a pH of 7.8 and a hardness of 273 ppm $CaCO_3$ based on a major cation-anion laboratory analysis (Appendix H). According to Bucks and Nakayama (1985), the main reasons for emitter plugging are foreign particles, algae and bacteria, and $CaCO_3$ blockage. The foreign particles are screened in-line by a 200 mesh filter in the field trailer. Algae should not appear unless the water is exposed to light, and the city water is treated with chlorine to control bacteria (Kieft, NMIMT, personal communication, 1986). pH of the water should be maintained at 6.5 to prevent carbonate precipitation in the emitters (Bucks and Nakayama, 1985).

To lower the pH of the city water to 6.5, muriatic acid (31.41%) is added to the water in the water supply tank. A 40 gallon chemical feed tank supplies a mixture of 1 part acid to 13 parts tap water to the water supply tank. A chemical feed pump is activated simultaneously with the gear pump. As water is withdrawn from the water storage tank, the acid mixture is injected in the storage tank. The volume of acid injection is proportional to the volume of water used for each cycle. The acid injection rate was determined by laboratory experiments. The pH of the water storage tank is checked periodically with pH paper to insure a proper pH is maintained.

5. SOIL WATER MONITORING SYSTEM

Twenty-one (21) soil water monitoring stations are used to monitor the changes in soil moisture and pressure head at the field site. Each monitoring station contains a neutron access tube and duplicate nests of tensiometers. The monitoring stations are identified by station description number based on the X-Y coordinate grid system (Figure 3.2).

The monitoring stations are placed such that a higher density is located near the center of the field site. Most of the stations are located on the east-west and north-south transects across the site. Four stations are found at 45-degree angles from the transects (Figure 3.2). This array of soil-water monitoring stations allowed close observation of the wetting front movement and moisture content profiles throughout the infiltration experiment.

5.1. SOIL WATER MONITORING

The neutron moisture probe (Model 503DR, CPN Corp., Pacheco, CA) was used to determine the moisture content and the wetting front location in this field study. The neutron probe method has the advantage of being non-destructive, fast, less laborious than destructive sampling, and providing repeatable measurements with

time. However, disadvantages are health considerations, difficulty with near surface measurements, and a low degree of spatial resolution (Hillel, 1980). The low degree of spatial resolution creates difficulties when calibrating a layered medium. The probe's sphere of influence may intersect multiple layers of soil resulting in a probe response which would represent a type of an average moisture content of the layers.

Major soil parameters that affect probe response are dry bulk density, hydrogen molecules of soil-water, and soil elements which have a high affinity to adsorb thermal neutrons. Hydrogen molecules of adsorbed soil-water and soil elements with high neutron affinity are not present in the soils found near Socorro. Of the soil parameters, bulk density will have the greatest affect on the probe response. Other factors influencing the neutron probe response are the installation technique and material of the access tube. Hillel (1980) provides an overview of the theory of the neutron probe operation. Greacen (1981) examines the theory and methodology of neutron logging in more detail.

5.1.1. Neutron Access Tube Installation

Because of the dry caving soil conditions, layers of cobbles in the soil profile, and the length of the access tubes, a 20.3 cm (8 in) hollow stem rotary auger was used to install the access tubes at the field site. The access tube is a thin wall aluminum pipe, 9.1 meters (30 ft) long with a diameter of 5.1 cm (2 in). Both ends were sealed with rubber stoppers to prevent moisture

from entering the access tube. A small sack of silica desiccant was attached to the upper stopper to prevent moisture from condensing on the interior of the tube.

The aluminum access tube was inserted through the hollow stem after the hole was drilled to a depth of 9.1 meters. While the auger flight was slowly raised, the rotation was reversed. Approximately every 75 cm (2.5 ft), rotation was stopped and the flight was lowered to compact the soil in the annulus of the hole. This process was continued to the surface. The final lift was hand tamped using a rod. A layer of dry bentonite powder was placed just below the ground surface to prevent channeling of runoff water. The same method of installation was used with the neutron probe calibrations. Care must be taken when sealing the neutron access tubes. Experience has shown that the bentonite in contact with the aluminum tubing will corrode the tubing in approximately one year. The high alkalinity of the moist bentonite is believed to be the cause for corrosion (R.S. Bowman, personal communication, 1988).

5.1.2. Neutron Probe Calibration

Calibration of the neutron probe is conducted by comparison of the neutron probe readings to a range of field moisture contents determined by destructive sampling. The relationship between the neutron probe readings and the destructive soil sample moisture content values provide the calibration curve. The calibration curve often takes the form of the equation:

$$\theta = b(NP) + a \qquad (5.1)$$

where θ (cc/cc) is the volumetric water content, NP is the neutron probe reading, b is the calibration coefficient, and a is the intercept constant.

Three methods were utilized to obtain destructive samples to use in calibrating the neutron probes. The three sampling methods were: shelby tubes, hand augering, and split spoon sampling.

Destructive sampling using the shelby tube soil sample collection method was conducted at a test site directly west and adjacent to the water hazard on the 13^{th} hole of the New Mexico Tech golf course shown on figure 4.1. This site was chosen because of the similar silty sand soil conditions, lack of cobbles in the soil profile, and a wide range of moisture contents due to the water hazard. A week before acquiring the destructive soil samples, three neutron access tubes were installed to a maximum depth of 150 cm at the site. Destructive samples were collected at a distance of not more than 61 cm (24 in) from the access tubes. A series of shelby tubes were pushed and pounded using the 144 pound hammer of the drill rig (B-52, Mobil Drill, Indianapolis, IN). After the shelby tube reached the desired depth, it was extracted and sealed to prevent evaporation. The shelby tubes were promptly brought to the laboratory, where the soil sample was extruded using a hydraulic ram. Each shelby tube soil sample length was recorded to account for compaction of the soil sample. The sample was then sliced in 7.6 cm (3 in) segments, weighed and oven dried at 105°C for a

period of two days. The segments were weighed again and the gravimetric water content, w, was determined.

To estimate the bulk density, the assumption of a linear compaction factor, lcf, was made. The lcf was determined by dividing the length pushed in the field by the length of the soil sample after extraction. The adjusted segment length was determined by multiplying the segment length by the lcf. The lcf had a mean of 1.13 with a standard deviation of 0.10. This method was used to calculate the volume and vertical location of each soil segment. Using the calculated volume, the volumetric water content was determined. A linear least squares regression was determined for the gravimetric water content versus volumetric water content. The slope of the regressed line was 1.32 g/cc, an estimate of the average bulk density for this soil. The revised volumetric water content for each segment was determined from the gravimetric water content multiplied by the average bulk density, assuming the density of water is 1 gm/cc.

It is not known precisely how the measurements of moisture content from the neutron probe are affected by moisture content discontinuities in layered media. Due to the thin layering structure of the soil profile, the volumetric water content of the shelby tube 7.6 cm segments varied greatly; thus, a computer program was necessary to compute thickness-weighted mean water content at each neutron probe measurement depth. A computer program, NP.FOR (Appendix I), was used to compute volumetric water contents at locations where neutron probe measurements were

taken. In the program, a spherical weighted average of each of the layers that intersected a calculated sphere of influence of the probe was used to determine an equivalent volumetric water content. Hillel (1980) states that the sphere of influence radius ranges from approximately 10 cm in a wet soil to 25 cm or more in a dry soil. The program NP.FOR assumes that the functional relationship between the sphere of influence and soil moisture is linear. Thus, a moisture content of 32% corresponds to a 10 cm sphere of influence radius whereas 0% moisture content (oven-dried conditions) is assumed to have a sphere of influence radius of 25 cm. Appendix I describes NP.FOR in more detail. Sixty-four (64) second counts were used to take neutron probe measurements. Data pairs of volumetric water content and neutron probe readings are shown in Appendix J.

The second sample collection method involved collecting destructive samples outside the edge of the drip irrigation plot. At stations 8-16 and 15-5, continuous grab samples were collected from 5.1 cm (2 inch) hand augered holes. The samples were weighed and oven dried at 105°C for 24 hours to determine gravimetric water content. Based on 22 core samples (100 cc) previously collected from the field site, the average bulk density of this soil was calculated to be 1.6 gm/cc. Volumetric water content was determined from gravimetric water content. Again, NP.FOR was used to compute volumetric water content at the depths of the neutron probe measurements. Sixteen (16) second counts were used during these probe measurements. The data pairs

of volumetric water content and neutron probe readings are shown in Appendix J.

The third sample collection method used split-spoon sampling during installation of the monitoring equipment. Gravimetric and volumetric water contents were determined using the same technique as for the hand auger method. For this sample collection method, NP.FOR was not used to adjust volumetric water contents to neutron probe reading depths, since the destructive sampling frequency was larger than the maximum determined sphere of influence. Instead, the nearest neutron probe reading to each sample was used. Sixteen (16) second counts were used to determine the moisture content. Appendix J contains the paired results.

For ease of reference, the two neutron probes (both identical models) used in this project, serial numbers H34045324 and H36036601, will be referred to as the 'old' and 'new' probe, respectively. The 'old' probe had an electrical failure early in the experiment, and the 'new' probe was used as a temporary replacement. Additionally, calibration of both probes added flexibility to the monitoring program. Either probe could be used at the site depending on availability.

A linear least squares regression was performed to determine the calibration for both neutron probes from all sampling methods. The calibration equation for the old probe is:

$$\theta_C = 0.8982*\theta_{np} - 1.87 \qquad (5.2)$$

where θ_c is the calibrated volumetric moisture content, and θ_{np} is the neutron probe reading. The r^2 for this fit is 0.82. The regressed line is shown in Figure 5.1 with the 95% confidence interval. The new probe calibration equation is:

$$\theta_c = 0.9152*\theta_{np} + 0.82 \qquad (5.3)$$

with an r^2 of 0.85. The neutron probe readings and true water contents with a regressed fit are shown in Figure 5.2.

The regression fit for the 2.3 cm (8 inch) diameter borehole installation method used in this study compares well with four previous regressions where the neutron access tube was installed in 5.1 cm (2 inch) hand augered boreholes (Figure 5.3). Knowlton (1984) flooded an area similar to an instantaneous profile site. He obtained fourteen fine to medium sand samples in a range of water contents from 6 to 25% at the Sevilleta National Wildlife refuge. Herst (1986) collected sixteen silty soil samples from M-mountain in the moisture range of 13.5 to 27%. McCord (1986) used the above two sets of data and added 11 more points, from the Sevilleta, in the dry range (3 to 12% water content) to determine an exponential fit. Harris (1987) calibrated the neutron probe in a mill tailings pile containing water contents over the range of 12 to 65% (% vol), a substantially higher moisture content range than the other calibrations. Mill tailings contain large amounts of iron and calcium (Harris, 1987). According to Hammermeister and others (1985), the slow neutrons are absorbed by boron, iron, calcium, titanium, and cadmium, changing the probe calibration for soils which contain

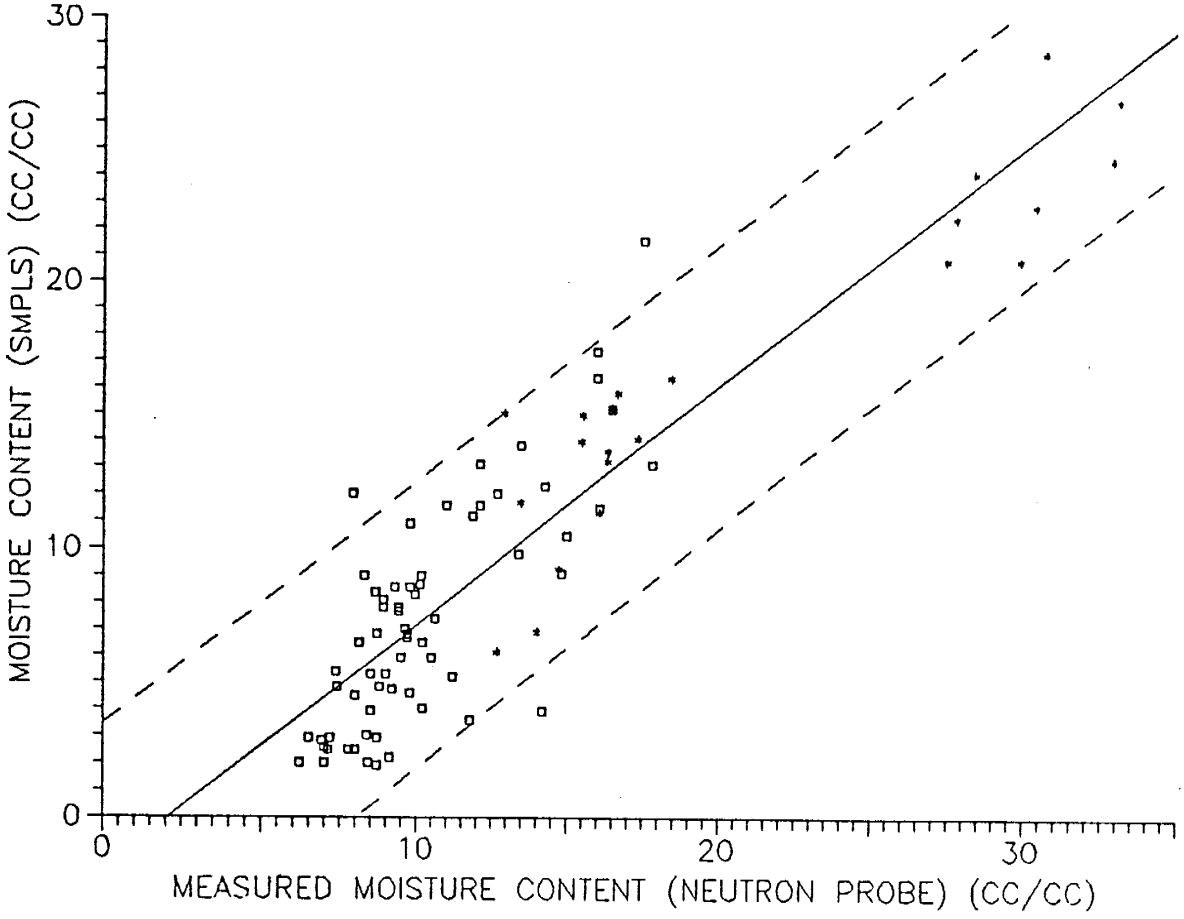

Figure 5.1. Calibration curve for the 'old' neutron probe. Solid line is the regressed fit, dashed lines show upper and lower 95% confidence intervals. Squares represent split spoon samples from the field site, and stars are shelby tube samples from the golf course.

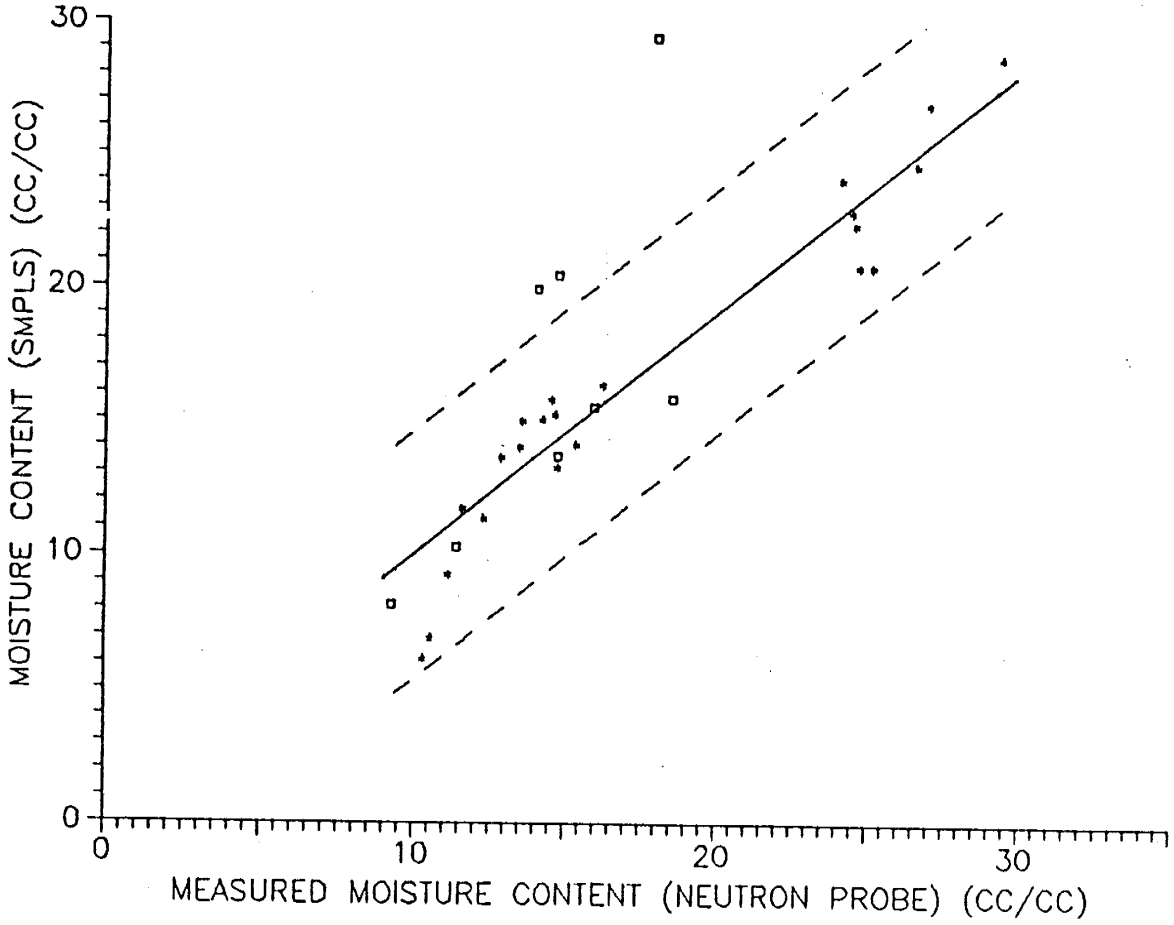

Figure 5.2. Calibration curve for the 'new' neutron probe. Solid line is the regressed fit, dashed lines show upper and lower 95% confidence intervals. Squares represent hand augered samples from the field site, and stars are shelby tube samples from the golf course.

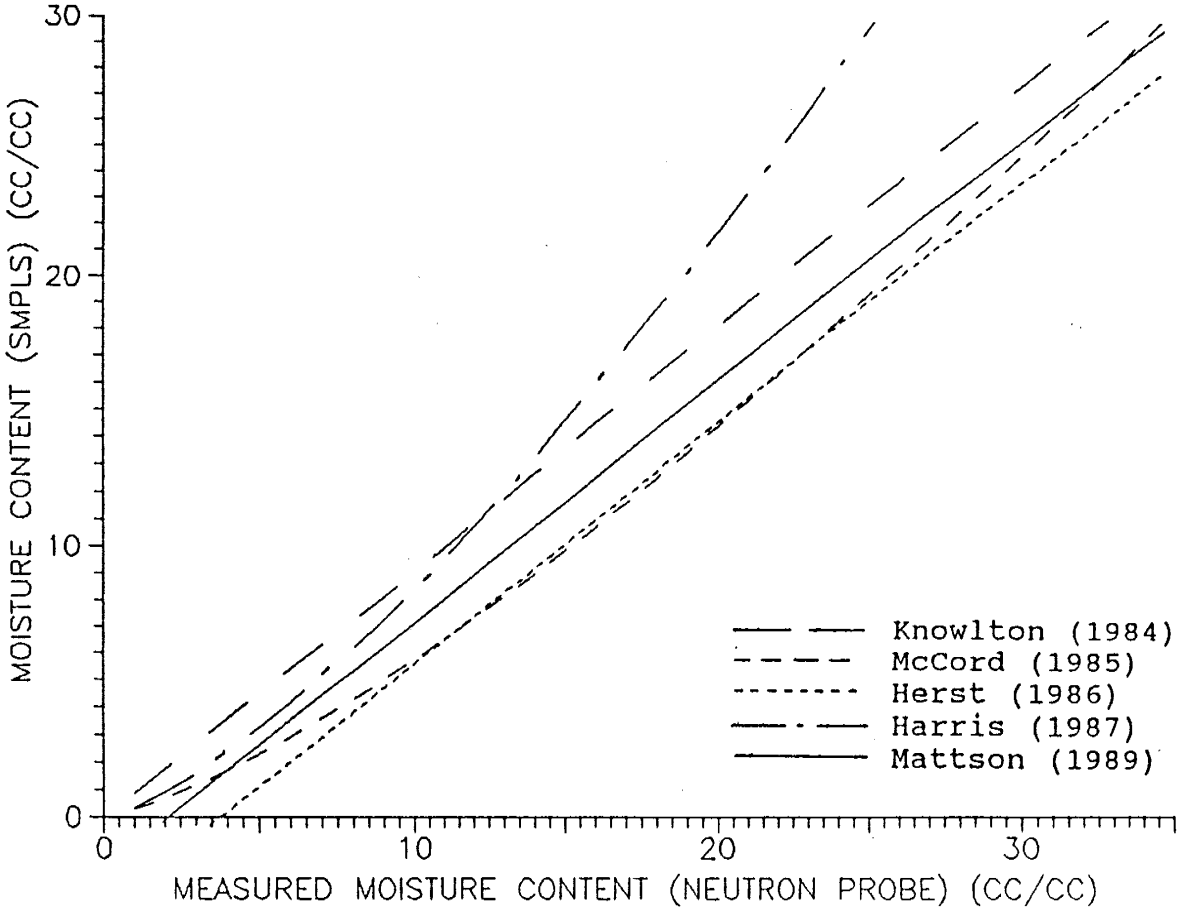

Figure 5.3. Comparison of all calibration curves for the 'old' neutron probe.

these elements. Therefore, Harris's (1987) calibration will not be used in the neutron probe calibration comparison. Calibration equations for the 'old' probe are summarized in Table 5.1.

The method of installation does not seem to affect the calibration. The previous calibration investigations use a 5.1 cm (2 inch) hand auger to install their neutron access tubes. The slope of the linear regression for the 20.3 cm (8 inch) installation method determined in this study differs by less than one percent from the slopes of the previous linear calibrations performed (Table 5.1). Furthermore, the intercept lies in the mid-range of the linear regression intercepts. The range of intercepts may be due to the difference in dry bulk densities and soil composition of the sites. Greacen (1981) concluded that variations of dry bulk density will shift the intercept of the regressed line and will not substantially change the slope. The 20.3 cm (8 inch) calibration differs by less than two percent water content from three of the four regressed fits as shown in Figure 5.3. The result of the 20.3 cm calibration intercept bracketed by the other linear calibration intercepts with nearly the same slope as the previous calibrations provides confidence that the 20.3 cm (8 inch) installation method does not seem to change the calibration equation of the 'old' probe.

5.1.3. Bias and Precision of the Neutron Probe

Moisture contents determined by the neutron probe may contain measurement and sampling bias. Bias is the difference between the statistical true value and the scientific true value.

TABLE 5.1. Neutron Probe Calibrations for the 'Old' Probe.

Author	Equation	r^2	# of pts
Knowlton (1984)	$0.9068*\theta_{np} + 0.035$	0.97	14
McCord (1985)	$\exp\{-1.29+1.34*\ln(\theta_{np})\}$	NA	41
Herst (1986)	$0.8999*\theta_{np} - 3.24$	0.99	16
Harris (1987)	$\exp\{-1.34+1.45*\ln(\theta_{np})\}$	0.86	NA
Mattson (1989)	$0.8982*\theta_{np} - 1.87$	0.82	89

NA = not available

Measurement bias can arise in the calibration equation, variation in access tube diameter, access tube wall thickness, distortion caused by drilling, and drift or changes in the probe's detector electronics. Sampling bias is associated with mode of access tube installation and the use of samples of the soil system not representative of the whole soil profile (Greacen, 1981). Bias of the neutron probe determined moisture contents can only be addressed by comparison with independent measurements of moisture content.

Bias in the slope and intercept of the neutron probe calibration are important in the estimation of moisture content. A bias in the slope will affect both the absolute value of the moisture content as well as the change in moisture content measure over time. A bias in the neutron probe intercept only will affect the absolute value of the moisture content. Bias in the calibration may occur because the calibration was developed in a different soil horizon or the method used to develop the calibration introduced bias.

The development of the calibration equation using soil samples near the NM Tech golf course (13^{th} hole) may have introduced bias. The stars in Figure 5.1 represent shelby tube destructive samples from the golf course. Had a calibration curve been developed without the golf course shelby tube samples, the calibration curve slope may have been greater and the intercept lower than the values calculated from equation 5.2. At this time it is not known if bias has been introduced into the

neutron probe calibration equation. Destructive sampling beneath the drip irrigation system in the areas of greatest moisture would help determine if the calibration equation is biased.

Installation of the neutron access tubes may have incorporated sampling bias into the moisture content data. As discussed in Section 5.1.2, the aluminum access tubes were installed through a 20.3 cm hollow stem rotary auger. Compaction of soil in the hole annulus about the neutron probe was accomplished by lowering the auger flights at approximately 75 cm intervals. It is not known if a uniform compaction was accomplished using this compaction method. Assuming that much of the neutron access tube backfill bulk density was compacted at a lower bulk density than the native material in situ bulk density, the neutron probe would likely underestimate the true soil moisture content.

Precision of the neutron probe measurement is affected by heterogeneity of the soil moisture distribution, instrument random error, neutron probe detector electronics, and calibration equation. Precision is defined here to be a random error of measurement about a mean value, whether or not the mean value represents the scientific true value.

The precision of the heterogeneity of the soil moisture distribution can be increased by increasing the number of monitoring stations. Random error of the neutron probe detector electronics are usually considered to be small and can be reduced by taking longer count times. The calibration equation precision

can be increased by decreasing the variance of the regressed calibration equation parameters.

The expected variation for two standard deviations (95.5%) of a single measurement can be expressed as the percent error of the count precision as follows:

$$\%E = 200/\sqrt{CN} \qquad (5.4)$$

where %E is the percent error of the count precision, and CN is the number of counts detected.

Assuming the neutron probe measured value of θ was 20% and the neutron probe standard count equals 10,000 (an approximate value for the 'old' neutron probe), an estimate of the 95% confidence interval was made. Using equation 5.2 and the factory calibration of the 'old' neutron probe a moisture content of 20% corresponds to 13,630 detected counts. According to equation 5.4, the percent error of the count precision is 1.71%, equivalent to a variation in the volumetric moisture content of ± 0.41% using the 'old' probe calibration equation (equation 5.2).

5.2. PRESSURE HEAD MONITORING

Tensiometers were used to measure negative pressure head at the field site. Hillel (1980) describes the principals of the tensiometer operation. The tensiometers were constructed of 1.9 cm (0.75 inch) PVC pipe, one bar standard ceramic cups, and septum rubber stoppers. The vacuum beneath the rubber stopper was measured using a Tensimeter (Soil Moisture Measurement

Systems, Las Cruces, NM), a pressure transducer connected to a hypodermic needle. The depth to each ceramic cup was determined using surveying techniques and field measurements.

5.2.1. Tensiometer Installation

The nests of tensiometers were installed in a similar method as the neutron access tubes (Section 5.1.1.). A borehole was drilled to the desired depth using the 20.3 (8 inch) diameter hollow stem augers. A tensiometer was lowered through the hollow stem and the augers were lifted approximately 30 cm while slowly reversing the rotation to place backfill at the base of the augers. The auger flight was lowered to compact the soil in the annulus. The auger flight was lifted approximately 5 cm, then powdered bentonite was poured through the hollow stem in an attempt to form a bentonite clay layer above the porous cup. Success in forming a clay layer across the entire borehole is unknown, but the method was believed to have created a partial clay layer at the least. The auger flight was further lifted with reverse rotation another 25 cm. The soil was compacted by lowering the auger, then another tensiometer was emplaced by the method previously described. The process was repeated until six to eight tensiometers were installed in the borehole. A layer of bentonite was emplaced just below the land surface (or drip irrigation system) and covered with soil to prevent channeling. A duplicate nest of tensiometers was installed in the same manner within a meter of the first nest to provide duplicate pressure head measurements.

Twenty (20) cm (7.9 inch) clear PVC was cemented using PVC cement on the 1.9 cm (0.75 inch) diameter tensiometer PVC pipes. The depth to the cup was marked on the clear PVC for subsequent determination of the water column height. The cup elevation was later verified in the field by lowering a wire down the PVC pipe and measuring the distance measured on the wire compared to the scale marked on the tensiometer top.

5.2.2. Tensimeter Calibration

Three portable Tensimeters were calibrated to determine pressure head from tensiometers at the field site. The Tensimeters use pressure transducers to linearly convert pressures to voltages. The voltage is displayed digitally in terms of millibars of pressure. To ensure accurate determination of pressure head, it is necessary to calibrate each of the transducers. Appendix K describes the Tensimeter calibration procedure in detail.

Three Tensimeters were calibrated in the laboratory: the 'E&A' Tensimeter, Jim's Tensimeter, and Warren's Tensimeter, serial numbers 773863, 774309, and 8510007 respectively. The resulting calibration equations are respectively:

$$P = 2.35 + 1.06*TR \quad (5.4)$$

$$P = 0.05 + 1.03*TR \quad (5.5)$$

$$P = -1.0 + 1.02*TR \quad (5.6)$$

where P, the pressure head (cm); and TR, the Tensimeter reading (mbar), are considered positive values.

5.3. SOIL TEMPERATURE MONITORING

Three nests of five (5) thermistor probes (107B, Campbell Scientific, Logan, UT) were installed at the field site. Table 3.2 lists the X-Y coordinates of the three nests. The thermistor probes were installed to measure temperature profiles at the site. Analysis of the temperature profile is outside the scope of this work and will not be discussed.

Thermistors were prepared for field installation by running the thermistor cable through a 1.3 cm (0.5 in.) PVC pipe. The thermistor end protruded from an end of the PVC and was sealed with silicon cement. The PVC pipe allows for easy instrument removal and assists in placing the thermistor through the hollow stem auger.

Boreholes were drilled using a 20.3 cm hollow stem auger. After the borehole reached the proper depth, a thermistor and PVC pie was lowered through the hollow stem to the base of the borehole. The auger flight was slowly raised approximately 30 cm while reversing the auger rotation to place backfill material about the thermistor. The auger flight was lowered to compact the soil in the annulus. A bentonite seal was placed similar to those used in tensiometer installation. The process was repeated for the other thermistors in the nest with the exception of the shallow thermistor which was placed by hand. The thermistor nest located near station 15-15 was installed before the drip

irrigation system was in place. Table 5.2 shows the depth of each of the thermistors.

Data of temperature is reached by the CR-7 data logger on an hourly basis. The data is transferred to floppy diskettes using the procedures outlined in section 4.2.4.

Table 5.2. THERMISTOR DEPTHS

STATION 15-2		STATION 15-8		STATION 15-15	
DEPTH BELOW LAND-SURFACE (CM)	DEPTH BELOW DATUM (M)	DEPTH BELOW LAND-SURFACE (CM)	DEPTH BELOW DATUM (M)	DEPTH BELOW DRIP IRRIG. (CM)	DEPTH BELOW DATUM (M)
20	0.47	18	0.44	9	0.95
106	1.33	110	1.36	80	1.66
260	2.87	256	2.82	220	3.06
322	3.49	332	3.58	300	3.86
422	4.49	458	4.84	461	5.47

6. FIELD EXPERIMENT RESULTS

Experiment results affecting model input, and soil-water monitoring used in the comparison of model predictions of moisture content distribution, are discussed in the following sections. Model predictions are presented in two-dimensional symmetric vertical transects. Therefore emphasis is placed on the field results observed along the east-west and north-south cross-sections (Figure 3.2).

6.1 WATER APPLICATION

The water applied to the undisturbed soil surface was monitored using a totalizing flow meter. The flow meter, located in the field office, was read manually during monitoring of the experiment. Flow meter readings were converted to emitter discharge (i.e. source strength) by dividing the average flow rates by 441 emitters. Figure 6.1 shows the emitter discharge during the first 160 days of infiltration. The large variation of the metered discharge at the beginning of the experiment was due to manual adjustment of the water tank floats (Section 4.2.). Sharp increases or decreases in the discharge rates are noted at these times. A decreasing trend after adjustments of the floats may indicate water imbibition into the float material.

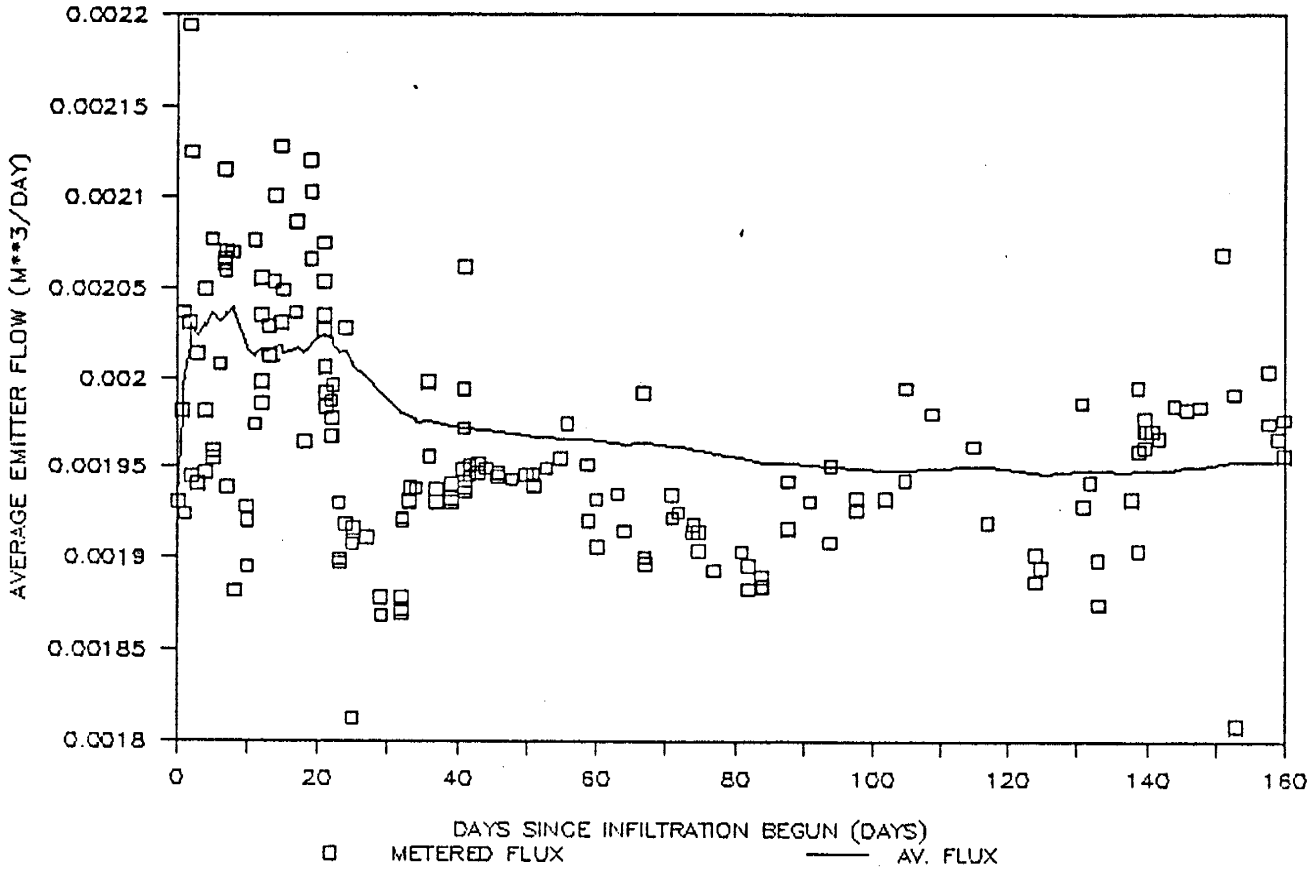

Figure 6.1. Metered and time-weighted average of emitter discharge determined by a totalizing flow meter for the first 160 days of infiltration.

The average emitter discharge varies from a maximum of approximately 2.04×10^{-3} to 1.95×10^{-3} m^3/d during the first 160 days of infiltration (Figure 6.1). The average emitter discharge was calculated from the cummulative volume of water pumped as recorded from the totalizing meter (figure 4.1) divided by the time since infiltration began and the 441 emitters. The average emitter discharge range varies by less than 5% during this period. Figure 6.1 can be used to input the strength of the emitter source for various time lengths of the time dependent case. For example, the emitter discharge would be about 2.03×10^{-3} m^3/d for days 0 to 20, while a emitter discharge of 1.96×10^{-3} m^3/d would be more appropriate for 0 to 160 days. Appendix G contains the meter discharge data used to calculate the discharge depicted in Figure 6.1.

An unfortunate leak occurred in one of the emitter line connections to the water supply manifolds located in the northeast corner of the irrigation plot from experimental day 26.5 to 39. The time of the beginning of the leak was obtained from flow meter data. Figure 6.1 does not distinguish the amount of water that was lost through the broken connection during the period of leakage. It is estimated that 37% of the total metered flow (0.3 m^3/d) was discharged through the broken connection (Appendix L). Water from the broken connection flowed into the north end of the east header and likely spread in the clean sand layer that underlies the irrigation system infiltrating into the soil profile. It is unknown to what extent the broken connection

affected the uniformity of flow through the driplines.

For early and late time model predictions, it is assumed the effect of the leak is negligible. Model predictions before experimental day 26.5 will not be affected by the leak. At the time when repairs were made to the broken connection, the estimated leakage volume accounted for approximately 12% of the total injected volume of water for the 39 day period. By experimental day 81, the estimated volume of water which leaked was only 6% of the total amount of infiltrated water. Late time predictions will only be affected slightly because the total volume injected into the irrigation system increases relative to the volume that leaked. Appendix L contains a detailed description of the broken connection discharge calculations and later preventive measures.

The installation of three flow meters in the drip irrigation system on experimental day 22 allowed calculations of the uniformity of water flow to the emitters. Emitters in the southern area of the irrigation system (driplines 1-10) had a slightly greater discharge than the northern area (driplines 11-21) (Figure 4.3). Calculations show that the average emitter discharge ratio of the northern emitters to the southern emitters is approximately 0.90 from experimental days 22 to 153, disregarding the time period of the connection leak. Appendix-- tabulates the average north-south emitter discharge to experimental day 153.

There are several possible explanations for the apparent

non-uniform emitter discharge. First, the three flow meters installed in the irrigation system on experimental day 22 were not calibrated in the laboratory prior to installation. Time constraints prevented calibration on experimental day 22, however, the meters were installed so that they could be removed at a later date. Calibration of the three flow meters has not taken place to date to the author's knowledge.

Second, the non-uniform discharge may be due to the non-symmetric layout of the water flow system possibly creating lower in-line pressures at the northern end of the irrigation system. Water enters the drip irrigation system between driplines 10 and 11 on the east header (Figure 4.3). Because of the greater number of driplines in the northern half of the plot, more water must flow north in the east header. Greater flow rates imply greater head losses, hence lower pressure and lower discharge at the emitters. An iterative procedure in a computer program would be necessary to calculate whether the non-symmetric location of the water inlet to the irrigation system was responsible for the non-uniform discharge. Due to the relatively low flow rates, it is the author's opinion that the non-symmetric water distribution would not account for the lower average emitter discharge to the north. Finally, the non-uniform emitter discharge may be due to greater head losses in the flow meter and gate valve located to the north of the water inlet than to the south, Figure 4.7. Significantly greater head losses in identical equipment would not be normally expected. However, the flow meters installed on

experimental day 22 were used in a previous research project. Used equipment may tend to have variable resistance to flow.

6.2. MASS BALANCE

By mass balance principles, the known amount of water injected through the emitters should equal the change in the amount of water in the soil profile measured by the neutron probe. Calculations show that only approximately 70% of the water applied to the soil can be accounted for by neutron probe measurements. This section describes the methodology used in the mass balance calculations and compares the calculated change of the volume of water in the soil profile to the amount measured by the flow meters at selected times.

The water balance calculations were conducted by comparing the change in moisture content from initial conditions to that condition at selected times after infiltration began. The initial moisture content profile was assumed to be represented by data collected on 1/29/88, just prior to the injection of water. At selected times, the moisture content profile was compared to the initial moisture content at 0.15 meter increments at each of the 21 monitoring stations. The change in moisture content for each depth increment is multiplied by the 0.15 meter depth interval, calculating an equivalent depth of water for that depth interval. The equivalent depth of water is calculated with depth

until the change in moisture content approaches zero. The total equivalent depth of water is determined by summing the equivalent depths of water at each station. The total equivalent depth of water for the selected time is plotted on a plan view map and contoured by hand (Appendix M). The contoured intervals are planimetered to compute the area between contour lines. The area is multiplied by the average of the two contour lines to calculate a volume. A summation of the volumes for each contour interval produces the change of the volume of water within the soil profile.

The cumulative volume of water measured by the totalizing flow meters and calculated by neutron probe readings as described above are compared in Table 6.1 for the first 125 days of infiltration. The calculated amount of injected water is always less than the measured amount. The mass of the injected water accounted for by the mass balance calculations after seven days was approximately 40%, and increases to about 70% for the remainder of the 125 days (Table 6.1.). The discrepancy between the measured and calculated water volumes may be due to several factors.

First, boundary effects near the driplines may cause the neutron probe calibration equation to be inaccurate near the driplines. The neutron probe measurements were within 15 cm of the drip irrigation system. The area near the driplines contains PVC pipe, sheets of plastic, hay, and bentonite overlain by fill material. The effect of many of these materials on the neutron

Table 6.1. Calculated and measured amounts of injected water for selected experimental dates.

Experimental Day	Vol of Water Calc. (gal)	Vol of Water Measured (gal)	% Water Accounted
7	643	1,596	40
25	3,480	5,700	61
39	6,131	8,892	69
60	8,974	13,680	66
81	15,797	18,468	85
125	20,287	28,500	71

probe is unknown. However, the gross underestimation of the water volume at early time implies the boundary effect can be large.

Secondly, drafting bias of the hand-drawn contour lines may largely underestimate the volume of water due to the unknown extent of lateral spreading. The lateral extent of the spreading is unknown after the wetting front passes a monitoring station until it reaches the next outer station. Contour lines inside the pit area are estimated linearly.

Preferential flow creating fingering effects at the wetting front are not believed to have been responsible for the low calculated mass of infiltrated water. Fingering tends to occur in a homogeneous profile when the initial conditions are very dry. The upper piedmont slope facies is highly variable in hydraulic properties, composed of stratified layers which contain small scale features (Parsons, 1988a). Additionally, due to the water which infiltrated into the excavated area prior to the irrigation system installation (Parsons, 1988a, Section 6.1), the volumetric moisture content near the surface of the excavated plot increased up to 8.5%. Hence, large-scale fingering effects would be less likely to occur at the field site. Small scale fingering within individual layers may have occurred, but on the average, the wetting front was assumed to be fairly uniform.

A biased neutron probe calibration curve could cause an inaccurate measurement of the change in moisture content. As discussed in Section 5.1.3, a bias in the slope will cause errors

in the change in calibrated moisture content. For example, if the slope of the neutron probe calibration is higher than the regressed slope reported in equation 5.2, the result would be a greater calibrated moisture content change implying a higher calculated mass balance of water than reported in Table 6.1.

Finally, a possible error would result from monitoring equipment installation techniques affecting the moisture movement. The neutron tubes were installed in 20.3 cm (8") boreholes (Section 5.2.1.). The backfill, if it were more porous than the formation, may not wet to the same degree as the formation. The pressure head would have to increase to higher levels (less negative values) before moisture could pass into the homogenized borehole. Such a scenario would cause the neutron probe to read a lower moisture content than is actually present outside the borehole.

6.3. MEASURED TWO-DIMENSIONAL MOISTURE CONTENT

Volumetric moisture content distributions measured by the neutron probe were developed for the east-west and north-south transects. The corresponding geologic cross-sections are shown at a one-to-one horizontal to vertical scale in Figure 6.2.

Prior to the beginning of infiltration, neutron logging was performed for several months on a weekly basis to establish the background moisture content at the field site. Figure 6.3 presents the initial moisture content distributions present on

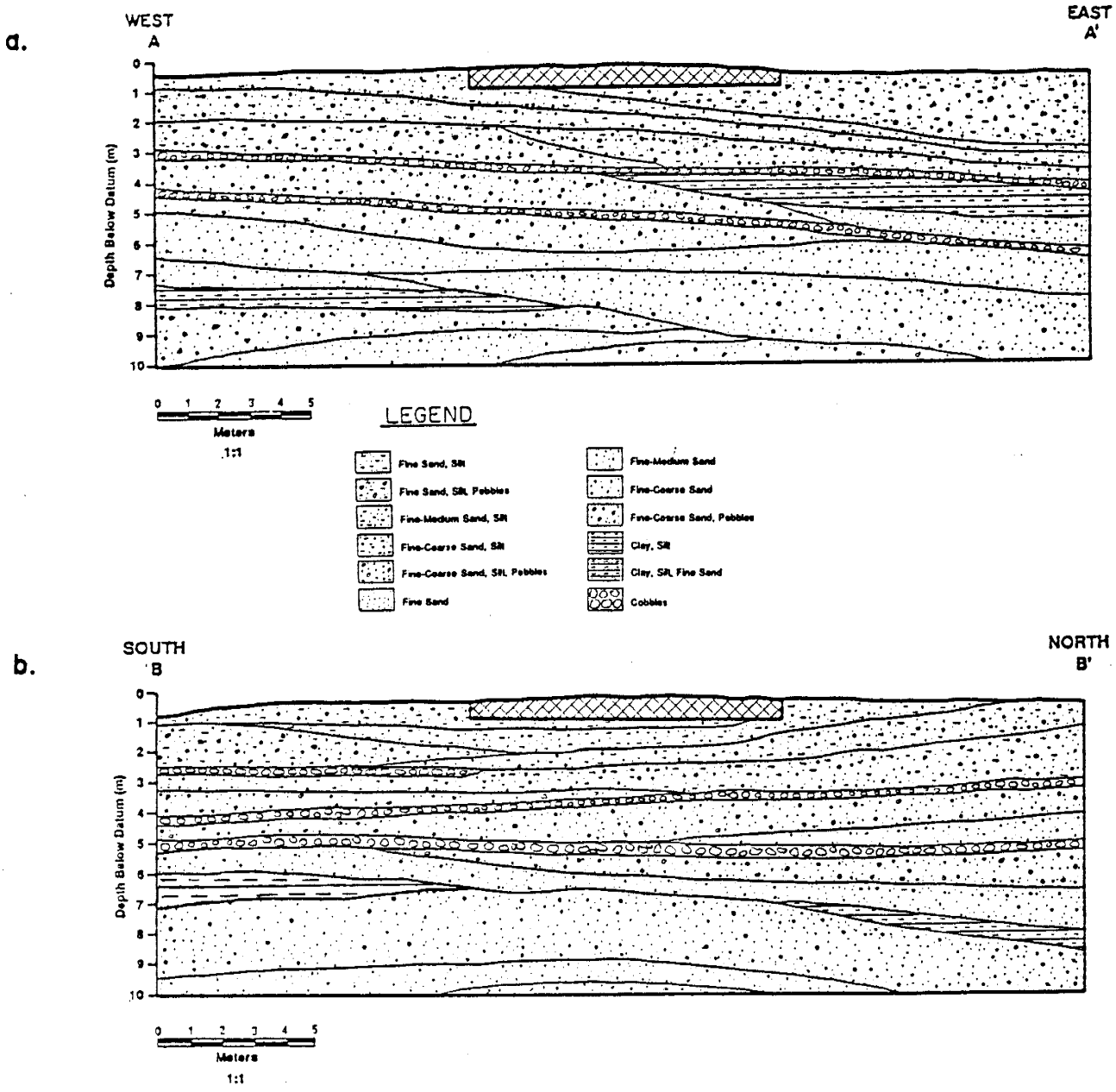

Figure 6.2. Geologic cross-sections for the a) east-west and b) north-south transects.

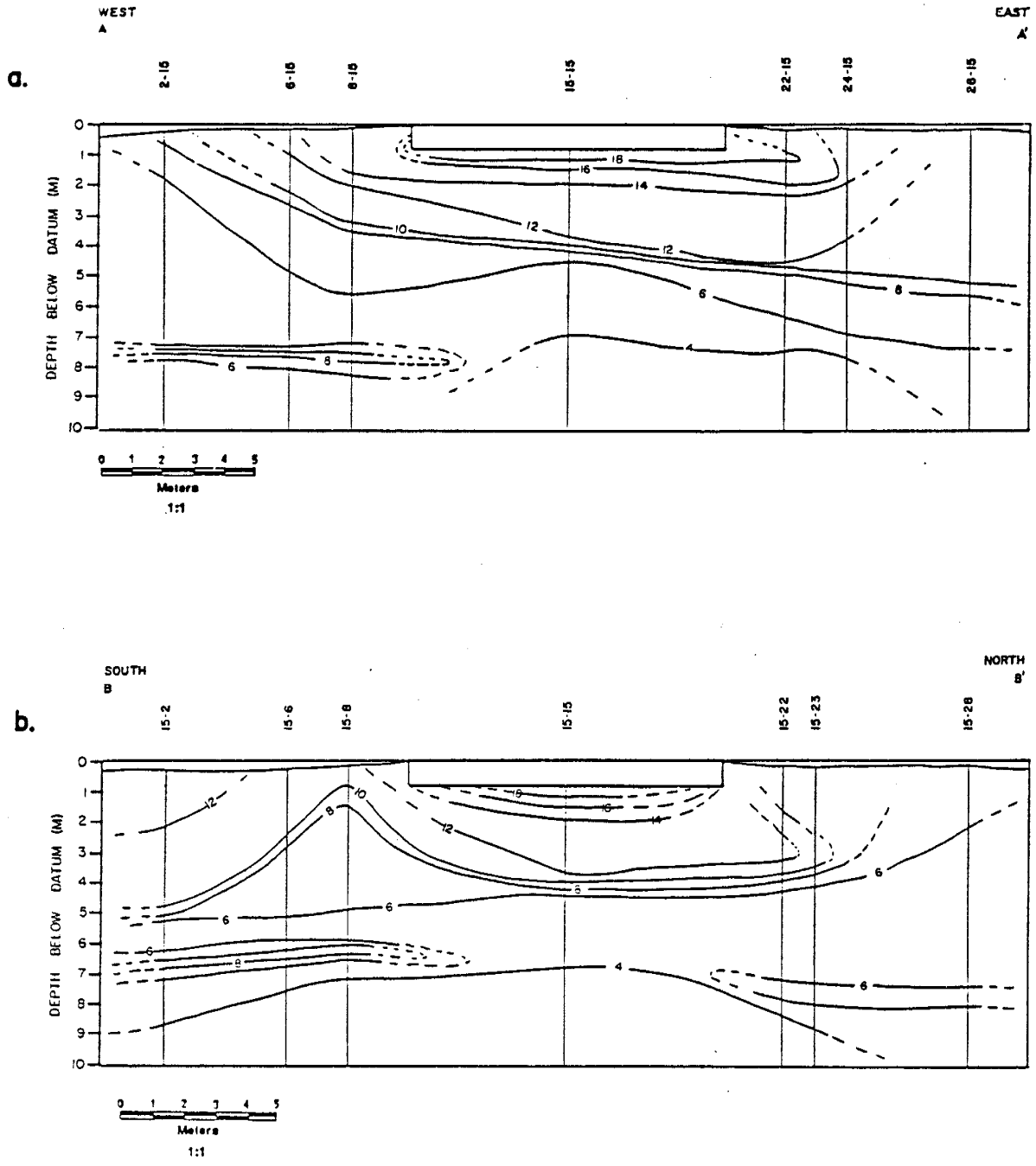

Figure 6.3. Initial moisture content distributions determined by neutron logging before infiltration occurred along the a) east-west and b)north-south transects.

the day prior to the experiment start. The moisture ccntent in the piedmont slope facies beneath the irrigation plot was approximately 14%. However, the moisture contents decrease with horizontal distance from the emitters from a maximum of 18% to a minimum value of about 6% in the north and west (Figure 6.3). The increased moisture beneath the irrigation plot is believed to be due to infiltration of water which ponded mostly in the NE part of the plot after a large precipitation event which occurred prior to installation of the driplines and the plastic layers. Parsons (1988a) discusses the infiltration of precipitation in more detail.

After seven days of infiltration, the maximum moisture content increased from 18 to 20% directly beneath the emitters (Figure 6.4). Vertical wetting occurred to a depth of approximately 2 meters below datum. No moisture content increases were noted at the monitoring stations 2 meters beyond the edge of the emitters.

Figure 6.5 depicts the moisture content profile after 25 days of infiltration. The increased moisture content was observed to a depth of 5.5 meters below datum at the center of the plot (station 15-15) where the first major cobble layer is located (Figure 6.2). Lateral movement of the moisture was noted 2 meters to the east of the irrigation plot at station 22-15 and to the north at station 15-22. A steep moisture gradient is observed at approximately 4 meters below datum in the center of the field site, just above the interface between the piedmont

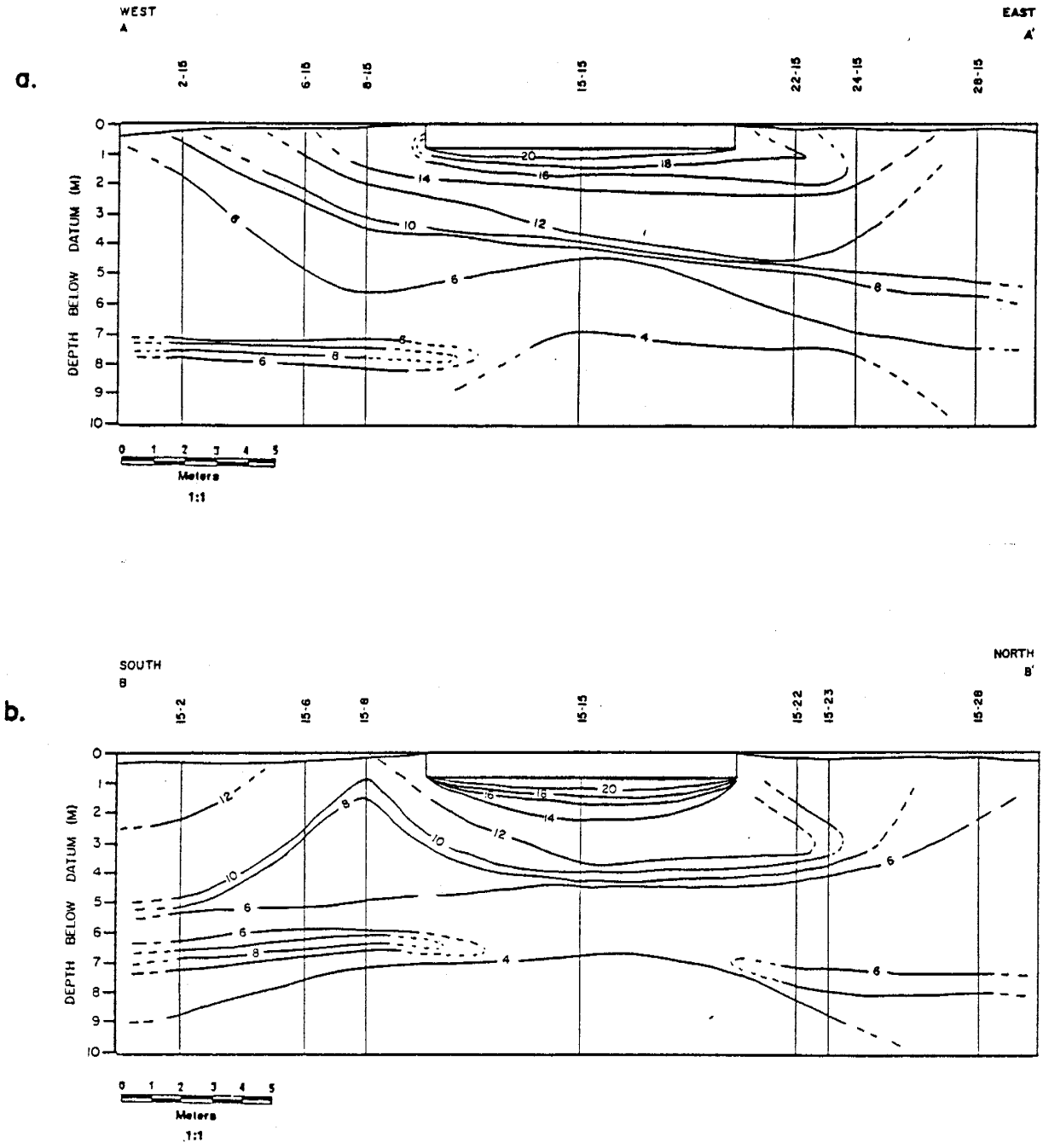

Figure 6.4. Moisture content distributions determined by neutron logging after 7 days of infiltration along the a) east-west and b)north-south transects.

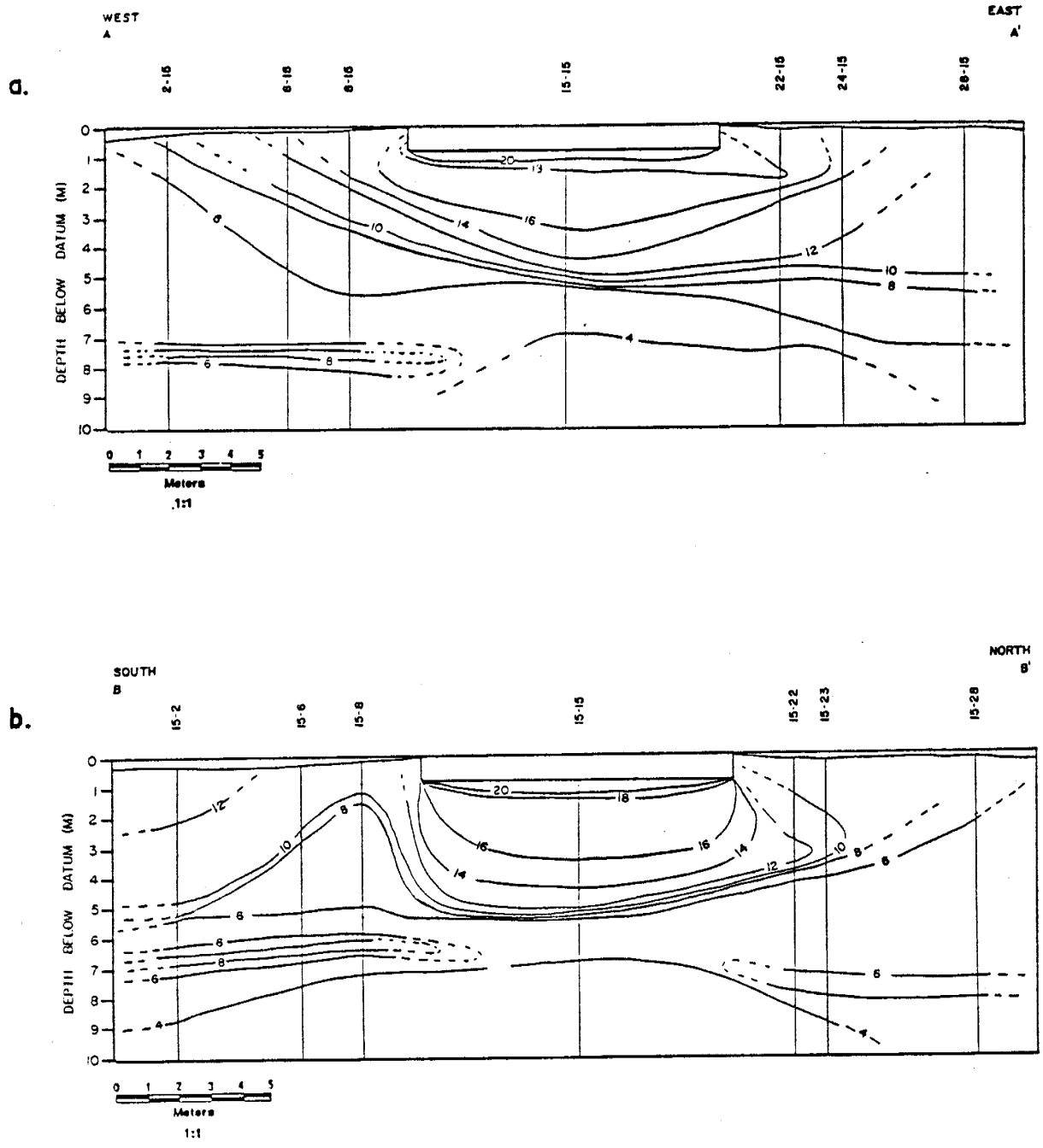

Figure 6.5. Moisture content distributions determined by neutron logging after 25 days of infiltration along the a) east-west and b)north-south transects.

slope and fluvial sand facies. The 20 and 18% contour intervals appear to have stabilized between experimental day 7 (Figure 6.4) and day 25 (Figure 6.5).

The moisture content profiles are significantly different by experimental day 153 (Figure 6.6). By this time the wetting front had propagated beyond the maximum limits of measurement (10 meters below datum) in the center of the field site, well into the fluvial sand facies. The east-west and north-south moisture content distributions are fairly symmetric with slightly more water in the east and north quadrants of the field site possibly due to the sloping soil layers. Lateral spreading greater than 4 and less than 8 meters from the edge of the driplines was observed. The 16% moisture content contour appears to have stabilized at this time.

6.4. MEASURED TWO-DIMENSIONAL PRESSURE HEAD

Pressure head distributions as determined by tensiometers were developed for the east-west and north-south transects to illustrate the initial and experimental day 153 pressure head distributions. The corresponding geologic cross-sections are shown on a one-to-one horizontal to vertical scale in Figure 6.2.

The negative pressure head was measured by the tensiometers. The tensiometers consisted of a PVC pipe filled with a water/antifreeze mixture with a ceramic cup at one end and a stopper and cap assembly at the other end. A Tensimeter recorded

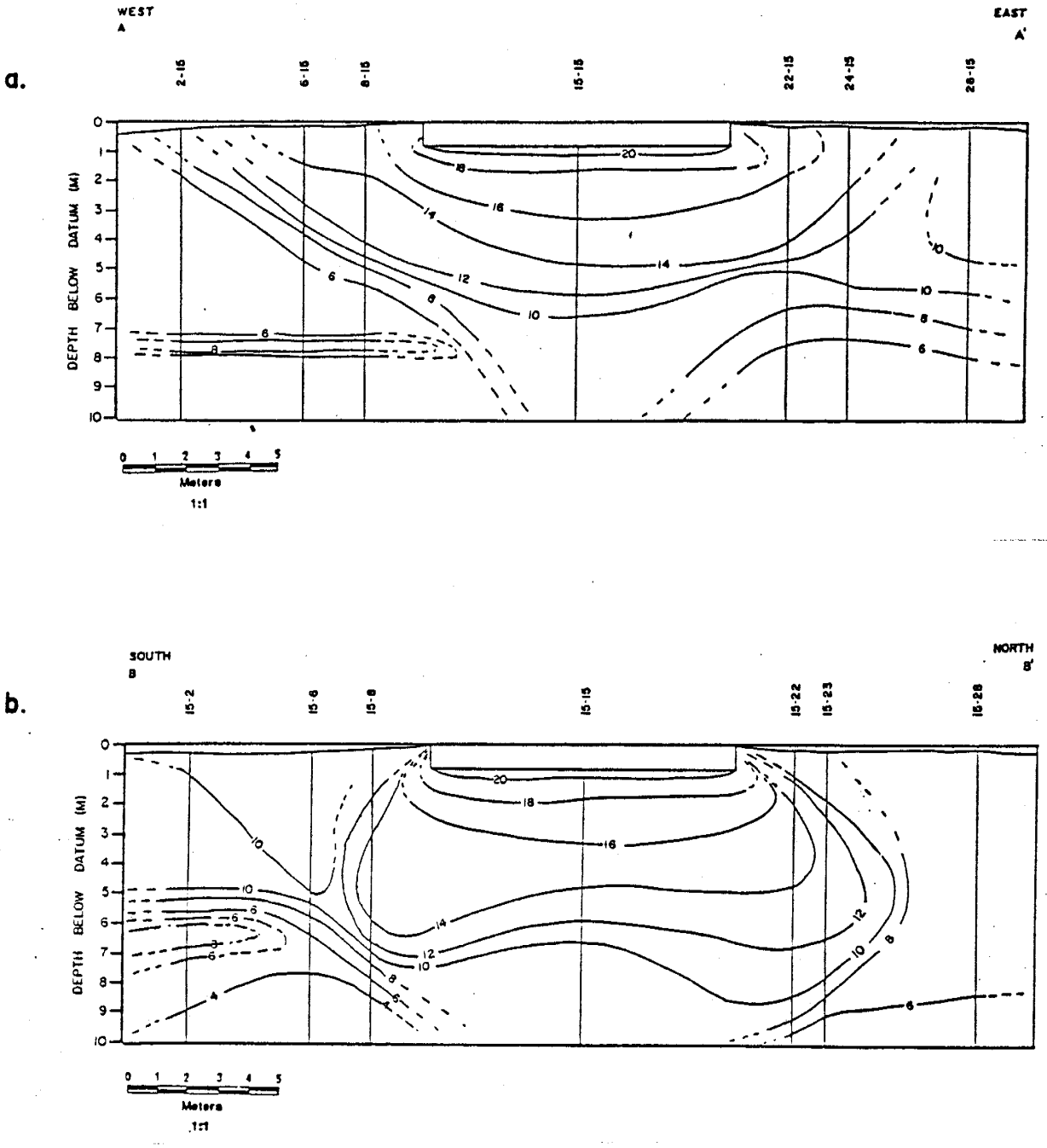

Figure 6.6. Moisture content distributions determined by neutron logging after 153 days of infiltration along the a) east-west and b)north-south transects.

the pressure above the column of water/antifreeze in the tensiometer. The negative pressure head (ψ) at the tensiometer ceramic cup was then calculated by:

$$\psi = -P + L\rho \qquad (6.1)$$

where P is the pressure head reading from the Tensimeter, L is the height of water/antifreeze above the ceramic cup, and ρ is the density of the water/antifreeze mixture.

A 50/50 mixture of water and Peak 1 antifreeze was used in the tensiometers to prevent freezing during the winter months. The addition of antifreeze affects the density of the water column, therefore also affecting the negative pressure head calculation (Equation 6.1). Laboratory experiments calculated the density of the water/antifreeze mixture to be 0.92 g/cc at 20°C. The antifreeze may also affect the surface tension of the fluid in the ceramic cup and surrounding soil. At this time it is unknown whether a change in surface tension caused a significant bias in the ψ measurements in the field, but a laboratory study is currently being conducted to study the surface tension effects of water/antifreeze mixtures in tensiometers (E. Hicks, NMIMT Research Assistant, personal communication, 1988).

Pressure head contours were developed using smoothed ψ values from tensiometer data. Figure 6.7 presents the initial ψ field prior to the start of the experiment. Pressure head ranges from greater than -50 cm to approximately -150 cm beneath the irrigation system in the piedmont slope facies.

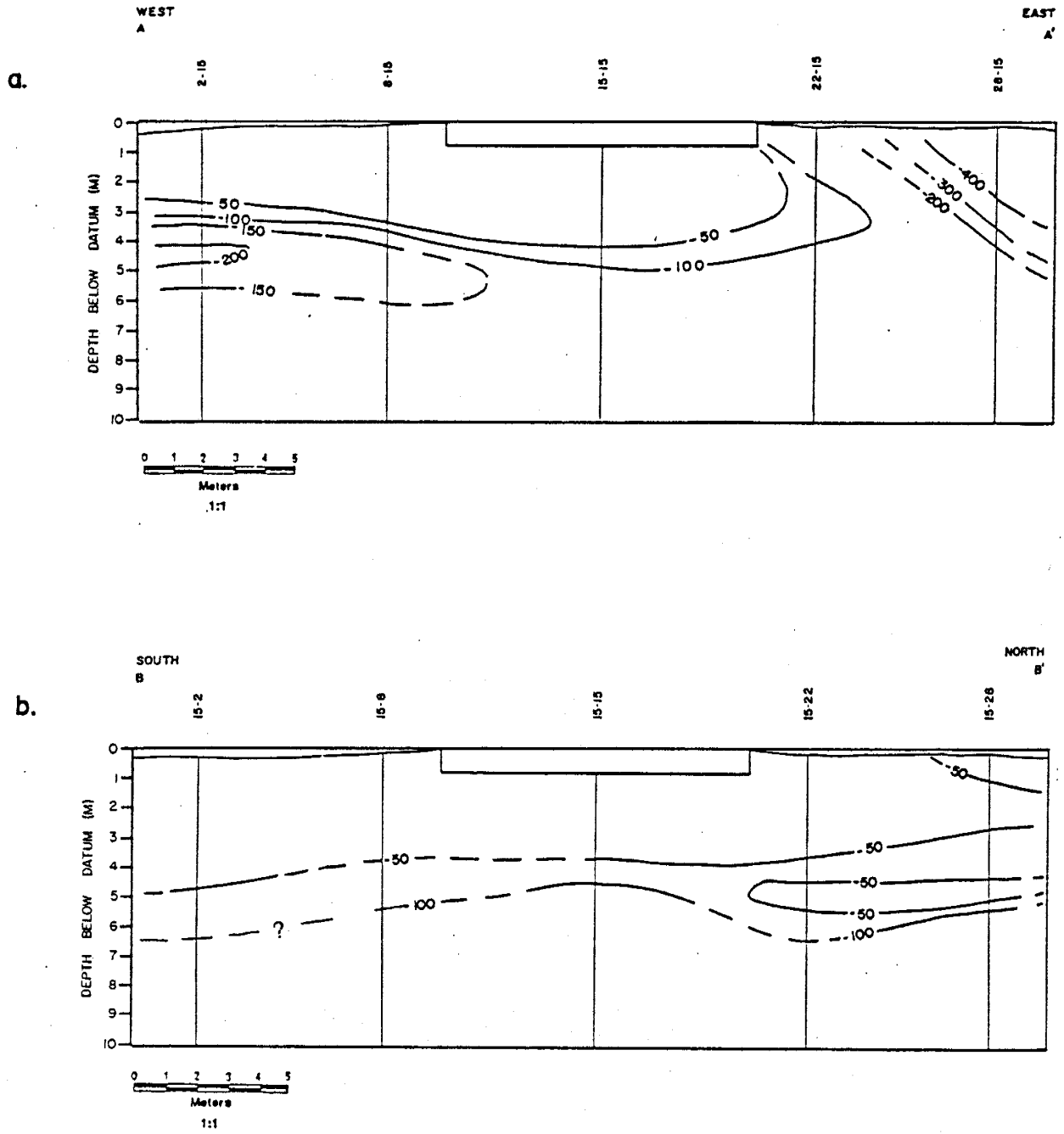

Figure 6.7. Initial pressure head distributions measured by tensiometers before infiltration occurred along the a) east-west and b)north-south transects.

Tensiometric data suggest there were large areas of positive pressure head ($\psi > 0$) were present beneath the irrigation plot after 153 days of infiltration (Figure 6.8). Although the contour shapes of the ψ distribution and the moisture content distribution were similar on experimental day 153 (Figures 6.8, 6.6), the moisture content distribution does not reflect a zone of saturation. If the θ-ψ relationship was developed using field data, it would tend to be positioned to the left of the laboratory θ-ψ relationship (Figure 3.8). These results indicate the neutron probe measured moisture contents may be lower than actual moisture content values.

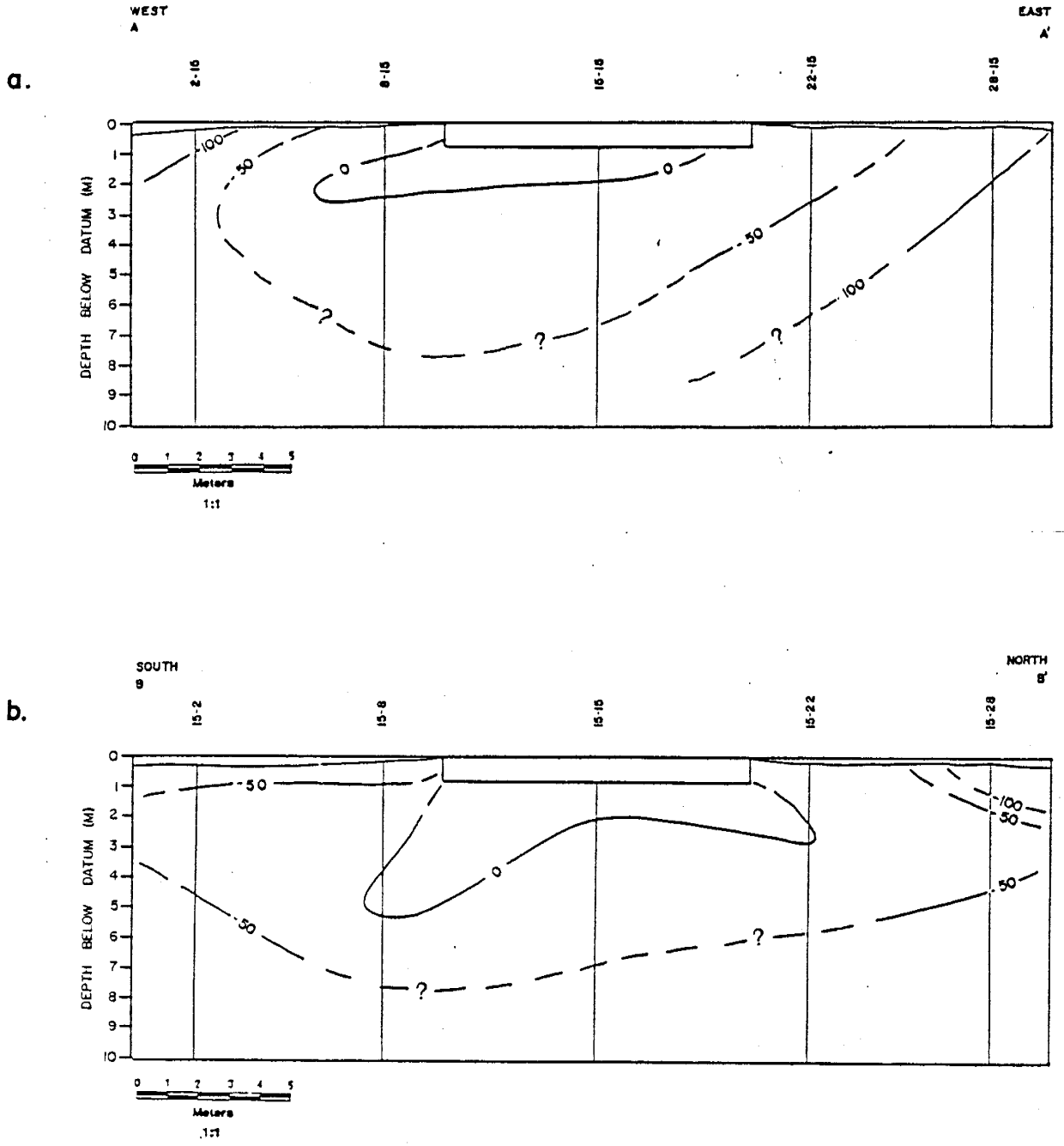

Figure 6.8. Pressure head distributions measured by tensiometers after 153 days of infiltration along the a) east-west and b)north-south transects.

7. TWO-DIMENSIONAL ANALYTICAL MODEL

Steady state and transient point source linearized solutions are used to predict moisture content distributions beneath the field site using the computer program TRANS.FOR. The upper boundary conditions designated for the analytical model are listed below. There is a constant discharge from the emitters located at 0.86 meters below datum. A no flow boundary directly above the emitters extends infinitely in the horizontal direction. The no flow boundary is accurately represented beneath the simulated impoundment by the plastic layer immediately above the emitters. However beyond the simulated impoundment boundaries, evaporation from the soil surface and infiltration of precipitation events may occur.

The following sections present 1) a verification of the computer program TRANS.FOR, 2) an analysis of the sensitivity of model dimensionless matric flux potential distribution to input parameters 3) calibration of the model using the steady state and time-dependent solutions using field data, 4) the comparison of model predicted moisture content distributions to field observations at experimental day 25, and 5) a discussion of the model prediction.

7.1. MODEL VERIFICATION

Two test cases were conducted using the computer program TRANS.FOR to compare the dimensionless matric flux potential, Φ, solutions to those published by Warrick (1974). The test solutions are presented in terms of dimensionless distance, time, and matric flux potential. Real distance, time, and matric flux potential can be determined using equations 2.17 through 2.20.

Figure 7.1 compares the shape and location of the 0.5 Φ contour solutions at various times for a single point source located at R = Z = 0. Contours were developed using a linear kriging technique (Surfer, Golden Software, Golden, CO). The results of TRANS.FOR compare well with Warrick's (1974) results at all times (Figure 7.1). To the author's knowledge, Warrick has not published the actual output from his point source solution, therefore the TRANS.FOR verification was accomplished by superimposing the TRANS.FOR solutions on Warrick's published figures. The minor discrepancies are likely due to different contour interpolation techniques, density of the dimensionless matric flux potential solution grid, and distortion of the R to Z ratio while enlarging Warrick's (1974) figure.

Figures 7.2.a and 7.2.b verify the superpositioning technique used by TRANS.FOR to Warrick's (1974) steady state superposition figure. Point sources of equal strength are located at X equal to 0 and 2. The selected Φ contours shown compare very well (Figures 7.2.a and 7.2.b). Again, the minor

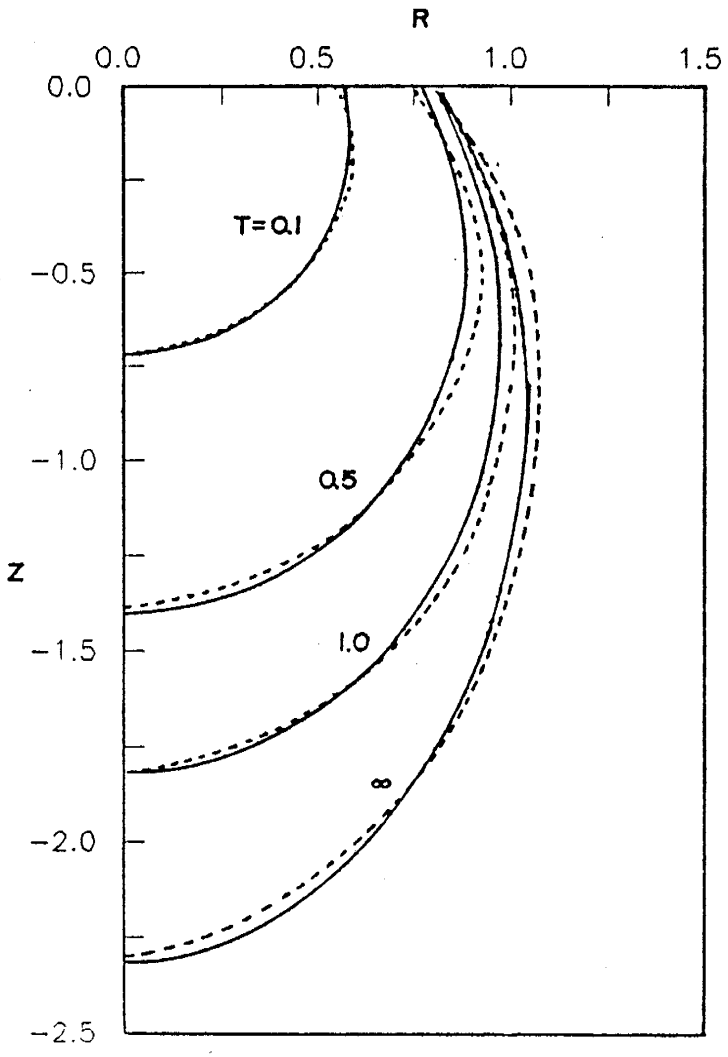

Figure 7.1. Comparison of the shape and advance of the 0.5 dimensionless matric flux potential, Φ, for a point source of constant flux. Solid lines show results computed by TRANS.FOR in this study. The dashed lines are Warrick's (1974) predictions.

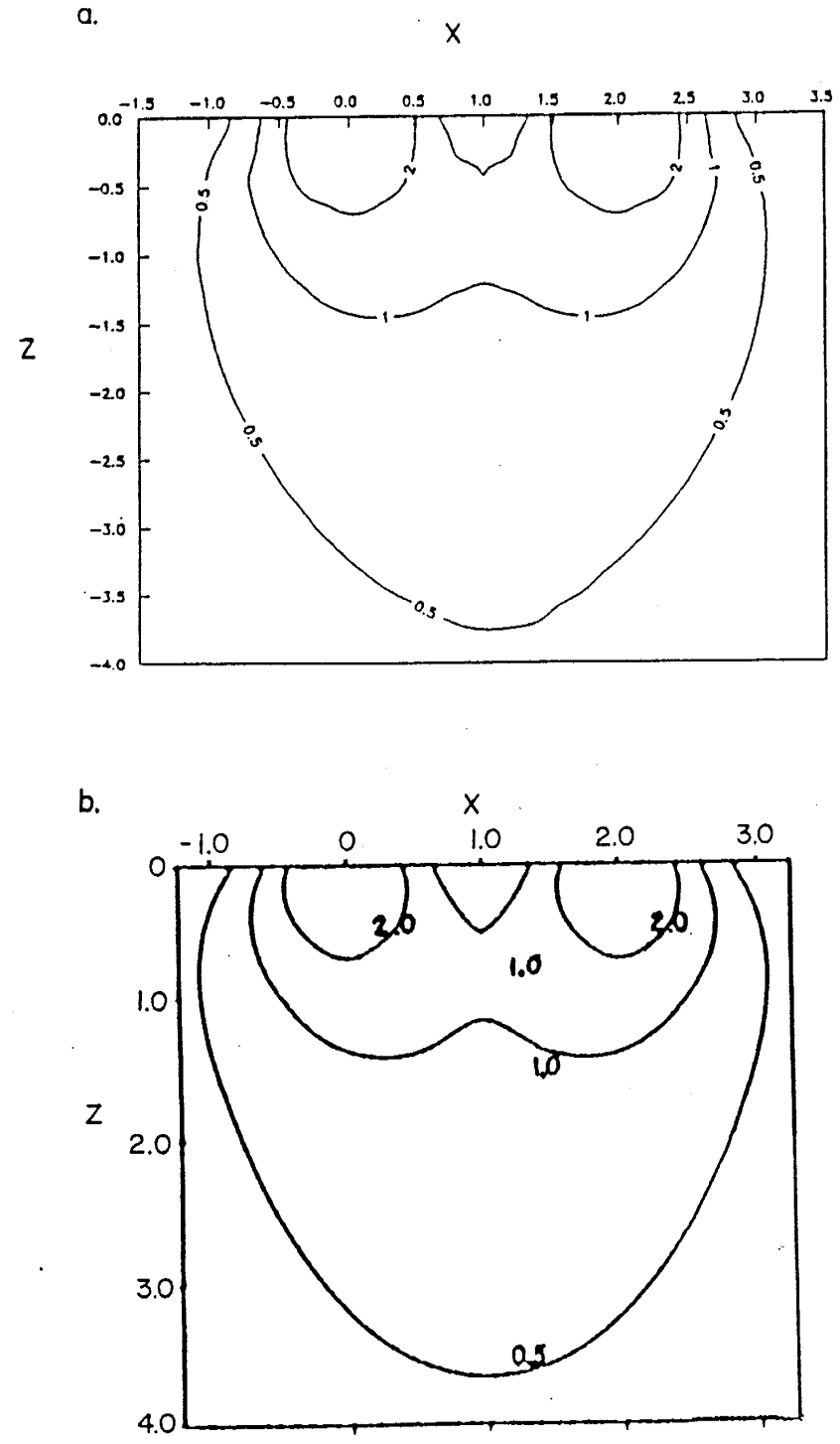

Figure 7.2. Comparison of dimensionless matric flux potential, Φ, superpostioning steady state solutions of a) this study and b) Warrick (1974). Point sources located at X = 0 and X = 2.

observed discrepancies are likely due to the contour interpolation technique, solution grid density, and distortion when enlarging Warrick's figure.

7.2. MODEL SENSITIVITY

Model sensitivity is discussed below for the five model input parameters. The five input parameters will be discussed in the following order; emitter discharge rate (q), the intercept of the K-ψ exponential relationship (K_0), the anisotropic ratio (K_h/K_z), the slope of the K-ψ exponential relationship (α), and the time-dependent linearization parameter (k). Effects of input perturbation will be discussed using a single point source in a dimensionless field.

The emitter discharge rate, q, does not affect the solution of dimensionless matric flux potential using equations 2.17 and 2.20. However, q is used to find the real matric flux potential (equation 2.16). Combining equations 2.4, 2.5 and 2.16 results in the following equation for ψ:

$$\psi = 1/\alpha \ln\{(\alpha^2 q\Phi)/(K_0 8\pi)\} \qquad (7.1)$$

Equation 7.1 shows that q is $\log_e$ proportional to the value of the pressure head. An increase in the discharge rate will increase the pressure head at any point.

Equation 7.1 is also useful for evaluating the model solution response to the intercept of the K-ψ exponential relationship, K_0. Like the emitter discharge, K_0 does not affect the dimensionless matric flux potential solutions of equations

2.17 and 2.20. K_0 is used in the conversion of matric flux potential to pressure head, equations 2.4 and 2.5. As shown in equation 7.1, an increase in K_0 will decrease the pressure head, which is intuitively correct.

The importance of anisotropy was studied by comparing dimensionless matric flux potential distribution for anisotropy ratios of 1, 2 and 5. As the anisotropy ratio increases, the dimensionless matric flux potential tends to spread laterally. Figures 7.3 through 7.5 illustrate the dimensionless matric flux potential distribution for the three anisotropic ratios. The geometric mean of the hydraulic conductivity was held constant (0.05 m/day) for all modeling runs.

A mass balance of the dimensionless matric flux potential was computed using Figures 7.3-7.5 in the following manner. Two hundred fifty five (255) data points were used to generate dimensionless matric flux potential contours (Figures 7.3-7.5). Each data point was treated as the centroid of a block centered grid with an area of 0.625 units^2. Multiplication of the area of the block, the distance from the z axis to the centroid, 2π, and the average value of the dimensionless matric flux potential for that block resulted in an estimate of the total Φ for that node. Summation of the dimensionless matric flux potential values for the 225 data points estimated the total Φ for each anisotropy ratio.

The mass balance results for each anisotropy ratio compare within 12% of each other. The summation of Φ was determined to

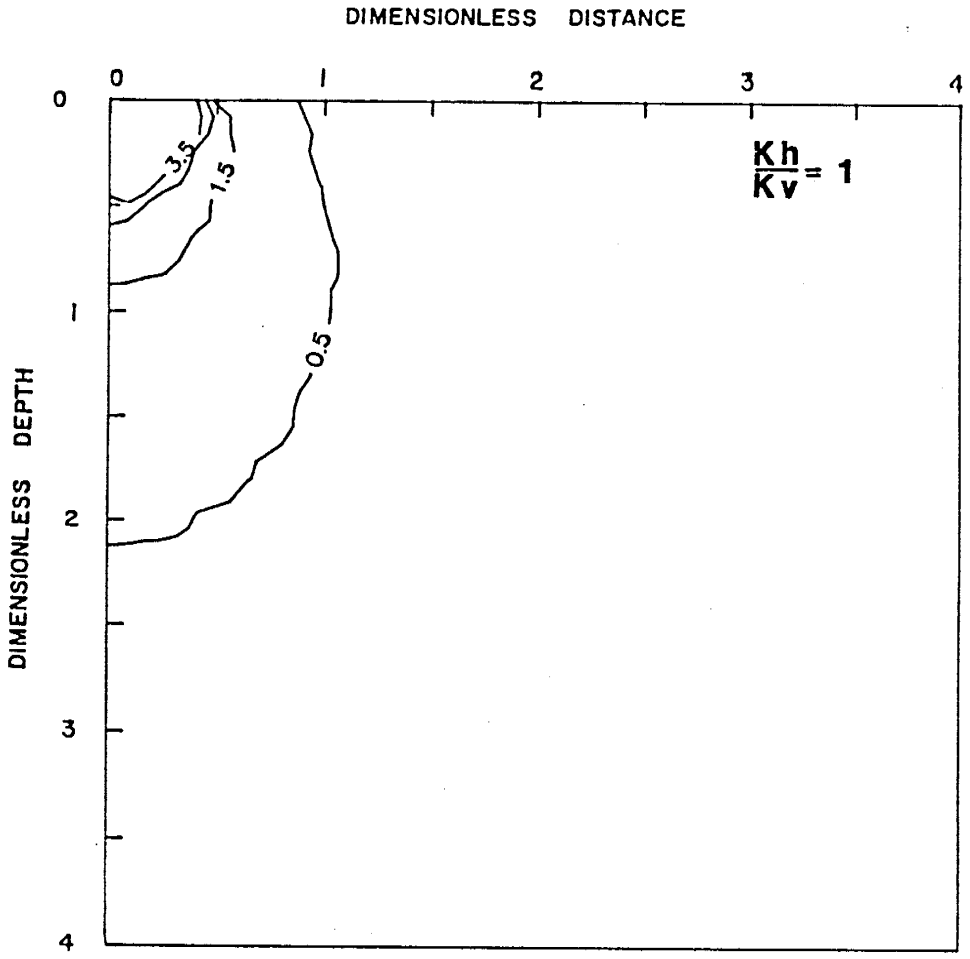

Figure 7.3. Dimensionless matric flux potential contours after 7 days of infiltration from a point source located at (0,0) for the isotropic case (α = 1 1/m, k = 1 m/d).

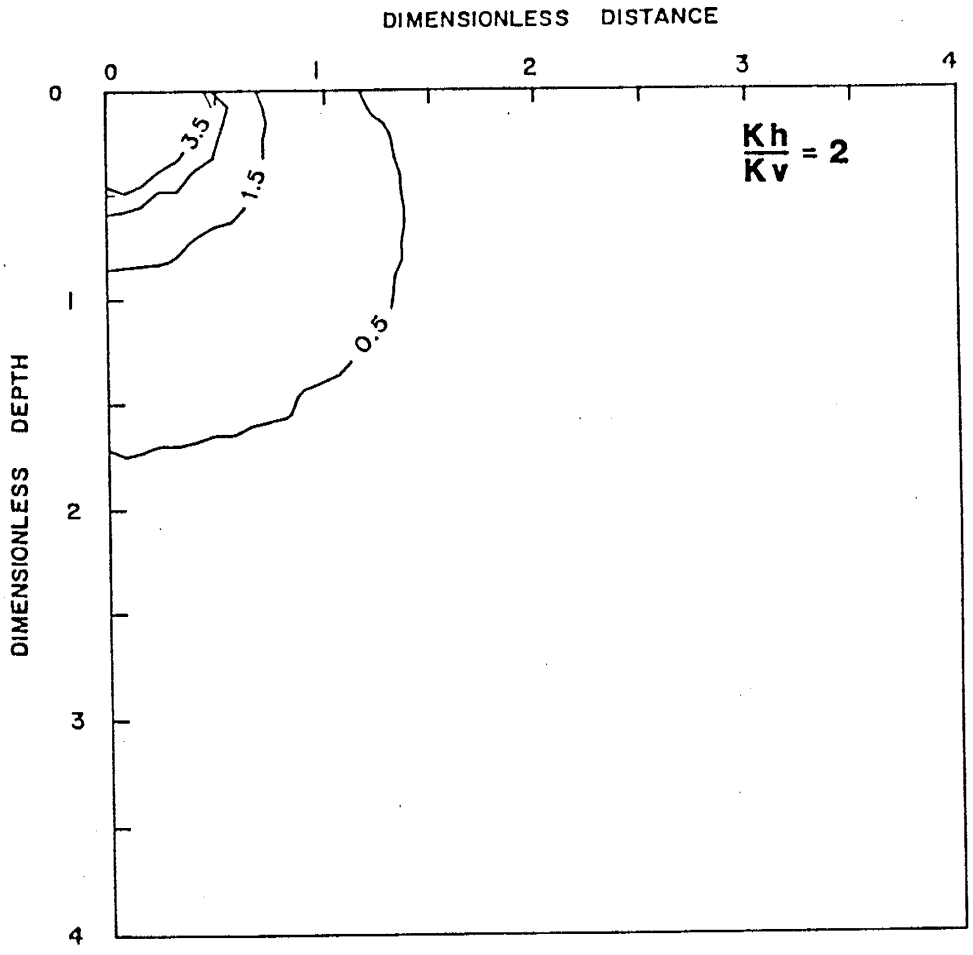

Figure 7.4. Dimensionless matric flux potential contours after 7 days of infiltration from a point source located at (0,0) for an anisotropic ratio equal to 2 (α = 1 1/m, k = 1 m/d).

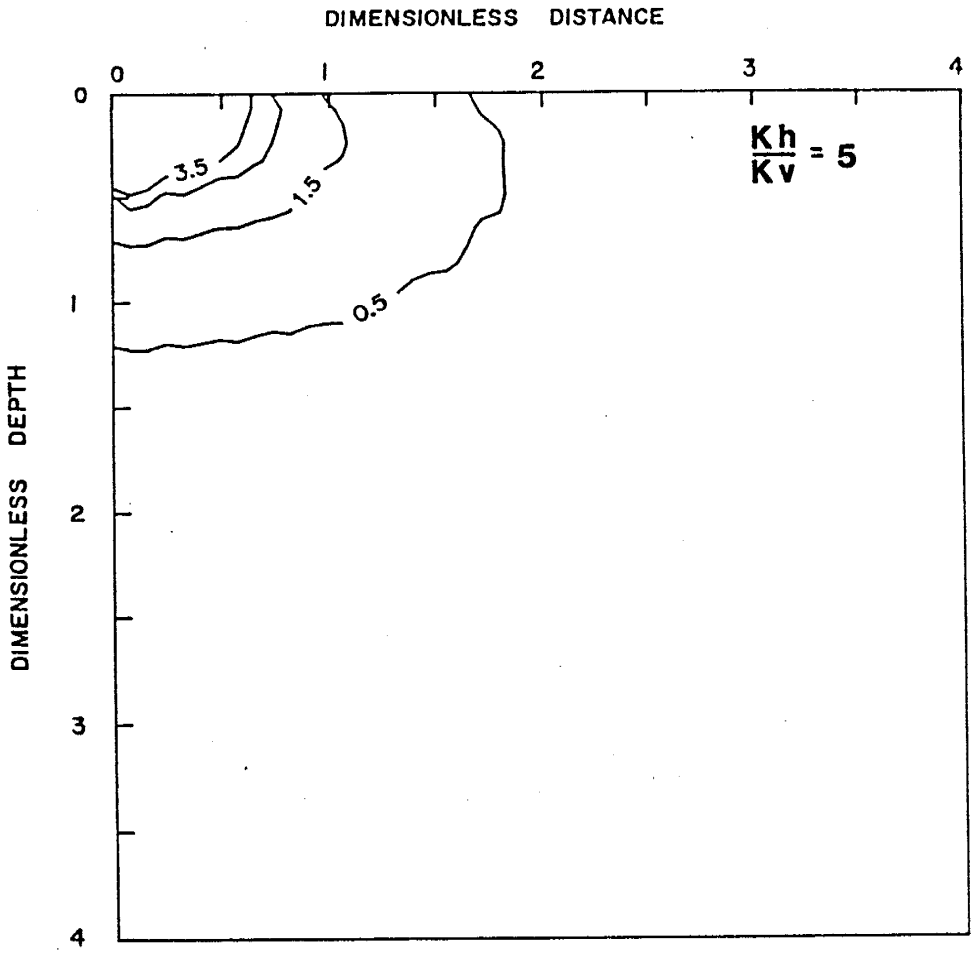

Figure 7.5. Dimensionless matric flux potential contours after 7 days of infiltration from a point source located at (0,0) for an anisotropic ratio equal to 5 (α = 1 1/m, k = 1 m/d).

be 18.80, 21.16, and 21.22 for the 1, 2, and 5 anisotropic ratios, respectively. A higher density of data points would likely lead to better accuracy of the summation of Φ.

Decreasing the slope of the K-ψ relationship, α, will decrease the dimensionless matric flux potential, Φ (Figures 7.3, 7.6). Furthermore, ψ will tend to decrease as α decreases according to equation 7.1.

A sensitivity analysis was performed on the range of pressure heads used to develop the K-ψ exponential relationship parameters α and K_0. Table 3.4 lists value of K_0 and α calculated over eight ranges of ψ. The ψ ranges used in the calibration analysis were: 0 to -1.5 m, 0 to -2.5 m, and 0 to-5.0 m. As the ψ range increases from -1.5 to -5 meters, the slope (α) and the intercept (K_0) decrease. Smaller values of K_0 and α tend to increase Φ, hence increasing the moisture content value. The reduction of K_0 and α will eventually cause $K(\psi)$ to be less than the applied flux at all ψ values (equation 2.5), resulting in saturated conditions.

A decrease in k has the effect of lessening the dimensionless time of infiltration (equation 2.15), and hence the extent of the wetting front. Figures 7.3 and 7.7 show the effect on Φ when decreasing k by an order of magnitude. The dry ranges seem to be affected the most by a decrease in k. For example, the position of the 0.5 Φ contour has decreased dramatically compared to the 3.5 Φ contour change of position with an order of magnitude decrease in k (Figures 7.3 and 7.7). A possible

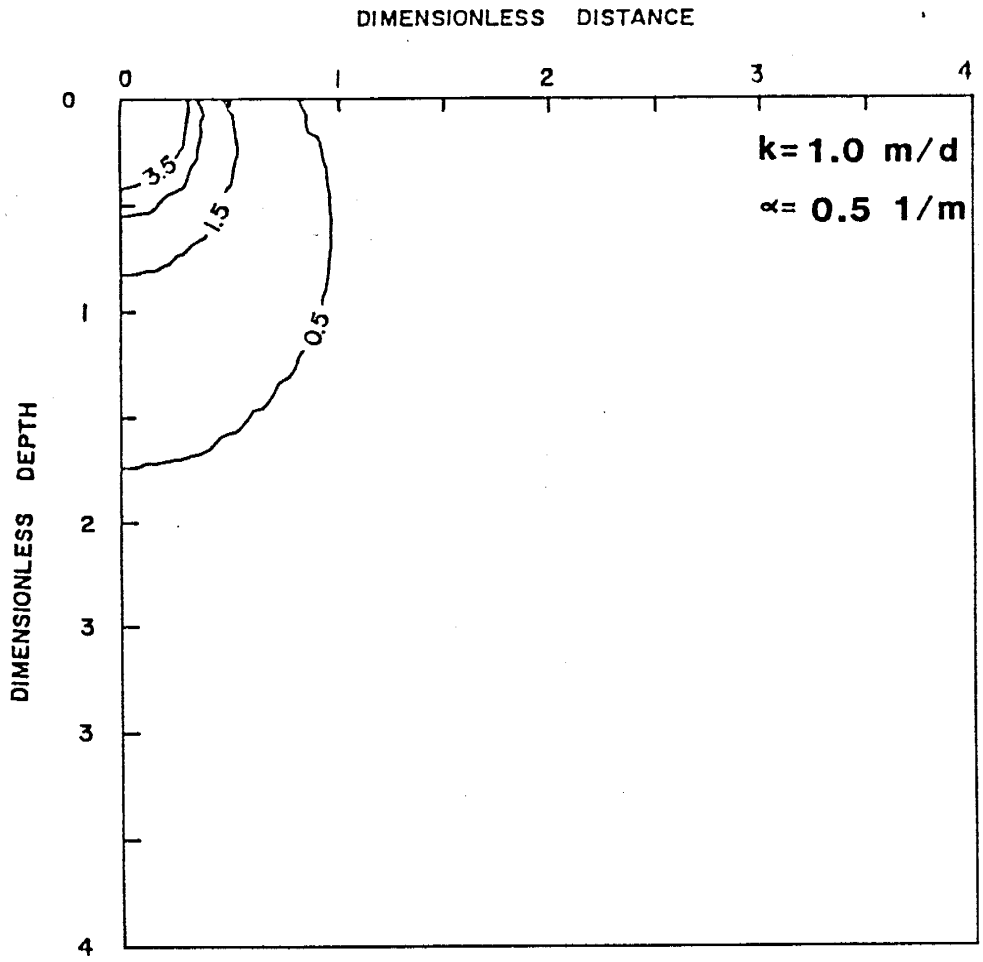

Figure 7.6. Dimensionless matric flux potential contours after 7 days of infiltration from a point source located at (0,0) for the isotropic case (α = 0.5 1/m, k = 1 m/d).

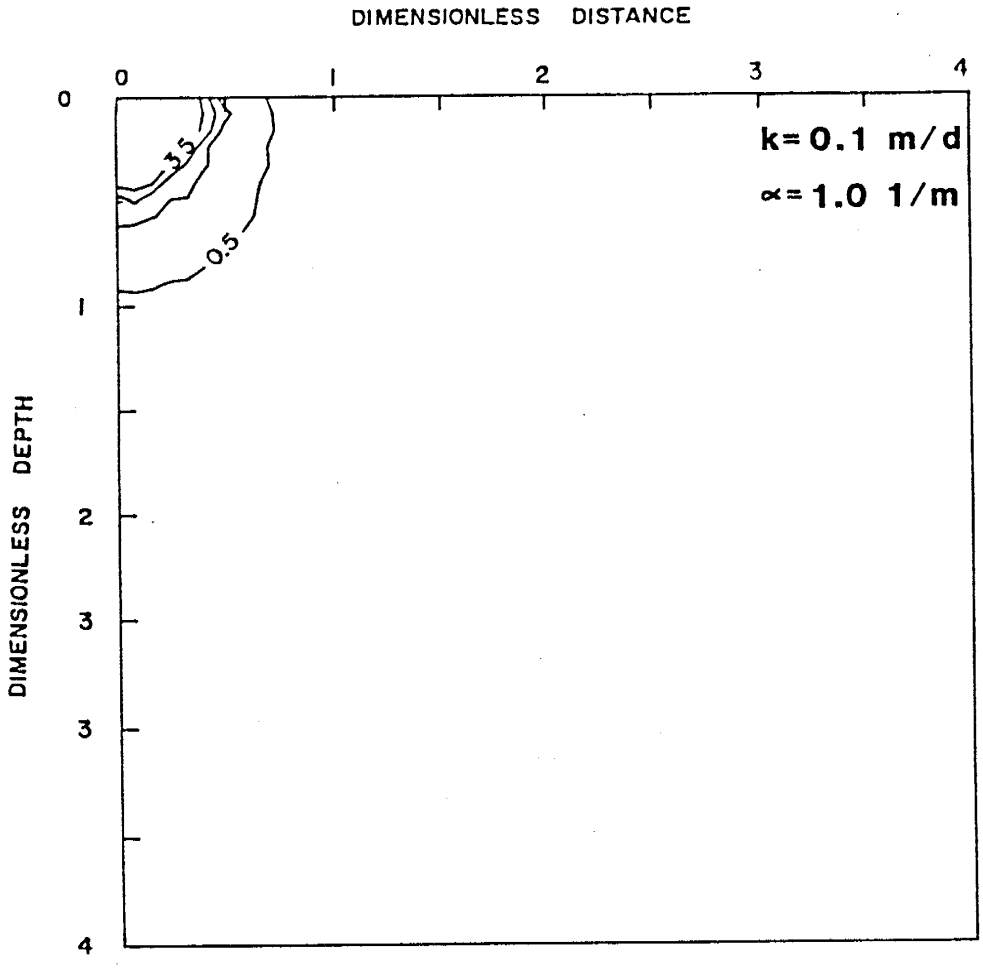

Figure 7.7. Dimensionless matric flux potential contours after 7 days of infiltration from a point source located at (0,0) for the isotropic case (α = 1 1/m, k = 0.1 m/d).

explanation may be that the Φ field near the emitter (e.g. 3.5 Φ contour) may have approached steady state by this time.

7.3. MODEL CALIBRATION

Calibration analysis of the model input parameters α,K_0 and k was attempted using a trial and error procedure which compared the computer predictions to field data. Steady state model predictions were used to calibrate α and K_0, whereas transient model predictions at experimental day 7 was used to calibrate k.

A calibration analysis was preformed on the ranges of pressure head used to develop the K-ψ exponential relationship parameters α and K_0. The ψ ranges used in the calibration analysis were; 0 to -1.5 m, 0 to -2.5 m, and 0 to -5.0 m. The above ψ range input parameters were used in steady state model predictions and were compared to experimental day 153 measured moisture contents. Experimental day 153 is assumed to represent steady state moisture content conditions, at least for the areas near the drip irrigation system. Model output was converted to moisture content values by applying equations 3.1, 3.2, and 7.1. Residual and satiated moisture contents equal 11.7% and 37.7%, respectively for the piedmont slope facies.

Maximum moisture content beneath the drip irrigation system was used to choose an appropriate value of α and K_0. Maximum

moisture observed by the neutron probe measurements was 20% at day 153 (Figure 6.6). This may be the expected steady state moisture content inasmuch as the location of the 20% contour did not change substantially from day 25 to 153 (Figures 6.5 and 6.6).

Of the three ψ ranges used in this calibration, the ψ range 0 to -1.5 m best predicts the maximum moisture content at day 153, Figure 7.8. The maximum predicted moisture content is 26% for the 0 to -1.5 m ψ range compared to 28% and saturated conditions for the 0 to -2.5 m and 0 to -5.0 m ψ ranges respectively. Additionally, the 0 to -1.5 m ψ range represents the ψ range found in the piedmont slope facies beneath the irrigation system prior to and during infiltration, Figures 6.7 and 6.8. Values for α and K_0 equal to 7.78 1/m and 0.421 m/d, respectively, will be used for the remainder of the simulations.

The last model input calibration involves the parameter k, used to linearize the time-dependent solution. Figure 7.9 illustrates the effect of the moisture content profile beneath the irrigation system where k varies from 0.1 to 0.01 m/d after 7 days of infiltration for the isotropic case. Comparison of the model predictions of Figure 7.9 to that of the observed moisture content illustrated in Figure 6.4 indicates an input value of 0.01 m/d for k most closely predicts the measured moisture content profile.

However, there was a discrepancy between the initial field conditions and the model initial conditions. The model assumes

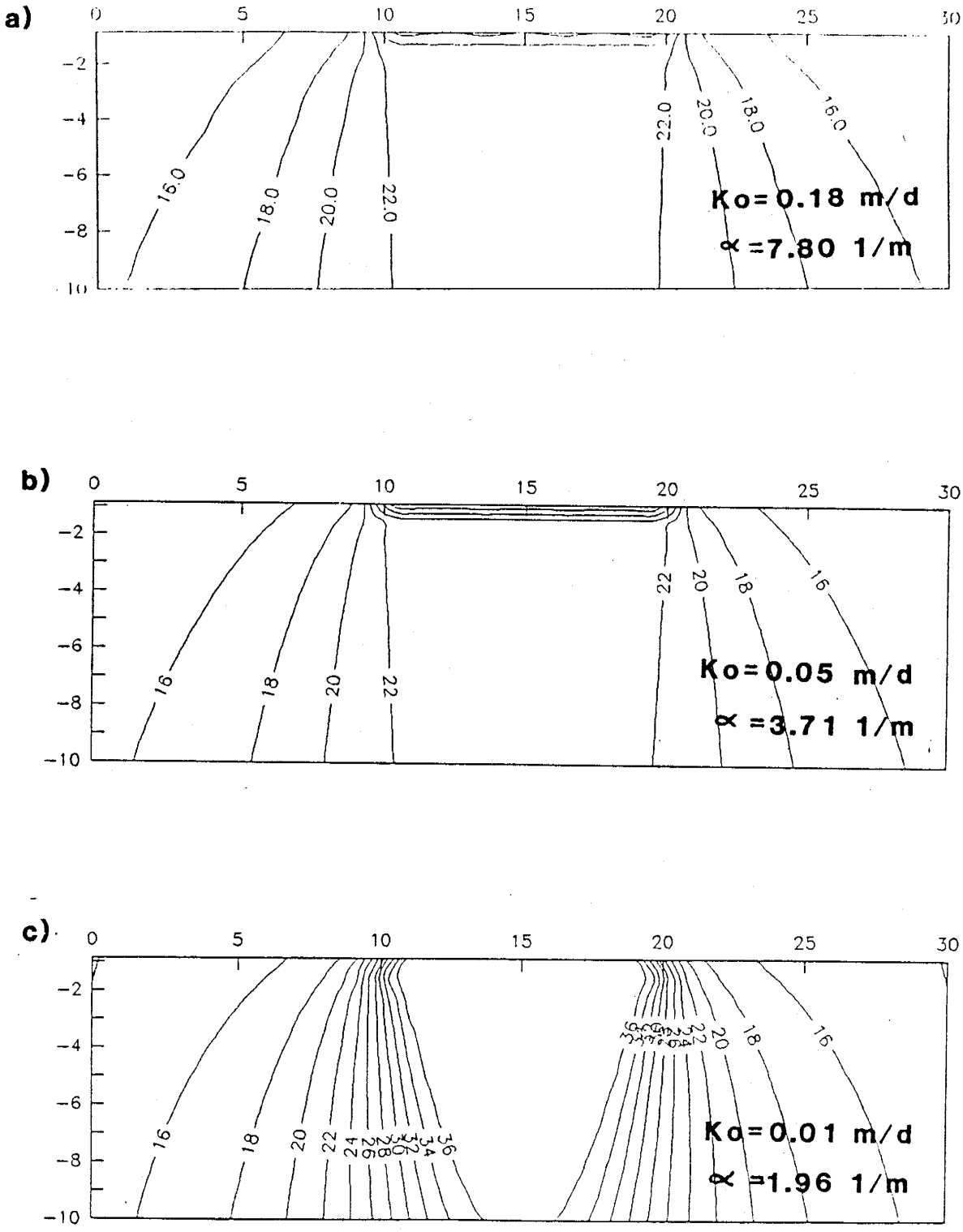

Figure 7.8. Steady state predicted moisture content contours beneath the drip irrigation system for selected ψ ranges used to calibrate K_0 and α: a) ψ range 0 to -1.5 m (K_0 = 0.18 m/d, α = 7.80 1/m); b) ψ range 0 to -2.5 m (K_0 = 0.05 m/d, α = 3.71 1/m); c) ψ range 0 to -5.0 m (K_0 = 0.01 m/d, α = 1.98 1/m).

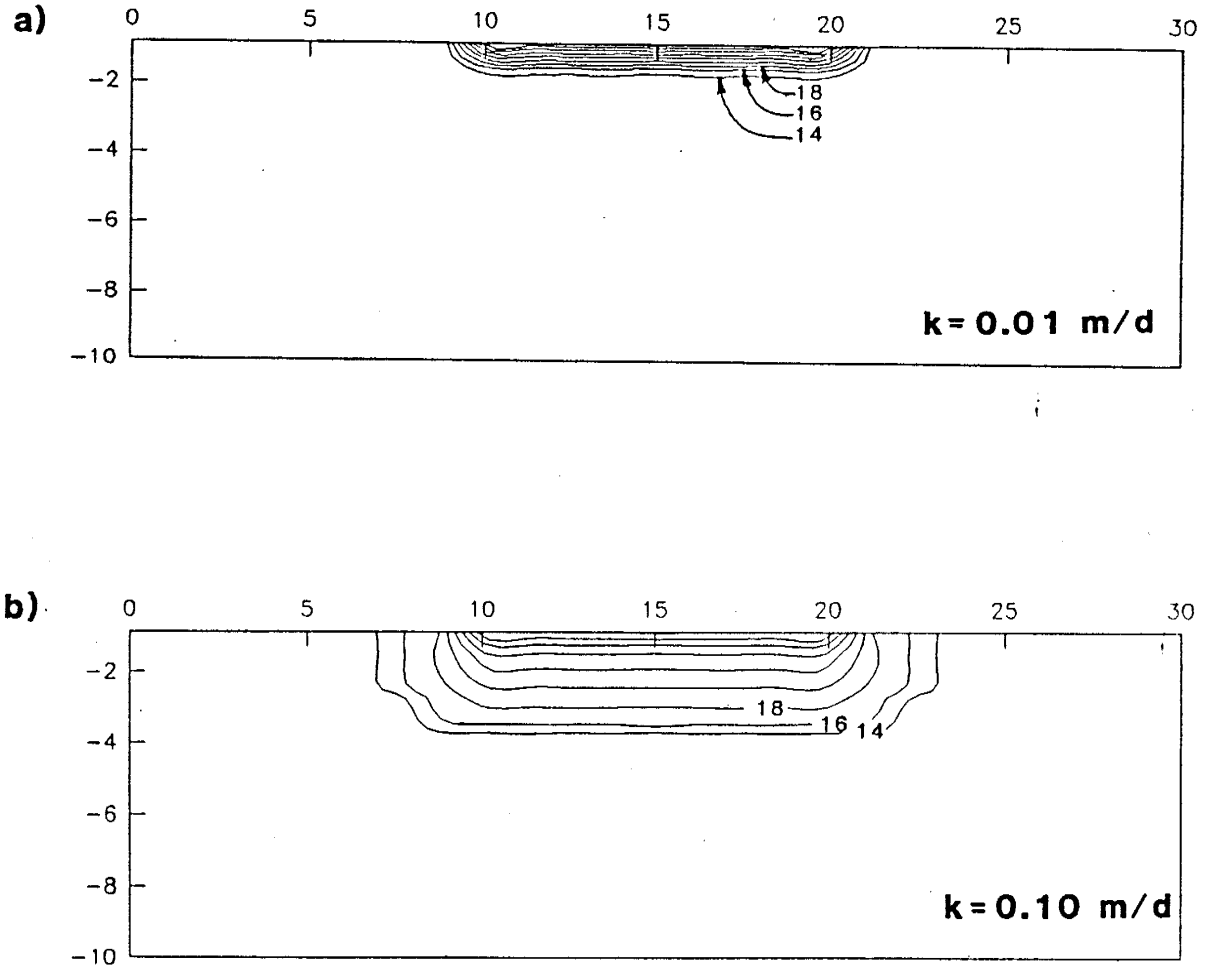

Figure 7.9. Predicted moisture content contours at day 7 for selected k values. Other input parameters held constant (K_0 = 0.421 m/d, α = 7.78 1/m, q = 0.00196 m^3/d): a) k = 0.01 m/d; b) k = 0.1 m/d.

that the soil beneath the irrigation system had a Φ equal to zero before infiltration began. A Φ of zero implies that ψ would be equal to negative infinity (θ equals residual moisture). Due to a large precipitation event, as discussed previously, the moisture content beneath the irrigation system ranged from 18% to 8%, Figure 6.3. Residual moisture content determined by laboratory analysis was 11.7%. The higher moisture immediately beneath the irrigation system would tend to increase the rate of the wetting front advance which would cause the calibrated k of 0.01 m/d to be overestimated. It is not known to what extent this overestimation of k affects the model output.

7.4. MODEL PREDICTIONS

Isotropic model predictions underestimates the vertical extent the increase of moisture content at experimental day 25. The moisture content profile was predicted using the above calibrated model input parameters (α = 7.78 1/m, K_0 = 0.421 m/d, and k = 0.01 m/d). An increase in moisture content from the model simulation was noted to a depth of 3 mbd and extends laterally approximately 2 m beyond the edge of the drip irrigation system (Figure 7.10). Increases of field measured moisture content were noted to extend to 5.5 mbd and 2 m from the edge of the irrigation system. The model predicts the lateral extent well, but it grossly under predicts the vertical extent of the moisture increase.

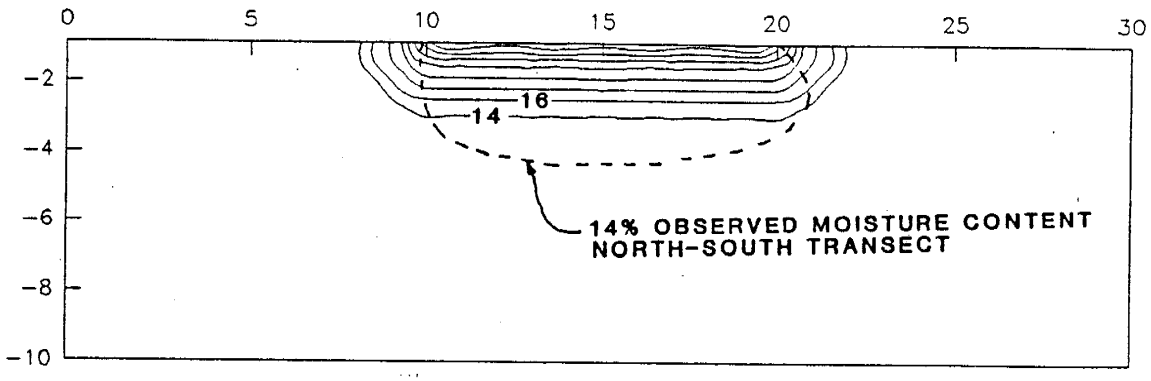

Figure 7.10. Predicted and 14% observed moisture content contours for day 25. Model input parameters: K_0 = 0.421 m/d, α = 7.78 1/m, q = 0.00196 m^3/d, k = 0.01 m/d, $K_H = K_Z$ = 1.

7.5. DISCUSSION

An attempt was made to calibrate and validate the Warrick's 1974 time-dependent linearized point source solution to a large scale field experiment. Violation of the model initial conditions prevented conclusive calibration of the model input parameters. Large errors in the prediction of the magnitude and extent of the moisture content and pressure head could result from biased input parameters. Assuming the input parameters are correct, comparison of the field data to model prediction imply that the piedmont slope is anisotropic, where K_z is greater than K_h, inspite the highly stratified soil of the piedmont slope which should tend to enhance the effects of lateral spreading.

Multiple reasons may account for the discrepancies between model and field data. First, the field conditions violates the model initial condition. Φ is assumed to be equal to 0 before infiltration began. The greater than residual moisture beneath the irrigation system would tend to increase the rate of advance of the wetting front.

Secondly, possible fingering of the wetting front may be responsible for the greater depth to wetness noted in the field, however there is no field evidence to support such a claim.

Thirdly, uncertainty of the calibration of the model input parameters may cause the model to under predict the extent of moisture increase. K_0 and α were calibrated to day 153 moisture

content. Possible biases of the neutron probe calibration would propagate in the estimation of K_0 and α. k was calibrated to day 7. Mass balance at day 7 only accounts for 40% of the infiltrated water. As seen in the calibration of k, small deviation in this input parameter has a great effect on the lateral and vertical extent of the moisture content increase.

The effect of an implied constant diffusivity may tend to predict unrealistic moisture content profiles. Clothier and Scotter (1982) demonstrated that using a constant diffusivity could not predict a sharp wetting front. The effect of a constant diffusivity will be minimized with a small change in moisture content.

Finally, the assumption that the piedmont slope facies can be simulated as a homogeneous system may be in error. Parsons (1988a) states that the piedmont slope facies is highly heterogeneous. The moisture content profiles shown in figures 6.3 to 6.5 illustrates that moisture content is not symmetrical. The scale of the field experiment was not large enough to minimize the effect of the heterogeneity in the piedmont slope.

8.0 SUMMARY AND CONCLUSIONS

A field experiment was conducted to simulate uniform seepage from a lined 10.5 m x 10.5 m impoundment into a stratified soil in the vadose zone. Water was applied through a drip irrigation system containing 441 emitters spaced 50 cm apart. The discharge rate was approximately 2×10^{-3} m^3/d per emitter, which represents a flux averaged over the irrigated area of approximately 7.8×10^{-3} m/d. The flux was approximately 100 times less than the mean saturated hydraulic conductivity of the soil profile, and therefore the most of the soil beneath the irrigated area remained unsaturated.

The soil profile is stratified, consisting of two major facies. The piedmont slope facies, comprised of red brown silty sand and pebbles, is the upper unit which extends to a depth of about 5.5 meters below datum. The lower unit is a fluvial sand facies derived from the ancestral Rio Grande River. Soil core samples (100 cc) and split spoon samples were analyzed in the laboratory to determine the geologic and hydraulic properties of the field site.

Neutron probe measured moisture contents may underestimate the actual moisture contents in the piedmont slope facies. Moisture movement was monitored through neutron logging equipment and tensiometers. A mass balance analysis was conducted to

compare the known amount of injected water (measured by totalizing flow meters) to the water increase measured by neutron logging techniques in the soil profile. The results of the mass balance indicate that the neutron probe only account for approximately 70% of the injected water. Furthermore, the field estimated θ-ψ relationship was located to the left of the laboratory determined θ-ψ relationship, indicating that the moisture content (or pressure head) values may be in error.

Model predictions of moisture content do not represent field observations in the piedmont slope facies. Warrick's (1974) time-dependent linearized surface point source solution was used to predict the moisture content distribution beneath the irrigation system in the upper piedmont slope facies. The analytical model was modified to account for anisotropy by scaling the input parameters and coordinates. Biases in the model initial conditions, calibration of the neutron probe, model input parameter uncertainties, and the requirement of a constant diffusivity results in an unrealistic moisture content profile which bears little resemblance to field observed moisture contents.

9. RECOMMENDATIONS FOR FUTURE WORK

Only forty-nine (49) 100 cc soil core samples were used to characterize the piedmont slope facies near the irrigation plot. Clearly this is not enough samples to characterize such a highly variable hydrogeologic unit. Additional soil samples should be collected when installing future monitoring equipment. Additionally, in situ testing would provide helpful information about the larger scale hydraulic properties. Bore hole permeameter data could eliminate the effective conductivity averaging scheme used to estimate saturated hydraulic conductivity. If excavation of the borehole was possible, qualitative information about the anisotropic ratio could also be obtained.

Neutron probe calibration verification would be appropriate. Conduct small scale field experiments to determine the lateral and vertical unsaturated moisture movement in plots instrumented with neutron tubes installed in a similar manner to those at the field site. Comparison of destructive sampling within the disturbed annulus as well as in the surrounding native material to the neutron probe measurement would assist in a quality assurance program.

The validity of creating effective θ-ψ and unsaturated conductivity curves should be studied in further detail. A

separate research program could be conducted to demonstrate the appropriateness of this method.

Model calibration of input parameters need to be determined with better confidence. This independent study used steady state and transient model predictions to calibrate α, K_0 and k. Independent calibration of the above parameters would be more appropriate.

Violation of the model initial conditions implies that analytical models such as TRANS.FOR are inappropriate for comparison purposes for this field experiment. The precipitation event which happened before the installation of the irrigation system increased the moisture content beneath the pit. The model assumes that the moisture content of the soil prior to infiltration is at residual. A numerical model such as VAM2D would be more appropriate to this field experiment.

If TRANS.FOR is to be used further, the integration scheme should be modified. Currently the trapezoidal rule is used to numerically integrate. An alternative integration scheme would improve the program's accuracy and speed. Typical transient solution times are 1.5 to 2.0 hours on a Compact 386 computer. Conversion of TRANS.FOR to UNIX fortran from PROFORT fortran would probably additionally increase the speed of the program. A numerical polar integration scheme could be conducted to give additional confidence of the mass balance of the anisotropic versus isotropic dimensionless matric flux potential calculations.

With modifications, TRANS.FOR could be applied to more controlled small field or laboratory experiments to validate or estimate laboratory or field anisotropic ratios. The time-dependent solution would be more accurate if the change in moisture content is small.

10. REFERENCES

Abramowitz, M., and Stegun, 1964, Handbook of Mathematical Functions, Nat. Bur. Stand. Appl. Math Ser., 55, U.S. Government Printing Office, Washington, D.C.

Ben-Asher, J., D.O. Lomen, and A.W. Warrick, 1978, Linear and Nonlinear models of infiltration from a point source, Soil Sci. Soc. Am. J., 42: 3-6.

Ben-Asher, J., N. Diner, A. Brandt, and D. Goldberg, 1975, Measurement of hydraulic conductivity and diffusivity for predicting the process of soil water infiltration from a trickle source, Water Resour. Bull., 11: 1187-1197.

Black, T.A., W.R. Gardner, and G.W. Thurbell, 1969, The prediction of evaporation, drainage, and soil water storage for a bare soil, Soil Sci. Soc. Am. Proc., 33: 655-660.

Bowmen, R.S., 1988, personal communication on 1/15/88, Assistant Professor, NMIMT, Socorro, NM.

Braester, C., 1973, Moisture variation at the soil surface and the advance of the wetting front during infiltration at constant flux, Water Resour. Res., 9: 687-694.

Bresler, E., 1978, Analysis of trickle irrigation with application to design problems, Irrigation Sci., 1: 3-17.

Bucks, D.A., and F.S. Nakayama, 1985, Guidelines for maintenance of a trickle irrigation system IN Drip/Trickle Irrigation in Action, Proceedings of the Third International Drip/Trickle Irrigation Congress, Nov. 18-21, Fresno, CA, ASCE, 119-126.

Bumb, A.C., 1988, personal communication on 10/31/88, Hydrologist, In-Situ, Inc., Laramie, WY.

Chamberlain, R.M., 1980, Cenozoic stratigraphy and structure of the Socorro Peak volcanic center, central New Mexico, New Mexico Bureau of Mines and Mineral Resources, Open-file Rpt. 118, 2 vol, 495 p.

Clothier, B.E., and D.R. Scotter, 1982, Constant-flux infiltration from a hemispherical cavity, Soil Sci. Soc. Amer. J., 46(4): 696-700.

Denny, C.S., 1940, Tertiary geology of the San Acacia area, New Mexico, J. of Geology, 48: 73-106.

Elrick, D.E., and D.H. Bowerman, 1964, Note on an improved apparatus for soil flow measurements, Soil Sci. Soc. Am. Proc., 28: 450-453.

Ferreira, P.A., 1977, Ph.D. Dissertation, University of Arizona, Tucson, AZ, 43 p.

Gardner, W.R., 1958, Some steady-state solutions of the unsaturated moisture flow equation with application to evaporation from a water table, Soil Sci., 85: 228-232.

Greacen, E.L., 1981, Soil Water Assessment by the Neutron Probe, CSIRO, Australia, 140 p.

Green, R.E., 1962, Infiltration of water into soils as influenced by antecedent moisture, Ph.D. Thesis, Iowa State University, Ames, IA.

Hammermeister D. etal., Borehole-logging and calibration methods used in cased and uncased test holes to determine moisture and porosity profiles in the unsaturated zone, Yucca mountain, Nevada, Proc. of the NWWA Conference on the Characterization and Monitoring of the Vadose Zone, Denver, Nov. 19-21, 1985, NWWA: 542-563

Harris, K.A., 1987, Incorporation of spatial variability of mill tailing hydraulic properties into a numerical model: Implications for movement and retention of moisture, Unpublished M.S. Independent Study, Geoscience Dept., New Mexico Inst. of Mining and Tech., Socorro, NM.

Herst, W., 1986, The Borehole Infiltration Method for Determining Saturated Hydraulic Conductivity in the Vadose Zone.. A Deep Water Table Case in Low Permeable Soils, Unpublished M.S. Independent Study, Geoscience Dept., New Mexico Inst. of Mining and Tech., Socorro, NM.

Hillel, D., 1980, Fundamentals of Soil Physics, Academic Press, New York, 413 p.

Johnson, T.M., K. Cartwright, and R.M. Schuller, 1981, Monitoring of leachate migration in the unsaturated zone in the vicinity of sanitary landfills, Groundwater Monit. Rev., Fall: 55-63.

Kieft, T., 1986, personal communication on 12/86, Asst. Professor, Biology Department, New Mexico Tech, Socorro, NM.

Klute, A., 1952, A numerical method for solving the flow equation for water in unsaturated materials, Soil Sci., 73: 105-116.

Knowlton, R.G., 1984, A field study and numerical simulation of natural ground-water recharge, Unpublished M.S. Independent Study, Geoscience Dept., New Mexico Inst. of Mining and Tech., Socorro, NM.

Kool, J.B., J.C. Parker, and M.Th. van Genuchten, 1985, ONESTEP: A nonlinear parameter estimation program for evaluating soil hydraulic properties from one-step outflow experiments, Virginia Agric. Exp. Station Bull 85-3.

Larson, M.B., and D.B. Stephens, 1985, A comparison of methods to characterize unsaturated hydraulic properties of mill tailings, Proc. Seventh Symposium on Management of Uranium Mill Tailings, Low Level Waste and Hazardous Waste, Fort Collins, CO.

Liliberte, G.E., A.T. Corey, and R.H. Brooks, 1966, Properties of unsaturated porous media, Hydrology Paper No. 17, Colorado State University, Ft. Collins, CO.

Lomen, D.O., and A.W. Warrick, 1978, Linearized moisture flow with loss at the soil surface, Soil Sci. Soc. Am. J., 42: 396-400.

McCord, J., 1986, Topographic control on ground water recharge at a sandy arid site, Unpublished M.S. Independent Study, Geoscience Dept., New Mexico Inst. of Mining and Tech., Socorro, NM.

McKee, C.R., and A.C. Bumb, 1988, A three-dimensional analytical model to aid in selecting monitoring locations in the vadose zone, Groundwater Monit. Rev., Spring.

McKee, C.R., A.C. Bumb, and T.L. Dresler, 1983, A three-dimensional computer model to aid in selecting monitor locations in the vadose zone, IN Conference on Characterization and Monitoring of the Vadose Zone, Las Vegas, Dec. 8, 1983, NWWA: 133-161.

McWhorter, D.B., and J.D. Nelson, 1979, Unsaturated flow beneath tailings impoundments, J. Geotech. Eng. Div. Am. Soc. Civil Eng., 105(GT11): 1317-1334.

Miller, D.E., 1963, Lateral flow as a source of error in moisture retention studies, Soil Sci. Soc. Am. Proc., 27: 716-717.

Miller, D.E., and W.H. Gardner, 1962, Water infiltration into stratified soil, Soil Sci. Soc. Am. Proc., 26: 115-118.

Moore, I.D., and J.D. Eigel, 1981, Infiltration into two-layered soil profiles, Am. Soc. Agric. Eng. Trans., 24(6): 1496-1503.

Moore, R.E., 1939, Water conducting from shallow water tables, Hilgardia, 12: 383-426.

Morin, G.C.A., 1977, Soil moisture regimes with desert strip farming, Ph.D. Dissertation, University of Arizona, Tucson, AZ, pp. 60, 61.

Mualem, Y., 1984, Soil anisotropy of unsaturated soils, Soil Sci. Soc. Am. J., 48: 505-509.

Mualem, Y., 1976, A new model for predicting the hydraulic conductivity of unsaturated porous media, Water Resour. Res., 12(3): 513-522.

Palmquist, W.N., and A.I. Johnson, 1962, Vadose flow in layered and non-layered materials, USGS Prof. Paper, 450-C: C142-C143.

Parsons, A.M., 1988a, Field Simulation of Waste Impoundment Seepage in the Vadose Zone: Site Characterization and One-Dimensional Analytical Modeling, Unpublished Masters Independent Study, New Mexico Inst. of Mining and Tech., Socorro, NM, 165 p.

Parsons, A.M., 1988b, 9I-KB Laboratory Analysis Notebooks: Volumes I,II,III, New Mexico Tech, Socorro, NM.

Philip, J.R., 1972, Steady infiltration from buried, surface, and perched point and line sources in heterogeneous soils: I. Analysis, Soil Sci. Soc. Amer. Proc., 36: 268-273.

Philip, J.R., 1971, General theorem on steady infiltration from surface sources, with application to point and line sources, Soil Sci. Soc. Amer. Proc., 35: 867-871.

Philip, J.R., 1969, Theory of infiltration, Advan. Hydrosci., 5: 215-296.

Philip, J.R., 1968, Steady infiltration from buried point sources and spherical cavities, Water Resour. Res., 4(5): 1039-1047.

Raats, P.A.C., 1972, Steady infiltration from sources at arbitrary depth, Soil Sci. Soc. Am. Proc., 36: 399-401.

Raats, P.A.C., 1971, Steady infiltration from point sources, cavities, and basins, Soil Sci. Soc. Amer. Proc., 35: 689-694.

Raats, P.A.C., 1970, Steady infiltration from line sources and furrows, Soil Sci. Soc. Amer. Proc., 34(5): 709-714.

Routson, R.C., W.H. Price, D.J. Brown, and K.R. Fecht, 1979, High level waste leakage from the 241-T-106 tank at Hanford, Rockwell Intl. Rpt. RHO-ST-14, Richland, WA, 37 p.

Stephens, D.B., and S. Heerman, 1988, Dependence of anisotropy on saturation in a stratified sand, Water Resour. Res., 24(5): 770-778.

Stephens, D.B., 1988, personal communication on 3/10/88, Assc. Professor, Hydrology Program, New Mexico Tech, Socorro, NM.

Thomas, A.W., H.R. Duke, D.W. Zachman, and E.G. Kruse, 1976, Comparisons of calculated and measured capillary potentials from line sources, Soil Sci. Soc. Am. J., 40: 11.

van Genuchten, M.Th., 1980, A closed-from equation for predicting the hydraulic conductivity of unsaturated soil, Soil Sci. Soc. Am. J., 44: 892-898.

Vomocil, J.A., 1965, Porosity IN Methods of Soil Analysis, Part 1, 1st Edition, ed. C.A. Black, Am. Soc. of Agron. Inc., WI, 299-314.

Warrick, A.W., 1988, personal communication in 11/88, Assoc. Professor, University of Arizona, Tucson, AZ.

Warrick, A.W., 1975, Analytical solutions to the one-dimensional linearized moisture flow equation for arbitrary input, Soil Sci., 120: 79-84.

Warrick, A.W., 1974, Time-dependent linearized infiltration. 1. Point Sources, Soil Sci. Soc. Am. J., 38: 383-386.

Warrick, A.W., and D.O. Lomen, 1983, Linearized moisture flow with root extraction over two-dimensional zones, Soil Sci. Soc. Am. J., 47: 869-872.

Warrick, A.W., and D.O. Lomen, 1976, Time dependent linearized infiltration: III. Strip and disc sources, Soil Soc. Soc. Am. J., 40: 639-643.

Warrick, A.W., D.O. Lomen, and A. Amoozegar-Fard, 1980, Linearized moisture flow with root extraction for three dimensional, steady conditions, Soil Sci. Soc. Am. J., 44: 911-914.

Wooding, R.A., 1968, Steady infiltration from a shallow circular pond, Water Resour. Res., 4(6): 1259-1273.

Youngs, E.G., 1964, An infiltration method of measuring the hydraulic conductivity of unsaturated porous materials, Soil Sci., 109: 307-311.

LIST OF APPENDICES

Appendix A. Program TRANS.FOR

```
C     ------------------
        PROGRAM DRIP
C     ------------------

C     THIS PROGRAM WAS MODIFIED ON 9-10-88
C     S.T. TO REDUCE COMPUTER TIME
C     MODIFIED AGAIN TO INCORPORATE ANISOTROPIC BEHAVIOR
C     ON 11-10-88
C
C     THIS PROGRAM WILL COMPUTE THE MOISTURE CONTENT FIELD CROSS
C     SECTIONS FOR THE 441 EMITTERS SPACED FOR OUR EXPERIMENT.
C     IT USES SUPERPOSITION TO TAKE INTO THE ACCOUNT THE EFFECT
C     OF EACH OF THE EMITTERS.


        DIMENSION R(10000), V(10000)
        REAL KO,KH,KZ

C     READS INPUT FROM FILE CALLED INDRIP.DAT

        OPEN(UNIT=20, FILE='INDRIP.DAT', STATUS='OLD')
        READ (20,*) SMT
        READ (20,*) SMK
        READ (20,*) Q
        READ (20,*) KO
        READ (20,*) ALPHA
        READ (20,*) KH
        READ (20,*) KZ

        READ (20,*) THETAR
        READ (20,*) THETAS
        READ (20,*) VANN
        READ (20,*) VANA

C     THE INPUT KO IS DETERMINED FROM THE RELATIVE K-PSI CURVE
        KO = KO * KH

C     ECHOS THE INPUT DATA
        WRITE(*,*) 'T,k,Q,KO,ALPHA',SMT,SMK,Q,KO,ALPHA

C     SETS REAL SPACE COORDINATES

        DO 30 RZ = .05,10,.5
C         RESETS THE REPEAT COUNTER
          NCNT = 0
          DO 40 RX = 0,15,.5
              SUMPHI = 0

C           SETS EMITTER COORDINATES
              DO 50 TX = -5,5,.5
                DO 60 TY = 0,5,.5
C                   COMPUTES THE DIST BETWEEN EMITTER AND
C                       REAL SPACE
                    DIST = SQRT((TX - RX)**2 + (TY - 0)**2)
```

```
C                    CHECKS TO SEE IF THE PROGRAM HAS
C                    MADE THIS CALCULATION EARLIER FOR THIS DEPTH
                     DO 65 I = 1,NCNT
                         IF (DIST .EQ. R(I))THEN
                           SMPHI = V(I)
                           GO TO 67
                         ENDIF
 65                   CONTINUE

C                    IF NOT IT CALCULATES THE NEW SMPHI
                     IF(SMT .EQ. 100000)THEN
                      CALL STDYPT(DIST,RZ,SMPHI,Q,KO,ALPHA,KH,KZ)
                     ELSE
                      CALL TRANPT(DIST,RZ,SMT,PHIDM,SMPHI,PSI,SMK,
     *                      Q,KO,ALPHA,KH,KZ)
                     ENDIF

                     R(NCNT+1) = DIST
                     V(NCNT+1) = SMPHI
                          NCNT = NCNT + 1
 67                   CONTINUE

                     IF(TY .NE. 0) SMPHI = 2*SMPHI
                     SUMPHI = SUMPHI + SMPHI
 60                 CONTINUE
 50             CONTINUE
                    write(*,*) 'X=',RX,'Z=',RZ,' IS FINISHED'
C      COMPUTES PSI VALUE
       IF(SUMPHI .EQ. 0)THEN
         PSI = -150
       ELSE
         PSI = ALOG(SUMPHI*ALPHA/KO)/ALPHA
       ENDIF
         WRITE (95,*) 15+RX,-RZ-.86,PSI
         WRITE (95,*) 15-RX,-RZ-.86,PSI

C    CALCULATES THE VOL. MOISTURE CONTENT
       VANM = 1 - 1/VANN
       XTEMP = VANA*PSI*(-1)
       IF(XTEMP .LE. 0)GOTO 40
       BOT = (1+ (VANA*PSI*(-100))**VANN)**VANM
       THETA = THETAR + (THETAS - THETAR)/BOT

       WRITE (96,*) 15+RX,-RZ-.86,THETA
       WRITE (96,*) 15-RX,-RZ-.86,THETA

 40      CONTINUE

C        RESETS THE REPEAT VALUES
         DO 45 I = 1,NCNT
          V(I) = 0
          R(I) = 0
 45      CONTINUE
```

```
30     CONTINUE

       STOP
       END
```

```
C     ************************************************************

        SUBROUTINE TRANPT(SMR,SMZ,SMT,PHIDM,SMPHI,PSI,SMK,Q,KO,
       *                  ALPHA,KH,KZ)
C     ************************************************************


C     REFERENCE
C     'TIME-DEPENDENT LINEARIZED INFILTRATION.
C        I. POINT SOURCES'
C     A.W.WARRICK
C     SSSAJ (38) 74 P383-386
C     EQ 13 AND EQ 16

        REAL KO,KH,KZ
        DIMENSION F(1001)
        PI = 3.1415927

C     SETS DIMENSIONLESS VARIABLES AND ANISOTROPIC RATIO
        R = SMR*ALPHA*SQRT(KZ/KH)/2
        Z = SMZ*ALPHA/2
        T = SMT*SMK*ALPHA*(KZ/KH)/4

        IF (R+Z .EQ. 0) GOTO 51

C     SOLVES EQ 13 FOR THE BURIED SOURCE
        CALL PHIB(R,Z,T,ANS)
        PBUR = ANS

C     SOLVES INTERGRATION OF EQ 16
C     LIMITS = DIMENSIONLESS Z TO INFINITY (IE. 100)
C     DISCRETIZATION = 1000

        ZBIG = 40
        DELZ = (ZBIG - Z)/1000
        I = 0
        DO 10 A = Z, ZBIG, DELZ
          I = I + 1
          CALL PHIB(R,A,T,ANS)

C         CHECKS LIMITS OF EXPONENTAL VARIABLE
C         IF LESS THAN -70 SETS EXP(X) = 0
          IF (-2*A .LT. -81)THEN
              F(I) = 0
          ELSE
              F(I) = EXP(-2*A)*ANS
          ENDIF

   10           CONTINUE

C     SOLVES THE INTERGAL BY THE TRAPIZOIDAL RULE

        SUM = 0
```

```
      DO 20 J = 1,(I-1)
        AVE = (F(J) + F(J+1))/2*delz
        SUM = SUM + AVE
 20    CONTINUE

      ANS = SUM
      PHIDM = 2*(PBUR - EXP(2*Z)*ANS)


      SMPHI = PHIDM*ALPHA*Q/(8*PI)
c    PSI    = ALOG(SMPHI*ALPHA/KO)/ALPHA


 51    CONTINUE

      RETURN
      END
```

```
C    ****************************
       SUBROUTINE PHIB(R,Z,T,ANS)
C    ****************************

C    SOLVES EQ. 13 FOR BURIED PHI

       RHO = SQRT(R**2 + Z**2)
       SRT = SQRT(T)

C    IF STATEMENT CHECKS LIMIT OF EXPONENTIAL
C       IF X > 70 ERFC = 0 TEMP1 = 0
C       IF X <-70 EXP = 0  TEMP2 = 0
C        THUS ANS = 0

       IF (RHO .GT. 70)THEN
         ANS = 0
       ELSE
         X = RHO/(2*SRT) + SRT
         CALL ERF(X,ERFN)
         ERFC = 1 - ERFN
         TEMP1 = EXP(RHO)*ERFC
         X = RHO/(2*SRT) - SRT
         CALL ERF(X,ERFN)
         ERFC = 1 - ERFN
         TEMP2 = EXP(-RHO)*ERFC
         ANS = EXP(Z)/(2*RHO) *(TEMP1 + TEMP2)
       ENDIF

       RETURN
       END
```

```
C     ********************
        SUBROUTINE ERF(W,ER)
C     ********************

C     THIS PART OF THE CODE HAS BEEN MODIFIED TO ACCEPT INPUT
C     TO THE ERROR FUNCTION FROM NEGITIVE AND POSITIVE INFINITY

        X = W
        IF (X .EQ. 0)THEN
          SIGN = 1
        ELSE
          SIGN = X/ABS(X)
        ENDIF

        X = ABS(X)

C     REFERENCE
C     ABRAMOWITZ AND STEGUN 1964
C     EQ. 7.1.26

        P =  0.3275911
        A1=  0.254829592
        A2= -0.284496736
        A3=  1.421413741
        A4= -1.453152027
        A5=  1.061405429

        T = 1/(1+P*X)
        TEMP = A1*T + A2*T**2 + A3*T**3 +A4*T**4 + A5*T**5
        DUM = -(X**2)
        IF(DUM .LT. -70)THEN
          ER = 1
        ELSE
          ER = 1 - TEMP*EXP(DUM)
        ENDIF

        ER = SIGN*ER

        RETURN
        END
```

```
C     ********************************************************
      SUBROUTINE STDYPT(SMRR,SMZR,SMPHI,Q,KO,ALPHA,HCONR,HCONZ)
C     ********************************************************


C     A.W. WARRICK
C     SSSAP VOL 38  1974
C     P 383-386
c     'TIME-DEPENDENT LINEARIZED INFILTRATION
C     I. POINT SOURCES'

C     EQUATION 18
      real ko

c     RESETS REAL COORDINATES
      smr = smrr
      smz = smzr

c     SETS DIMENSIONLESS AND ANISOTROPIC COORDINATES
      r = alpha*sqrt(hconz/hconr)*smr/2
      z = alpha*smz/2

      RHO = sqrt(R**2 + Z**2)
      if(rho .eq. 0.0)goto 20
      X = Z + RHO
      if (x .gt. 88)goto 20

      IF (X .LT. 1.0)THEN
        CALL ESMALL(X,ANS)
      ELSE
        CALL EBIG(X,ANS)
      ENDIF

      if(2*z .gt. 88)then
        temp2 = 3.4e38
      else
        temp2 = exp(2*z)*ans
      endif


      TEMP1 = EXP(Z - RHO)/RHO
      PHI = 2*(TEMP1 - TEMP2)

      smphi = phi*alpha*q/(8*3.1416)
 20     CONTINUE
      end
```

```
C     ************************
        SUBROUTINE ESMALL(X,ANS)
C     ************************

C     REFERENCE ABRAMOWITZ AND STEGUN
C     EQ. 5.1.53
C     0<X<1

        TEMP1 = -0.57721566 + 0.99999193*X - 0.24991055*X**2
        TEMP2 =  0.05519968*X**3 - 0.00976004*X**4
        TEMP3 =  0.00107857*X**5

        ANS   = (TEMP1 + TEMP2 + TEMP3) - ALOG(X)

        RETURN
        END
```

```
C     **********************
        SUBROUTINE EBIG(X,ANS)
C     **********************

c     REFERENCE ABRAMOWITZ AND STEGUN
c     EQ.  5.1.54
c     1<X<1000000

        TEMP1 = X**2 + 2.334733*X + 0.250621
        TEMP2 = X**2 + 3.330657*X + 1.681534

        ANS   = (TEMP1/TEMP2)/(X*EXP(X))

        RETURN
        END
```

```
153          :TIME (DAYS)
4.17         :SMALL k (M/D)
.00196       :Q PER EMITTER (M3/D)
1            :Ko INTERCEPT OF REGRESSION (M/D)
3.71         :ALPHA SLOPE OF REGRESSION (1/M)
.35          :Kh HORIZONTAL CONDUCTIVITY (M/D)
.0071        :Kz VERTICAL CONDUCTIVITY (M/D)
11.7         :RESIDUAL MOISTURE CONTENT (V/V %)
37.7         :SATURATED MOISTURE CONTENT (V/V %)
1.61         :vAN GENUCTEN n
0.068        :vAN GENUCTEN ALPHA
```

Appendix B. Verification of Coordinate Transformations of an Anisotropic Media to Obtain an Equivalent Isotropic Media.

Richard's Equation:

$$\partial\theta/\partial t = \nabla\circ(K(\psi)\nabla\psi) - \partial K(\psi)/\partial z' \tag{1}$$

expands to:

$$\partial\theta/\partial t = \partial/\partial x'\left(K_x(\psi)\partial\psi/\partial x' \right) + \partial/\partial y'\left(K_y(\psi)\partial\psi/\partial y' \right) + \partial/\partial z'\left(K_z(\psi)\partial\psi/\partial z' \right) - \partial K_z(\psi)/\partial z' \tag{2}$$

where x', y', z' are the anisotropic media coordinates and x, y, z are the equivalent isotropic media coordinates.

The coordinate transformations after McKee and Bumb (1988) are:

$$x = x'\{K_y(\psi)/K_x(\psi)\}^{1/4} \tag{3}$$

$$y = y'\{K_x(\psi)/K_y(\psi)\}^{1/4} \tag{4}$$

$$z = z'\{\sqrt{K_x(\psi)K_y(\psi)}/K_z(\psi)\}^{1/2} \tag{5}$$

$$\alpha = \alpha'\{K_z(\psi)/\sqrt{K_x(\psi)K_y(\psi)}\}^{1/2} \tag{6}$$

The derivatives of the space coordinates for equations 3 to 5 become:

$$\partial/\partial x = [\{K_y(\psi)/K_x(\psi)\}^{1/4}]\partial/\partial x' \tag{7}$$

$$\partial/\partial y = [\{K_x(\psi)/K_y(\psi)\}^{1/4}]\partial/\partial y' \tag{8}$$

$$\partial/\partial z = [\{\sqrt{K_x(\psi)K_y(\psi)}/K_z(\psi)\}^{1/2}]\partial/\partial z' \tag{9}$$

Substituting equations 7 through 9 into equation 2:

$$\partial\theta/\partial t = \partial/\partial x\{\sqrt{K_x(\psi)K_y(\psi)}\ \partial\psi/\partial x\} + \partial/\partial y\{\sqrt{K_x(\psi)K_y(\psi)}\ \partial\psi/\partial y\} + \partial/\partial z\{\sqrt{K_x(\psi)K_y(\psi)}\ \partial\psi/\partial z\} - [\{\sqrt{K_x(\psi)K_y(\psi)}/K_z(\psi)\}^{1/2}]\partial K_z(\psi)/\partial z \tag{10}$$

Defining the matric flux potential and its derivative as:

$$\phi = \int_{-\infty}^{\psi} K_H(h)\,dh \tag{11}$$

$$\partial\phi/\partial\psi = \partial/\partial\psi \int_{-\infty}^{\psi} K_H(h)\,dh \tag{12}$$

where

$$K_H(\psi) = K_{H0}e^{(\alpha'\psi)} \tag{13}$$

and

$$K_{H0} = \sqrt{K_{X0}K_{Y0}} \tag{14}$$

Substituting equations 13 and 14 into equation 12:

$$\partial\phi/\partial\psi = K_H(\psi) \tag{15}$$

Rearranging:

$$\partial\phi = K_H(\psi)\partial\psi = \sqrt{K_X(\psi)K_Y(\psi)}\ \partial\psi \tag{16}$$

Substituting equation 16 into equation 10:

$$\partial\theta/\partial t = \partial^2\phi/\partial x^2 + \partial^2\phi/\partial y^2 + \partial^2\phi/\partial z^2 - [\{\sqrt{K_X(\psi)K_Y(\psi)}/K_Z(\psi)\}^{1/2}]\ \partial K_Z(\psi)/\partial z \tag{17}$$

Substituting equation 13 into equation 11:

$$\phi = \int_{-\infty}^{\psi} K_{H0}e^{(\alpha'h)}\,dh \tag{18}$$

$$\phi = 1/\alpha'\{K_{H0}e^{(\alpha'h)}\}\Big|_{-\infty}^{\psi} \tag{19}$$

$$\phi = 1/\alpha'\{K_{H0}e^{(\alpha'\psi)}\} \tag{20}$$

$$\phi = 1/\alpha'\{K_{H0}e^{(\alpha'\psi)}\}K_{Z0}/K_{Z0} \tag{21}$$

$$\phi = 1/\alpha'\{K_{H0}/K_{Z0}\}K_{Z0}e^{(\alpha'\psi)} = 1/\alpha'(K_{H0}/K_{Z0})K_Z(\psi) \tag{22}$$

Solving for $K_Z(\psi)$:

$$K_Z(\psi) = \phi\alpha' K_{Z0}/K_{H0} \tag{23}$$

Substituting equation 23 into equation 17:

$$\partial\theta/\partial t = \partial^2\phi/\partial x^2 + \partial^2\phi/\partial y^2 + \partial^2\phi/\partial z^2 - \{\sqrt{K_x(\psi)K_y(\psi)}/K_z(\psi)\}^{1/2}\partial/\partial z\{\alpha'\phi K_{z0}/K_{H0}\} \quad (24)$$

Substituting equation 6 into equation 24:

$$\partial\theta/\partial t = \nabla^2\phi - \{\sqrt{K_x(\psi)K_y(\psi)}/K_z(\psi)\}^{1/2}\{K_{z0}/\sqrt{K_{x0}K_{y0}}\}\{\sqrt{K_x(\psi)K_y(\psi)}/K_z(\psi)\}^{1/2}\alpha\partial\phi/\partial z \quad (25)$$

Simplifying equation 25 to an isotropic non-linear moisture flow equation (Equation 3, Warrick, 1974) used to develop point source solutions:

$$\partial\theta/\partial t = \nabla^2\phi - \alpha\,\partial\phi/\partial z \quad (26)$$

BOREHOLE GEOLOGIC LOG

LOCATION: 15-2
DATUM EL: 1417.45
GND SURFACE EL: 1417.10

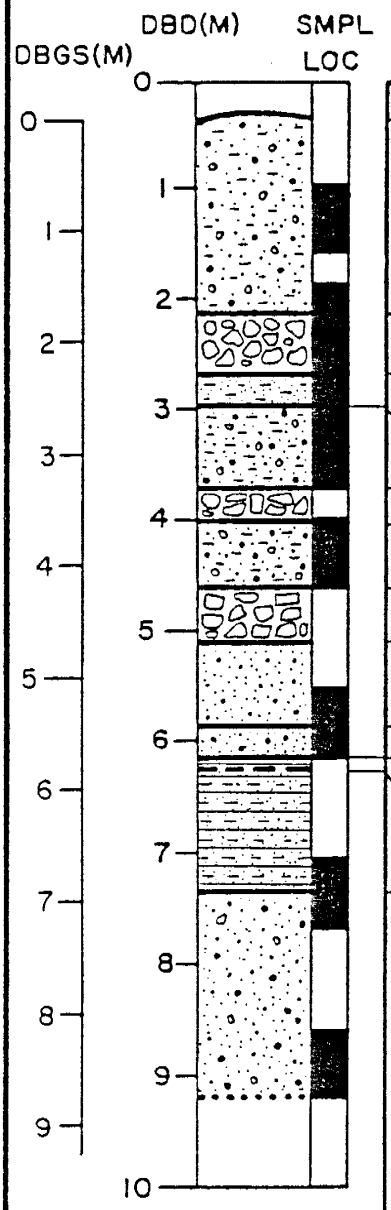

DESCRIPTION

Red brown fine-coarse sand, silt, 40% angular fine-medium pebbles

Cobbles

Red brown fine sand, silt

Poorly sorted red brown angular fine-coarse sand, silt, 30% subrounded medium-coarse pebbles

Cobbles

Poorly sorted red brown angular fine-coarse sand, silt, 30% subrounded medium-coarse pebbles

Cobbles

Clean yellow fine-medium sand

Tan fine-coarse sand

Green clay

Green fine sand, silt, clay

Tan fine-coarse sand, 5% rounded fine and coarse pebbles

BOREHOLE GEOLOGIC LOG

LOCATION: 15-6
DATUM EL: 1417.45
GND SURFACE EL: 1417.16

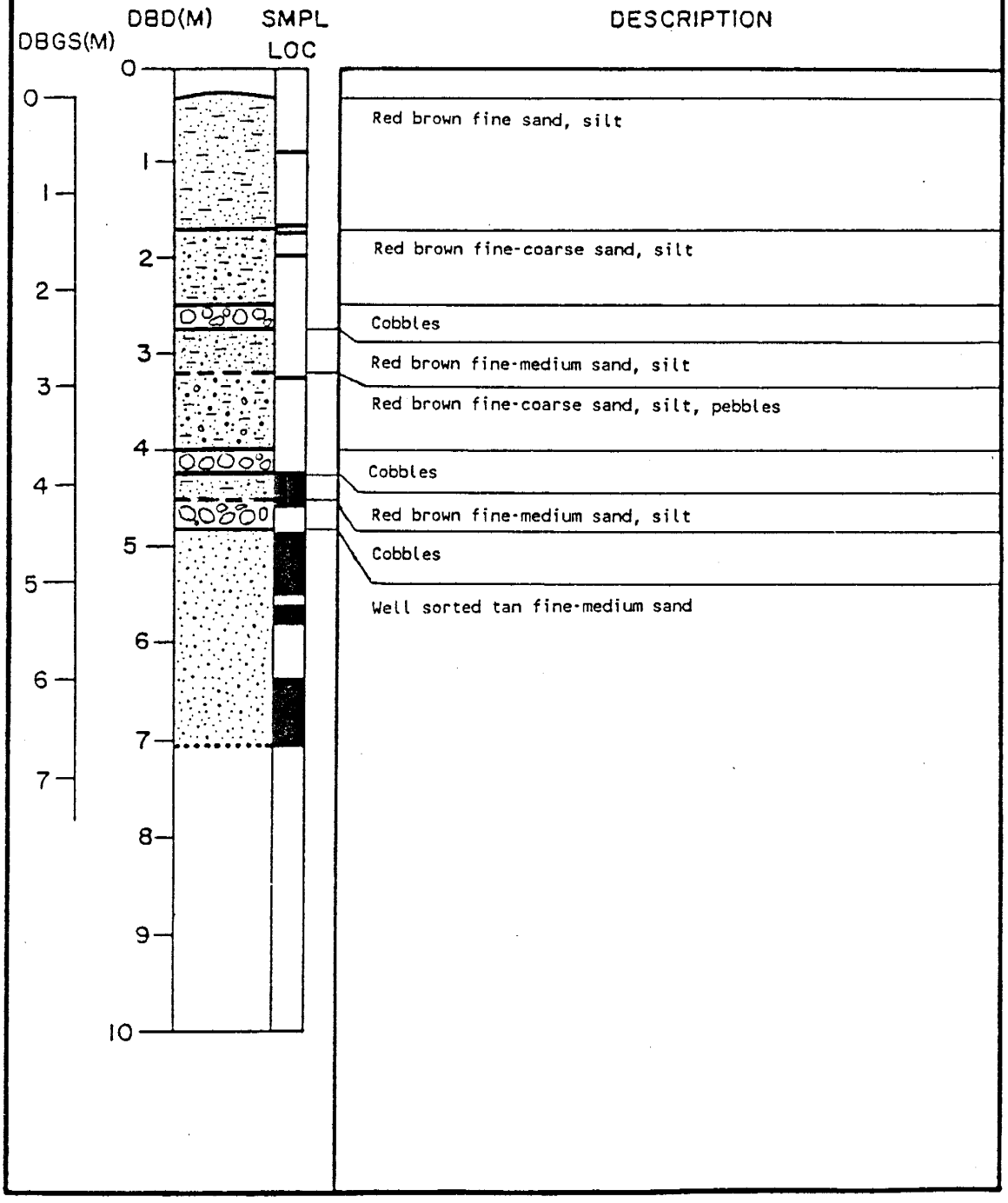

BOREHOLE GEOLOGIC LOG

LOCATION: 15-8
DATUM EL: 1417.45
GND SURFACE EL: 1417.18

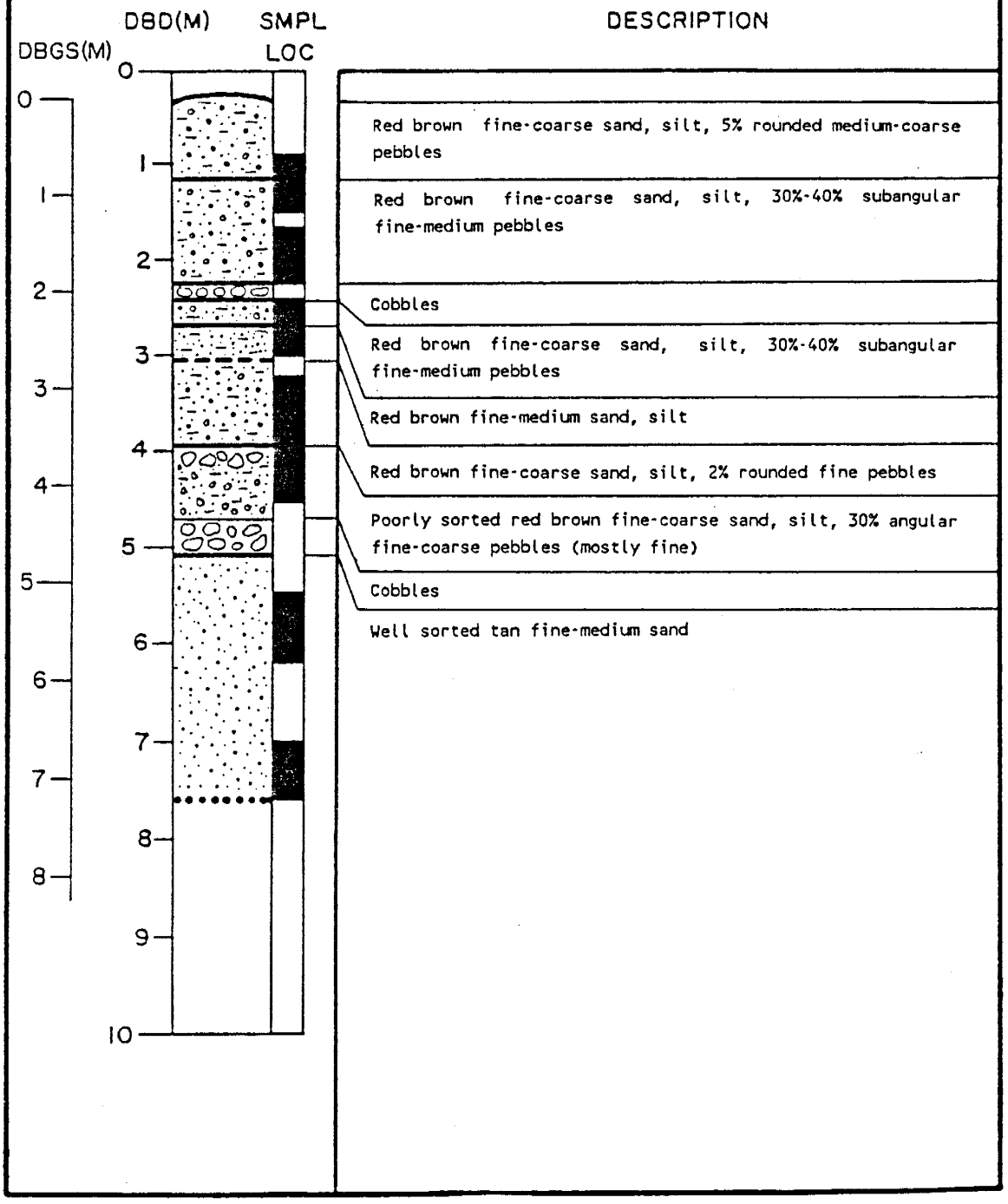

BOREHOLE GEOLOGIC LOG

LOCATION: 15-15
DATUM EL: 1417.45
GND SURFACE EL: 1416.59

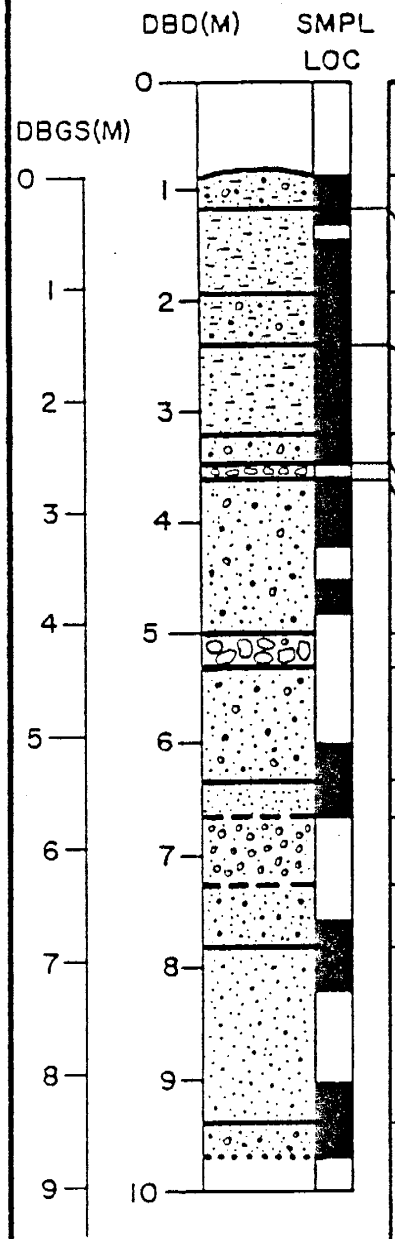

DESCRIPTION

Red brown fine-coarse angular sand, silt, 10% angular fine-medium pebbles

Red brown fine sand, silt

Red brown fine-coarse sand, silt, 5% rounded and angular medium pebbles

Red brown fine-medium sand, silt

Poorly sorted red brown fine-coarse sand, 20% rounded fine-coarse pebbles

Cobbles

Poorly sorted tan fine-coarse sand, 10-20% rounded fine-coarse pebbles

Cobbles

Poorly sorted tan fine-coarse sand, 10-20% rounded fine-coarse pebbles

Well sorted tan fine sand

Pebbles

Poorly sorted orange fine-coarse sand

Clean tan fine-medium subangular sand

Poorly sorted tan fine-coarse sand, 10% fine-coarse angular pebbles

BOREHOLE GEOLOGIC LOG

LOCATION: 15-22
DATUM EL: 1417.45
GND SURFACE EL: 1417.06

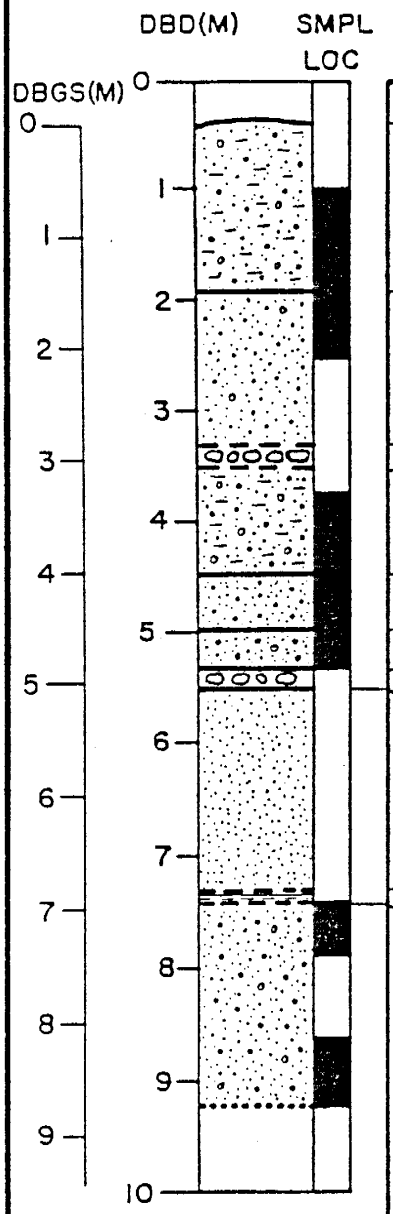

DESCRIPTION

Red brown fine-coarse sand, silt, 5% subrounded fine pebbles

Red brown fine-medium sand, 1% coarse pebbles

Cobbles

Poorly sorted red brown angular fine-coarse sand, silt, 20% rounded fine-coarse pebbles

Well sorted tan fine-medium sand

Tan fine-coarse sand, 2% subangular fine pebbles

Cobbles

Tan fine sand

Green clay

Poorly sorted tan fine-coarse subangular sand, 5% angular fine pebbles

BOREHOLE GEOLOGIC LOG

LOCATION: 15-23
DATUM EL: 1417.45
GND SURFACE EL: 1417.06

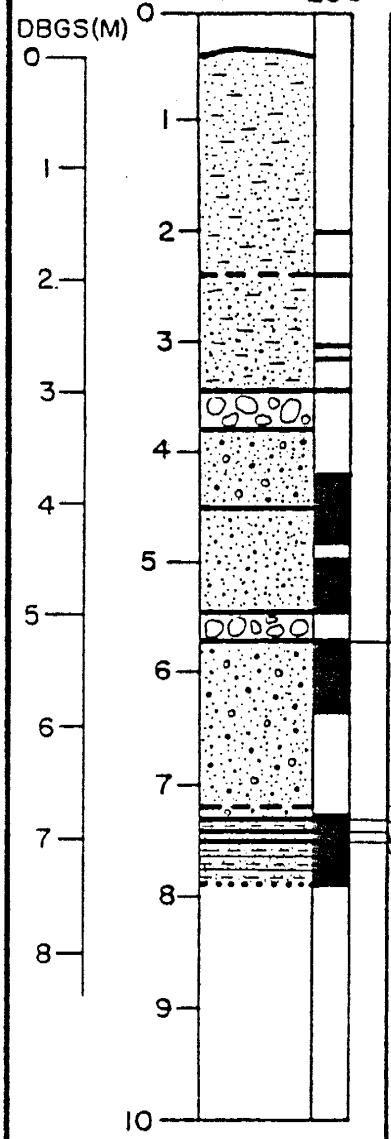

DESCRIPTION

Red brown fine sand, silt

Red brown fine-medium sand, silt

Cobbles

Clean brown subangular fine-coarse sand, 20% rounded fine-medium pebbles

Well sorted tan fine-medium sand

Cobbles

Poorly sorted tan subangular fine-coarse sand, 20% rounded fine-medium pebbles

Orange fine-coarse sand, 5% rounded fine pebbles

Green clay, orange fine sand, silt

Orange fine-coarse sand, silt, green clay, 5% fine pebbles

Green clay, fine-medium orange sand

BOREHOLE GEOLOGIC LOG

LOCATION: 15-28
DATUM EL: 1417.45
GND SURFACE EL: 1417.10

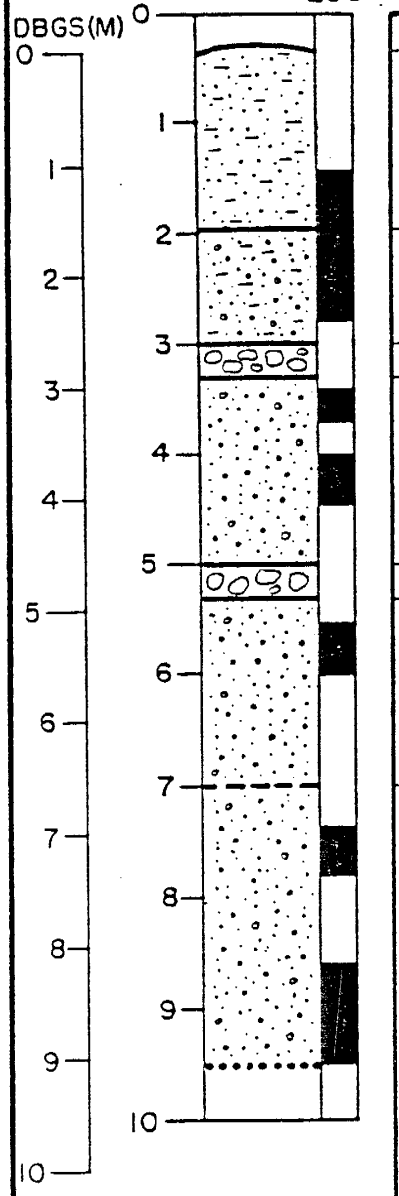

DESCRIPTION
Red brown fine-medium sand, silt
Red brown fine-coarse sand, silt, 5% subrounded fine pebbles
Cobbles
Poorly sorted tan subangular fine-coarse sand, 10% subangular fine pebbles
Cobbles
Poorly sorted tan subangular fine-coarse sand, 10% subangular fine pebbles
Poorly sorted tan fine-coarse sand, 5% rounded fine pebbles

BOREHOLE GEOLOGIC LOG

LOCATION: 2-15
DATUM EL: 1417.45
GND SURFACE EL: 1417.18

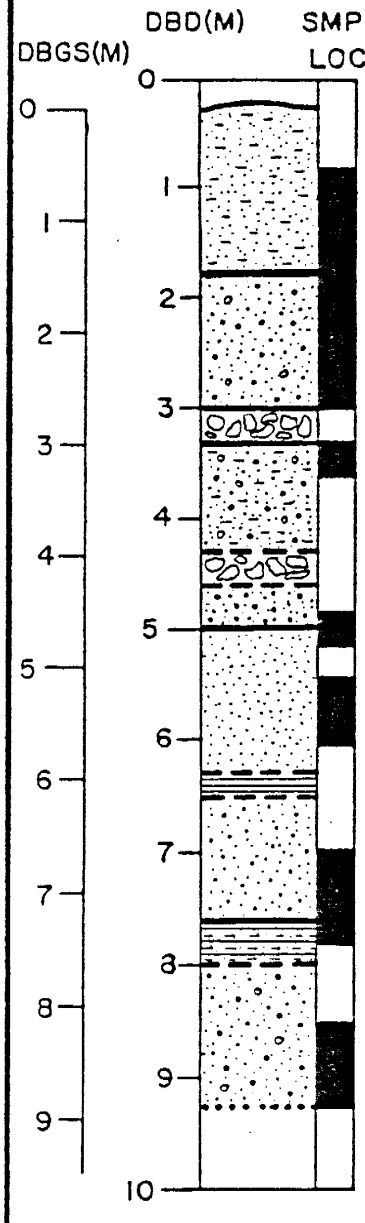

DESCRIPTION

Red brown fine sand, silt

Red brown fine-coarse sand, 10% subangular fine-medium pebbles

Cobbles

Red brown fine-coarse sand, 25% rounded medium-coarse pebbles, silt

Cobbles

Clean yellow subangular fine-coarse sand (mostly coarse)

Well sorted tan fine sand

Green clay

Well sorted tan fine-medium sand

Orange clay, silt, fine sand

Poorly sorted tan subangular fine-coarse sand, 10% fine-medium pebbles

BOREHOLE GEOLOGIC LOG

LOCATION: 6-15
DATUM EL: 1417.45
GND SURFACE EL: 1417.16

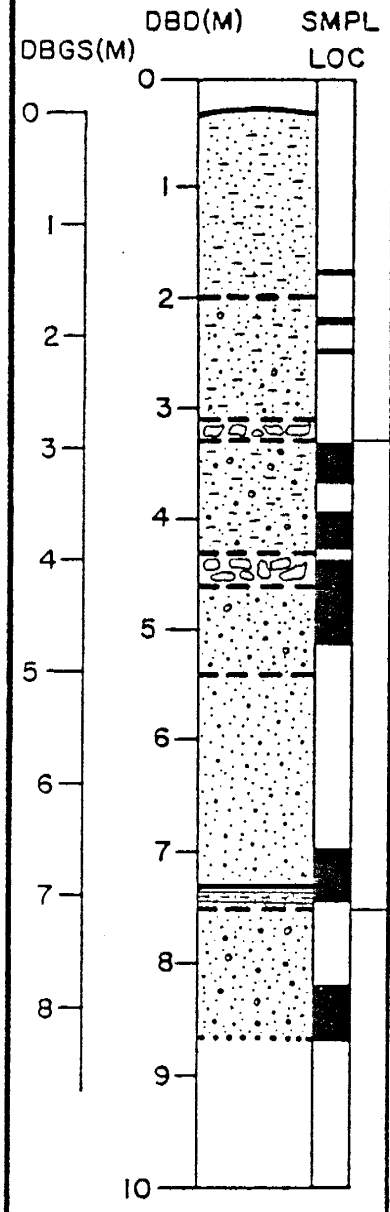

DESCRIPTION

Red brown fine sand, silt

Red brown fine-medium sand, silt, 3% angular fine-medium pebbles

Cobbles

Poorly sorted red brown subangular fine-coarse sand, silt 20% rounded fine-coarse pebbles

Cobbles

Poorly sorted tan subangular fine-coarse sand, 2% rounded medium pebbles

Well sorted tan fine-medium sand

Green clay, silt, fine sand

Poorly sorted tan fine-coarse sand, 15% rounded medium-coarse pebbles

BOREHOLE GEOLOGIC LOG

LOCATION: 8-15
DATUM EL: 1417.45
GND SURFACE EL: 1417.24

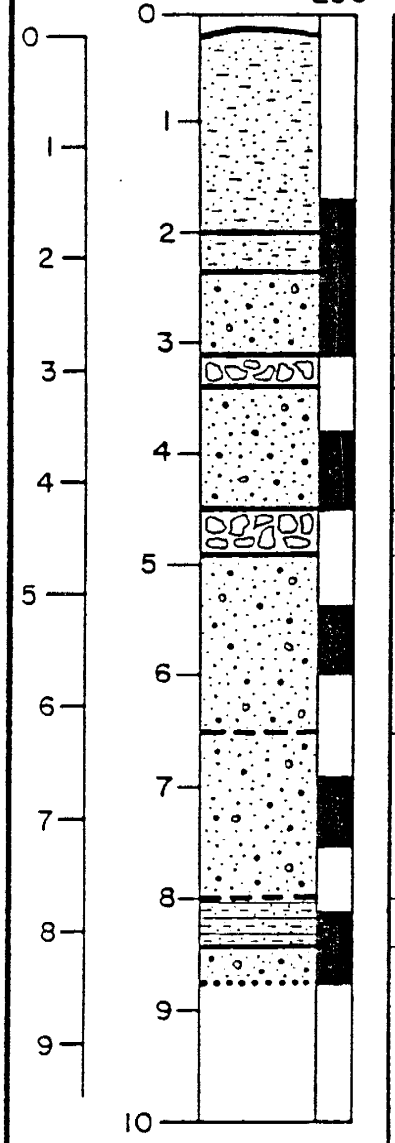

DESCRIPTION
Red brown fine sand, silt
Tan-brown fine-medium sand, silt
Red brown fine-coarse sand, 10% angular medium pebbles
Cobbles
Poorly sorted red brown subangular fine-coarse sand, 5% angular medium pebbles
Cobbles
Dark subangular - coarse sand, fine-medium sand, 10% rounded very coarse pebbles
Poorly sorted tan fine-coarse sand, 5% pebbles
Green clay, silt, fine-medium sand
Poorly sorted tan fine-coarse sand, 3% rounded fine pebbles

BOREHOLE GEOLOGIC LOG

LOCATION: 22-15
DATUM EL: 1417.45
GND SURFACE EL: 1416.92

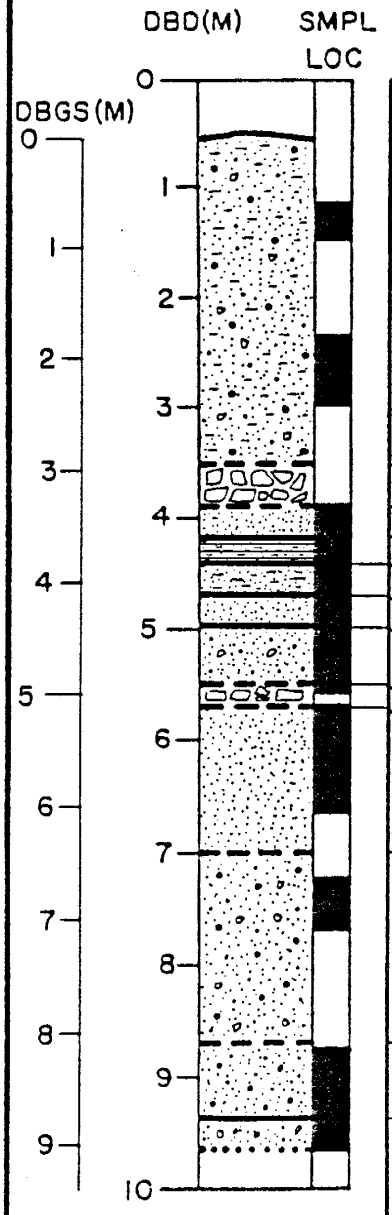

DESCRIPTION

Red brown fine-coarse sand, silt, 10% subangular pebbles

Cobbles

Well sorted tan fine sand

Green clay, tan fine sand, silt

Orange fine sand, silt

Well sorted tan fine sand

Poorly sorted tan fine-medium sand, 2% fine rounded pebbles

Cobbles

Well sorted tan fine sand

Poorly sorted fine-coarse tan sand, 20% rounded medium pebbles

Tan fine-coarse sand

Poorly sorted tan subangular fine-coarse sand, 15% subangular medium-coarse pebbles

BOREHOLE GEOLOGIC LOG

LOCATION: 28-15
DATUM EL: 1417.45
GND SURFACE EL: 1416.80

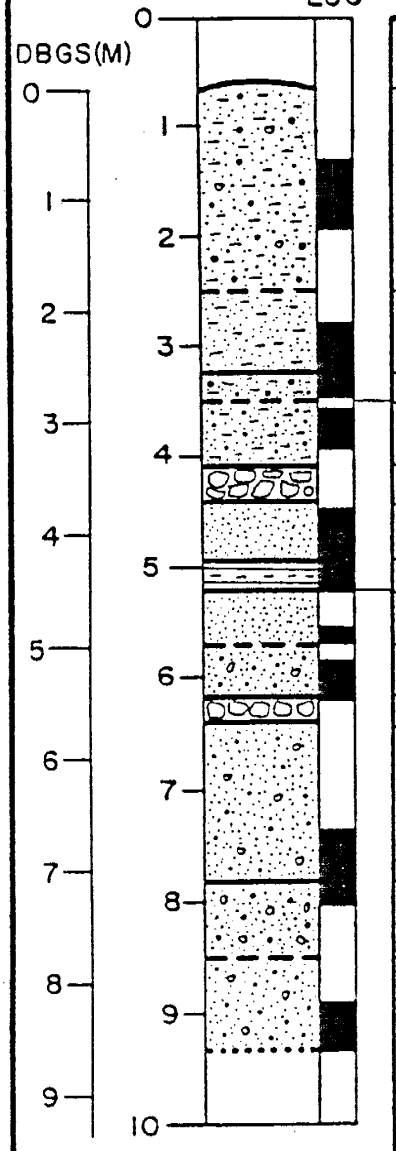

DESCRIPTION

Red brown fine-coarse sand, silt, 10% rounded fine-coarse pebbles

Red brown fine sand, silt

Red brown fine-coarse sand, silt

Red brown fine-medium sand, silt

Cobbles

Well sorted tan fine sand

Buff clay, silt

Well sorted tan fine sand

Tan subangular fine-medium sand, 5% rounded fine pebbles

Cobbles

Tan subangular fine-medium sand, 5% rounded fine pebbles

Tan angular fine-coarse sand, 25% angular and rounded medium pebbles

Tan subangular fine-medium sand, 5% rounded fine pebbles

APPENDIX D. HYDRAULIC PROPERTIES AND PARAMETERS

THETA sat = SATURATED MOISTURE CONTENT
THETA 15-bar = 15 BAR MOISTURE CONTENT
Ksat = SATURATED HYDRAULIC CONDUCTIVITY
ALPHAv, Nv = VAN GENUCHTEN FITTING PARAMETERS

PIEDMONT SLOPE FACIES SAMPLES NEAR THE IRRIGATION PLOT

SAMPLE LABEL	DBD (M)	THETA SAT. (%vol)	THETA 15-bar (%vol)	Ksat (m/day)	ALPHAv (1/cm)	Nv (-)
6-15-H9H	1.74	50.4	19.7	0.22	0.036	1.33
6-15-A8	2.15	43.6	17.6	0.85	0.048	1.27
6-15-A9	2.24	34.6		190.08	0.063	2.11
6-15-A3	2.47	34.3		1.47	0.106	1.98
8-16-B17	1.84	46.1	16.0	0.35	0.029	1.35
8-16-H15	1.99	47.9	7.4	1.90	0.059	1.26
8-16-H1	2.12	37.3	14.3	1.47	0.067	1.27
8-16-H13H	2.17	44.2	10.4	2.25	0.064	1.42
8-16-18CH	2.62	42.0	9.7	2.85	0.095	1.23
8-16-H5H	2.90	40.9		8.64	0.068	3.34
8-16-A14	3.03	36.9		15.55	0.068	2.66
11-15-A22H	1.26	36.2	23.6			
11-15-H8	1.56	37.8		0.11	0.038	1.86
11-15-H16	2.21	42.2		46.66	0.054	3.57
14-15-11C	1.27	34.1		5.27	0.284	1.59
14-15-H17	1.49	44.3	15.7	0.49	0.022	1.44
14-15-H22	1.81	44.6	27.3	0.01	0.048	1.17
14-15-H23	2.11	33.5	8.8	25.92	0.578	1.19
14-15-15C	2.64	33.8	14.3	9.50	0.029	1.16
14-15-A20	3.18	30.3	8.8	30.24	0.224	1.26
15-5-B13	1.41	50.3	13.7	55.30	2.454	1.10
15-5-A10H	1.69	51.1	11.5	2.51	0.267	1.21
15-5-B22	1.79	51.3	11.8	1.64	0.135	1.19
15-7.5-3C	2.87	50.1	10.2	6.39	0.037	1.52
5-7.5-H10	3.08	41.2	8.0	9.50	0.110	1.33
5-7.5-21C	3.13	45.7	5.7	13.82	0.037	1.94
5-11-H17H	1.16	44.5		21.60	0.042	1.89
15-11-B15	1.46	44.8		0.10	0.016	3.79
15-11-H12	1.96	46.3		0.14	0.022	2.76
15-19-B4	1.46	41.7		1.99	0.043	1.72
15-19-H18	1.78	46.0		4.75	0.024	2.42
15-19-A20	2.17	41.5		29.38	0.027	2.32
15-19-A1H	2.32	46.2		1.30	0.030	1.51
15-19-B7H	2.72	48.5		6.13	0.085	1.49
16-6-A1H	1.05	48.5	12.6			
16-6-B7H	1.33	41.6	11.5	0.60	0.182	1.19
16-6-B21H	1.64	45.7	10.7	0.80	0.206	1.09
16-6-B24	1.94	43.9	12.0	0.30	0.335	1.11
16-16-H11	1.00	39.7		24.19	0.068	2.56
16-16-B15	1.06	29.2	6.2	2.42	0.072	1.52
16-23-B20	1.68	57.6	13.5	0.20	0.037	1.12
6-23-B10H	1.76	49.2		3.46	0.033	1.83

APPENDIX D. HYDRAULIC PROPERTIES AND PARAMETERS

THETA sat = SATURATED MOISTURE CONTENT
THETA 15-bar = 15 BAR MOISTURE CONTENT
Ksat = SATURATED HYDRAULIC CONDUCTIVITY
ALPHAv, Nv = VAN GENUCHTEN FITTING PARAMETERS

PIEDMONT SLOPE FACIES SAMPLES NEAR THE IRRIGATION PLOT

SAMPLE LABEL	DBD (M)	THETA SAT. (%vol)	THETA 15-bar (%vol)	Ksat (m/day)	ALPHAv (1/cm)	Nv (-)
16-23-B4	2.24	44.5	11.8	1.30	0.075	1.16
16-23-B11	2.54	43.0	8.2	11.23	0.037	1.23
16-23-B12	2.84	39.3	9.9	4.41	0.038	1.34
16-23-B14	3.59	41.4		5.18	0.043	2.22
19-15-H6	1.30	31.0				
19-15-A16	1.36	39.5		371.52		
19-15-B8	1.51	37.8		0.42	0.049	2.27
NUMBER OF VALUES		49	28	46	45	45
GEOMETRIC MEAN		37.7	11.7	2.87	0.068	1.61

Appendix E. Effective ψ, η, and K Data

PSI (M)	THETA (V/V)	HYDRO. COND. (M/D)
0.00	0.3770	2.9E+00
0.05	0.3615	7.3E-01
0.10	0.3379	2.8E-01
0.15	0.3158	1.3E-01
0.20	0.2970	6.5E-02
0.25	0.2815	3.6E-02
0.30	0.2687	2.1E-02
0.35	0.2580	1.4E-02
0.40	0.2489	9.1E-03
0.45	0.2411	6.3E-03
0.50	0.2344	4.5E-03
0.55	0.2285	3.3E-03
0.60	0.2233	2.5E-03
0.65	0.2187	1.9E-03
0.70	0.2146	1.5E-03
0.75	0.2108	1.2E-03
0.80	0.2075	9.5E-04
0.85	0.2044	7.8E-04
0.90	0.2015	6.4E-04
0.95	0.1989	5.3E-04
1.00	0.1965	4.5E-04
1.05	0.1943	3.8E-04
1.10	0.1922	3.2E-04
1.15	0.1903	2.8E-04
1.20	0.1885	2.4E-04
1.25	0.1868	2.1E-04
1.30	0.1852	1.8E-04
1.35	0.1837	1.6E-04
1.40	0.1823	1.4E-04
1.45	0.1809	1.2E-04
1.50	0.1796	1.1E-04
1.55	0.1784	9.9E-05
1.60	0.1773	8.8E-05
1.65	0.1762	7.9E-05
1.70	0.1752	7.2E-05
1.75	0.1742	6.5E-05
1.80	0.1732	5.9E-05
1.85	0.1723	5.3E-05
1.90	0.1714	4.9E-05
1.95	0.1706	4.4E-05
2.00	0.1698	4.1E-05
2.05	0.1690	3.7E-05
2.10	0.1682	3.4E-05
2.15	0.1675	3.2E-05
2.20	0.1668	2.9E-05
2.25	0.1662	2.7E-05
2.30	0.1655	2.5E-05
2.35	0.1649	2.3E-05
2.40	0.1643	2.2E-05
2.45	0.1637	2.0E-05
2.50	0.1632	1.9E-05
2.55	0.1626	1.7E-05
2.60	0.1621	1.6E-05

PSI (M)	THETA (V/V)	HYDRO. COND. (M/D)
2.60	0.1621	1.6E-05
2.65	0.1616	1.5E-05
2.70	0.1611	1.4E-05
2.75	0.1606	1.3E-05
2.80	0.1601	1.3E-05
2.85	0.1597	1.2E-05
2.90	0.1592	1.1E-05
2.95	0.1588	1.0E-05
3.00	0.1584	9.8E-06
3.05	0.1580	9.3E-06
3.10	0.1576	8.8E-06
3.15	0.1572	8.3E-06
3.20	0.1568	7.8E-06
3.25	0.1564	7.4E-06
3.30	0.1561	7.1E-06
3.35	0.1557	6.7E-06
3.40	0.1554	6.4E-06
3.45	0.1550	6.0E-06
3.50	0.1547	5.7E-06
3.55	0.1544	5.5E-06
3.60	0.1541	5.2E-06
3.65	0.1537	5.0E-06
3.70	0.1534	4.7E-06
3.75	0.1532	4.5E-06
3.80	0.1529	4.3E-06
3.85	0.1526	4.1E-06
3.90	0.1523	3.9E-06
3.95	0.1520	3.8E-06
4.00	0.1518	3.6E-06
4.05	0.1515	3.4E-06
4.10	0.1513	3.3E-06
4.15	0.1510	3.1E-06
4.20	0.1508	3.0E-06
4.25	0.1505	2.9E-06
4.30	0.1503	2.8E-06
4.35	0.1501	2.7E-06
4.40	0.1498	2.6E-06
4.45	0.1496	2.5E-06
4.50	0.1494	2.4E-06
4.55	0.1492	2.3E-06
4.60	0.1490	2.2E-06
4.65	0.1488	2.1E-06
4.70	0.1485	2.0E-06
4.75	0.1483	2.0E-06
4.80	0.1481	1.9E-06
4.85	0.1480	1.8E-06
4.90	0.1478	1.8E-06
4.95	0.1476	1.7E-06
5.00	0.1474	1.6E-06
5.05	0.1472	1.6E-06
5.10	0.1470	1.5E-06
5.15	0.1469	1.5E-06
5.20	0.1467	1.4E-06

PSI (M)	THETA (V/V)	HYDRO. COND. (M/D)
5.25	0.1465	1.4E-06
5.30	0.1463	1.3E-06
5.35	0.1462	1.3E-06
5.40	0.1460	1.3E-06
5.45	0.1458	1.2E-06
5.50	0.1457	1.2E-06
5.55	0.1455	1.1E-06
5.60	0.1454	1.1E-06
5.65	0.1452	1.1E-06
5.70	0.1451	1.0E-06
5.75	0.1449	1.0E-06
5.80	0.1448	9.7E-07
5.85	0.1446	9.4E-07
5.90	0.1445	9.2E-07
5.95	0.1444	8.9E-07
6.00	0.1442	8.6E-07
6.05	0.1441	8.4E-07
6.10	0.1440	8.1E-07
6.15	0.1438	7.9E-07
6.20	0.1437	7.7E-07
6.25	0.1436	7.5E-07
6.30	0.1434	7.3E-07
6.35	0.1433	7.1E-07
6.40	0.1432	6.9E-07
6.45	0.1431	6.7E-07
6.50	0.1429	6.5E-07
6.55	0.1428	6.3E-07
6.60	0.1427	6.2E-07
6.65	0.1426	6.0E-07
6.70	0.1425	5.9E-07
6.75	0.1424	5.7E-07
6.80	0.1422	5.5E-07
6.85	0.1421	5.4E-07
6.90	0.1420	5.3E-07
6.95	0.1419	5.1E-07
7.00	0.1418	5.0E-07
7.05	0.1417	4.9E-07
7.10	0.1416	4.8E-07
7.15	0.1415	4.6E-07
7.20	0.1414	4.5E-07
7.25	0.1413	4.4E-07
7.30	0.1412	4.3E-07
7.35	0.1411	4.2E-07
7.40	0.1410	4.1E-07
7.45	0.1409	4.0E-07
7.50	0.1408	3.9E-07
7.55	0.1407	3.8E-07
7.60	0.1406	3.8E-07
7.65	0.1405	3.7E-07
7.70	0.1404	3.6E-07
7.75	0.1403	3.5E-07
7.80	0.1402	3.4E-07
7.85	0.1401	3.4E-07
7.90	0.1401	3.3E-07
7.95	0.1400	3.2E-07

PSI (M)	THETA (V/V)	HYDRO. COND. (M/D)
8.00	0.1399	3.1E-07
8.05	0.1398	3.1E-07
8.10	0.1397	3.0E-07
8.15	0.1396	2.9E-07
8.20	0.1395	2.9E-07
8.25	0.1395	2.8E-07
8.30	0.1394	2.8E-07
8.35	0.1393	2.7E-07
8.40	0.1392	2.6E-07
8.45	0.1391	2.6E-07
8.50	0.1391	2.5E-07
8.55	0.1390	2.5E-07
8.60	0.1389	2.4E-07
8.65	0.1388	2.4E-07
8.70	0.1388	2.3E-07
8.75	0.1387	2.3E-07
8.80	0.1386	2.2E-07
8.85	0.1385	2.2E-07
8.90	0.1385	2.2E-07
8.95	0.1384	2.1E-07
9.00	0.1383	2.1E-07
9.05	0.1382	2.0E-07
9.10	0.1382	2.0E-07
9.15	0.1381	2.0E-07
9.20	0.1380	1.9E-07
9.25	0.1380	1.9E-07
9.30	0.1379	1.8E-07
9.35	0.1378	1.8E-07
9.40	0.1378	1.8E-07
9.45	0.1377	1.7E-07
9.50	0.1376	1.7E-07
9.55	0.1376	1.7E-07
9.60	0.1375	1.7E-07
9.65	0.1374	1.6E-07
9.70	0.1374	1.6E-07
9.75	0.1373	1.6E-07
9.80	0.1372	1.5E-07
9.85	0.1372	1.5E-07
9.90	0.1371	1.5E-07
9.95	0.1371	1.4E-07
10	0.1370	1.4E-07

Appendix F. Irrigation System Test Results

Laboratory Test

Before the drip irrigation system was installed in the field, the system was tested outside the Eaton Hall hydrology laboratory. The purpose of this test was to determine that all the emitters were discharging water and that the water delivery design produced a uniform flux through the driplines.

The twenty-one (21) driplines were connected to a manifold header similar to the field design. However, in the laboratory test, the driplines were spaced at approximately 3 cm intervals, only one manifold was used, and the water supply was at the end of the headers. The system was supported, elevated, and leveled on the eastern exterior wall of Eaton Hall. The driplines were identified with numbers one through 21, and the emitters on each line were numbered in a similar fashion as to be installed in the field (Figure 4.3).

While the pump and electrical system test were in progress, water was pumped through the driplines once per hour. Water delivered from selected emitters was collected and measured with a 200 ml graduated cylinder.

Emitter uniformity testing was conducted in both the transverse and longitudinal direction of the driplines. The transverse emitter test determined the emitter output distribution across the driplines, while the longitudinal test found the distribution of water outflow along an individual

dripline.

Three pump cycles were analyzed on emitter number 8 across the twenty-one driplines in the transverse test. The average coefficient of variation for the transverse tests was 0.37 (Table F.1). The low coefficient of variation suggests emitter outflow is uniform and the measurement error small. A linear regression between dripline number and emitter number 8 outflow for the three tests show a small negative slope, indicating that dripline number 1 would most likely emit the highest flow. The magnitude of the regressed slope indicates less than a 1% difference in emitter outflow between dripline number 1 and 21. The correlation coefficient, r^2, is very low for each run (Table F.1), suggesting that the system design provides a uniform flow field transversely across the driplines.

The longitudinal emitter test was performed on driplines number 1 and 2. The emitter outflow was determined by the same method used in the transverse test. Water was collected from all odd numbered emitters along the length of both driplines. The three different longitudinal test runs have low coefficients of variation with the exception of test number three. The third run has a lower mean by about 16% and a coefficient of variation two times larger than the first two runs (Table F.2).

The emitter outflow appears to be uniform along the length of the driplines, based on the low coefficient of variation of the emitter outflow. There is little correlation between emitter outflow from the beginning to end of the dripline, as shown by the low r^2 for the regression between emitter number and emitter

Table F.1. Dripline Emitter Test - Transverse Direction on Emitter Number 8.

Test	1	2	3
Outflow Arith. Mean (ml)	435.2	431.9	439.6
Variance	2.6	2.4	1.6
Coefficient of Variation	0.4	0.4	0.3
Regressed Slope	-0.10	-0.16	-0.09
R^2	0.16	0.36	0.15

Table F.2. Dripline Emitter Test - Longitudinal Direction c
Driplines Number 1 and 2.

Test	1		2		3	
Dripline	1	2	1	2	1	2
Outflow Arith. Mean (ml)	454.4	454.4	419.2	420.0	367.8	368.2
Variance	5.8	5.1	3.5	2.4	7.2	8.4
Coefficient of Variation	0.5	0.5	0.4	0.4	0.7	0.8
Regressed Slope	0.28	0.16	-0.004	-0.06	0.12	-0.15
R^2	0.57	0.21	$2x10^{-4}$	0.06	0.09	0.11

outflow (Table F.2). The greatest correlation (r^2 = 0.57) was found in Test 1, dripline 1. The apparent correlation along the dripline is attributed to the fact that emitter number 1 emitted 3.4 ml of water less than the mean outflow and emitter number 21 emitted 3.6 ml more than the mean; between the three locations there was very little correlation.

Field Test

A field test was conducted to evaluate the performance of the emitters. The test compared two previously unused driplines (numbers 22 and 23) to dripline number 21 which was removed from the water application system after approximately 6.5 months of irrigation had occurred. Previously unused driplines number 22 and 23 showed very low coefficients of variation for the emitter outflow along the dripline length, while the used dripline number 21 coefficient of variation was 22 to 26% larger than the unused driplines (Table F.3). In fact, according to criteria cited by Braults and others (1981), the uniformity of flow in the previously unused driplines (numbers 21 and 22) was 'excellent' (90 to 100 U_S) while uniformity in used dripline was only considered 'fair' (70 to 80 U_S).

Emitter number 1 on dripline 21 had an outflow approximately 80% lower than the mean emitter outflow. This emitter was dissected and visually inspected. There was a small grain of sand trapped in the turbulent flow path of the emitter, restricting the outflow. Sand particle blockage is also believed to be the cause of the low outflow 50% less than the mean outflow

Table F.3. New versus Used Longitudinal Dripline Testing

Dripline Type	22 new	23 new	21 used	21 used	21 used
Outflow Arith. Mean (ml)	63.7	58.1	54.0	49.9	61.0
Variance	1.3	3.7	159.1	163.1	183.3
Coefficient of Variation (%)	1.8	3.3	23.4	25.6	22.2
U_s	98.2	96.7	76.6	74.4	77.8

observed at emitters 14 and 19 in line 21. There appears to be no observable trend in the results of this test of emitter plugging. If the emitter plugging is of a random nature, then the flow over the entire irrigated area should remain nearly uniform.

Appendix G. Discharge To Irrigation System vs. Time

TIME SINCE INFILTRATION BEGUN	EMITTER DISCHARGE	AVERAGE EMITTER DISCHARGE
DAY	M3/D/EMITTER	M3/D/EMITTER
0.00		
0.04	1.93E-03	1.93E-03
0.71	1.98E-03	1.98E-03
0.75	2.23E-03	1.99E-03
1.00	2.04E-03	2.00E-03
1.04	1.92E-03	2.00E-03
1.75	2.03E-03	2.01E-03
1.79	2.19E-03	2.02E-03
2.04	2.13E-03	2.03E-03
2.08	1.94E-03	2.03E-03
2.83	2.01E-03	2.02E-03
2.88	1.94E-03	2.02E-03
3.96	2.05E-03	2.03E-03
4.04	1.95E-03	2.03E-03
4.08	1.98E-03	2.03E-03
5.00	2.08E-03	2.04E-03
5.04	1.96E-03	2.04E-03
5.08	1.95E-03	2.04E-03
6.04	2.01E-03	2.03E-03
6.75	2.06E-03	2.03E-03
6.79	2.12E-03	2.04E-03
6.83	2.07E-03	2.04E-03
6.88	2.06E-03	2.04E-03
7.04	2.07E-03	2.04E-03
7.08	1.94E-03	2.04E-03
7.96	2.07E-03	2.04E-03
8.08	1.88E-03	2.04E-03
9.88	1.93E-03	2.02E-03
9.92	1.90E-03	2.02E-03
9.96	1.92E-03	2.02E-03
11.04	1.97E-03	2.01E-03
11.08	2.08E-03	2.01E-03
11.96	2.06E-03	2.02E-03
12.00	2.04E-03	2.02E-03
12.04	2.00E-03	2.02E-03
12.08	1.99E-03	2.02E-03
13.04	2.01E-03	2.02E-03
13.08	2.03E-03	2.02E-03
13.79	2.05E-03	2.02E-03
13.83	2.10E-03	2.02E-03
14.75	2.03E-03	2.02E-03
14.79	2.13E-03	2.02E-03
14.96		2.01E-03
15.08	2.05E-03	2.01E-03
16.88	2.04E-03	2.02E-03
16.96	2.09E-03	2.02E-03
18.04	1.96E-03	2.01E-03
18.96	2.12E-03	2.02E-03
19.00	2.10E-03	2.02E-03
19.04	2.07E-03	2.02E-03
20.79	2.07E-03	2.02E-03
20.83	2.05E-03	2.02E-03
20.88	2.04E-03	2.02E-03
20.92	2.03E-03	2.02E-03
21.00	2.01E-03	2.02E-03
21.04	1.98E-03	2.02E-03
21.08	1.99E-03	2.02E-03
21.83	1.99E-03	2.02E-03
21.88	1.97E-03	2.02E-03
21.92	1.98E-03	2.02E-03
21.96	1.97E-03	2.02E-03
22.04		2.02E-03
22.08	2.00E-03	2.02E-03
22.96	1.93E-03	2.01E-03
23.00	1.90E-03	2.01E-03
23.04	1.90E-03	2.01E-03
23.92	2.03E-03	2.01E-03

TIME SINCE INFILTRATION BEGUN	EMITTER DISCHARGE	AVERAGE EMITTER DISCHARGE
DAY	M3/D/EMITTER	M3/D/EMITTER
23.96	1.92E-03	2.01E-03
24.83	1.81E-03	2.01E-03
24.88	1.91E-03	2.01E-03
24.92	1.92E-03	2.01E-03
27.04	1.91E-03	2.00E-03
28.92	1.88E-03	1.99E-03
29.04	1.87E-03	1.99E-03
31.79	1.87E-03	1.98E-03
31.88	1.88E-03	1.98E-03
31.96	1.87E-03	1.98E-03
32.04	1.92E-03	1.98E-03
32.08	1.92E-03	1.98E-03
32.96	1.93E-03	1.98E-03
33.00	1.93E-03	1.98E-03
33.08	1.94E-03	1.98E-03
33.13	1.94E-03	1.98E-03
33.96	1.94E-03	1.98E-03
34.04		1.97E-03
35.79	2.00E-03	1.98E-03
35.96	1.96E-03	1.98E-03
36.83	1.94E-03	1.97E-03
36.88	1.93E-03	1.97E-03
39.04	1.94E-03	1.97E-03
39.08	1.93E-03	1.97E-03
39.13	1.93E-03	1.97E-03
40.75	1.95E-03	1.97E-03
40.88	1.97E-03	1.97E-03
40.92	1.99E-03	1.97E-03
41.00	2.06E-03	1.97E-03
41.04	1.94E-03	1.97E-03
41.08	1.94E-03	1.97E-03
41.71	1.95E-03	1.97E-03
41.75	1.95E-03	1.97E-03
42.96	1.95E-03	1.97E-03
43.04	1.95E-03	1.97E-03
44.04	1.95E-03	1.97E-03
45.79	1.94E-03	1.97E-03
45.83	1.95E-03	1.97E-03
47.79	1.94E-03	1.97E-03
49.92	1.95E-03	1.97E-03
50.83	1.95E-03	1.97E-03
51.00	1.94E-03	1.97E-03
52.75	1.95E-03	1.97E-03
54.92	1.96E-03	1.97E-03
55.79	1.97E-03	1.97E-03
58.79	1.95E-03	1.97E-03
58.83	1.92E-03	1.97E-03
59.96	1.93E-03	1.96E-03
60.04	1.91E-03	1.96E-03
62.96	1.93E-03	1.96E-03
63.88	1.91E-03	1.96E-03
66.71	1.99E-03	1.96E-03
66.92	1.90E-03	1.96E-03
67.00	1.90E-03	1.96E-03
70.96	1.93E-03	1.96E-03
71.04	1.92E-03	1.96E-03
71.83	1.92E-03	1.96E-03
73.92	1.91E-03	1.96E-03
74.00	1.92E-03	1.96E-03
74.75	1.91E-03	1.96E-03
74.79	1.90E-03	1.96E-03
77.00	1.89E-03	1.96E-03
80.92	1.90E-03	1.96E-03
81.92	1.90E-03	1.95E-03
81.96	1.88E-03	1.95E-03
83.92	1.89E-03	1.95E-03
84.00	1.88E-03	1.95E-03

TIME SINCE INFILTRATION BEGUN	EMITTER DISCHARGE	AVERAGE EMITTER DISCHARGE
DAY	M3/D/EMITTER	M3/D/EMITTER
87.75	1.94E-03	1.95E-03
87.79	1.92E-03	1.95E-03
90.92	1.93E-03	1.95E-03
93.92	1.91E-03	1.95E-03
93.96	1.95E-03	1.95E-03
97.71	1.93E-03	1.95E-03
97.75	1.93E-03	1.95E-03
101.88	1.93E-03	1.95E-03
104.71	1.94E-03	1.95E-03
104.83	1.99E-03	1.95E-03
108.71	1.98E-03	1.95E-03
114.83	1.96E-03	1.95E-03
116.88	1.92E-03	1.95E-03
123.92	1.90E-03	1.95E-03
123.96	1.89E-03	1.95E-03
124.79	1.89E-03	1.95E-03
130.71	1.99E-03	1.95E-03
130.75	1.93E-03	1.95E-03
131.79	1.94E-03	1.95E-03
132.92	1.90E-03	1.95E-03
132.96	1.87E-03	1.95E-03
137.71	1.93E-03	1.95E-03
137.79	2.22E-03	1.95E-03
138.75	2.00E-03	1.95E-03
138.79	1.90E-03	1.95E-03
138.96	1.96E-03	1.95E-03
139.67	1.97E-03	1.95E-03
139.71	1.96E-03	1.95E-03
139.75	1.98E-03	1.95E-03
139.83	1.97E-03	1.95E-03
140.83	1.97E-03	1.95E-03
141.75	1.97E-03	1.95E-03
143.92	1.98E-03	1.95E-03
144.00	2.27E-03	1.95E-03
145.79	1.98E-03	1.95E-03
147.75	1.98E-03	1.95E-03
151.00	2.07E-03	1.95E-03
152.75	1.99E-03	1.95E-03
153.00	1.81E-03	1.95E-03
157.71	1.98E-03	1.95E-03
157.75	2.00E-03	1.95E-03
158.96	1.97E-03	1.95E-03
159.79	1.98E-03	1.95E-03
159.83	1.96E-03	1.95E-03

New Mexico Bureau of Mines
Water Analysis

County Socorro Range _____ Township _____ Section _____ Collection Date Sept. 16, 1986
Collected by A. Parsons Special Handling _____ Remarks _____
Sample Identification V. Plant Tap Water Lab Number 145 Appearance _____

pH 7.4 Date 9/16/86 Analyst J.U.

Total Dissolved Solids
Residue at 180° + dish _____
dish _____
Solids _____
Date _____
Analyst _____
ppm 501

Conductivity
930 μmhos
Date 9/16/86
Analyst J.U.

Carbonate
Date 9/16/86
Sample size _____
Analyst JC
ml acid _____
ppm CO_3 0
epm _____

Bicarbonate
Date 9/16/86
Sample size _____
Analyst JC
Ml acid _____
ppm HCO_3 230
epm _____

Chloride
Date 9/20/86
Sample size _____
Analyst JC
Ml $HgCl_2$ _____
ppm Cl^- 56
epm _____

Sulfate
Date 9/20/86
Sample size _____
Analyst JC
crucible + ppt _____
ppt _____
ppm $SO_4^=$ 154
epm _____

Nitrate
Date 10/8/86
Sample size _____
Analyst JC
Abs. _____
ppm NO_3 <0.11
epm _____

Phosphate
Date _____
Aliquot _____
Analyst _____
Abs. _____
ppm PO_4' _____
epm _____

Fluoride
Date 9/19/86
Aliquot _____
Analyst J.U.
Mv _____
ppm F^- 0.56
epm _____

Total epm anions 8.1/7

Silica
Date _____
Aliquot _____
Analyst _____
Abs. _____

Hardness = 273 ppm $CaCO_3$

Sodium
Date 9/17/86
dilution _____
Analyst J.U.
Abs. _____
ppm Na^+ 62.0
epm _____

Potassium
Date 9/23/86
Dilution _____
Analyst J.U.
Abs. _____
ppm K^+ 3.6
epm _____

Magnesium
Date 10/3/86
Dilution _____
Analyst JC
Abs. _____
ppm Mg 13
epm _____

Calcium
Date 9/22/86
Dilution _____
Analyst JC
Abs. _____
ppm Ca 38
epm _____

Aluminum
Date _____
Aliquot _____
Analyst _____
Abs. _____
ppm Al^{+++} _____
epm _____

Iron
Date _____
Aliquot _____
Analyst _____
Abs. _____
ppm Fe _____
epm _____

Boron
Date _____
Aliquot _____
Analyst _____
Abs. _____
ppm B _____
epm _____

Manganese
Date _____
Aliquot _____
Analyst _____
Abs. _____
ppm Mn _____
epm _____

Total epm Cations 8.1/7
Cation-Anion Balance _____
% Error 0.27

Copper
Concentration _____
Analyst _____
Date _____
ppm Cu _____
epm _____

Cobalt
Concentration _____
Analyst _____
Date _____
ppm Co _____
epm _____

Chromium
Concentration _____
Analyst _____
Date _____
ppm Cr _____
epm _____

Cadmium
Concentration _____
Analyst _____
Date _____
ppm Cd _____
epm _____

Lead
Concentration _____
Analyst _____
Date _____
ppm Cd _____
epm _____

Molybdenum
Concentration _____
Analyst _____
Date _____
ppm Mo _____
epm _____

Nickel
Concentration _____
Analyst _____
Date _____
ppm Ni _____
epm _____

Zinc
Concentration _____
Analyst _____
Date _____
ppm Zn _____
epm _____

Mercury
Concentration _____
Analyst _____
Date _____
ppm _____
epm _____

Arsenic
Concentration _____
Analyst _____
Date _____
ppm _____
epm _____

APPENDIX . Tap Water Cation-Anion Analysis.

Appendix I. Program NP.FOR

```
      PROGRAM NP.FOR


C     THIS PROGRAM WEIGHTS DESTRUCTIVE SAMPLES AND DETERMINES
C     A VALUE AT A NEUTRON PROBE READING LOCATION.
C
C     THE WEIGHTING SCHEME TO BE USED IS A SPHERICAL
C     WEIGHTING APPROACH THAT MULTIPLIES THE MOISTURE
C     CONTENT BY THE VOLUME OF THE SLICE OF THE SPHERE
C     UNDER INFLUENCE FROM THE DESTRUCTIVE SAMPLE.
C
C     THE RADIUS OF INFLUENCE OF THE NEUTRON PROBE IS A FUNCTION
C     OF MOISTURE CONTENT.  IN THIS PROGRAM THE R. OF I. IS
C     DETERMINED BY A LINEAR INTERPLOLATION SCHEME WHERE AT 0%
C     MOISTURE THE ROI IS 10 INCHES AND AT A MOISTURE CONTENT OF
C     32% THE ROI IS 4 INCHES.
C     TO ACCOMPLISH THIS THE FIRST GUESS OF THE ROI IS 6 THEN THE
C     NEUTRON PROBE MOISTURE CONTENT IS DETERMINED.  USING THIS
C     MOISTURE CONTENT A NEW RADIUS OF INFLUENCE IS DETERMINED
C     AND THE PROCESS IS REPEATED TO FIND A NEW MOISTURE CONTENT.
C
C     THE INPUT FILE IS CALLED IN.PRN AND IS ON THE A DRIVE
C     THE FILE IS UNFORMATTED AND IS IN THE FOLLOWING FORM;
C     STARTING LOCATION OF THE NEUTRON PROBE (inches)
C     ENDING LOCATION OF THE NEUTRON PROBE (inches)
C     LIST;
C     MID-LOCATION OF THE DESTRUCTIVE SAMPLE, MOISTURE CONTENT
C                  (inches)          (% V/V)
C     NOTE:
C     THE INPUT FILE MUST BE BEYOND THE RADIUS OF INFLUENCE
C     OF THE NEUTRON PROBE FIRST AND LAST READINGS. (IE. IF THE
C     PROBE LOCATION IS AT 9 AND THE RADUIS OF INFLUENCE IS 6
C     THE FIRST DESTUCTIVE SAMPLE LOCATION SHOULD BE LOCATED
C      BEFORE 3.  IN FACT THE END OF THE FIRST DESTRUCTIVE SAMPLE
C     HAS TO BE BEFORE 3.  TO ACCOMPLISH THIS PLACE DUMBY POINTS
C     AT THE TOP WITH THE SAME MOISTURE CONTENT AND THE REAL TOP
C     POINT, SIMULARLY WITH THE BOTTOM.

      DIMENSION Y(100), DS(100), PR(100)
      REAL MULT, MOLD
      OPEN (UNIT = 90,FILE= 'A:IN.PRN',STATUS='OLD')
      OPEN (UNIT = 99,FILE='A:OUT.DAT',
     *     STATUS='NEW',IOSTAT=IO)

C     IO IS THE INPUT OUTPUT ERROR CODE
C     READS IN THE START AND END LOCATION OF THE NEUTRON PROBE
      PRINT*,  'IO= ',IO
      READ(90,*) ISTART
      READ(90,*) IEND

C     READS A MAXIMUM NUNBER OF 30 DESTRUCTIVE SAMPLES
C     FINDS THE NUMBER OF SAMPLE READ AND SETS IT TO N
 j^@^@^@^@^@    N = 30
```

```
      DO 10 I = 1,N
        READ(90,*,END = 15) Y(I), DS(I)
   10 CONTINUE
   15 CONTINUE
      N = I-1
      R = 6.

C     THIS LOOP FINDS THE MOISTURE CONTENT AT EACH NP LOCATION
      DO 30 NP = ISTART,IEND,6
        XLOW = NP-R
        XTOP = NP+R
        VOL = (4./3)*3.1416*(R**3)
        HTOTAL = 0.
        TEMP = 0.

C     THIS LOOP FINDS WHICH OF THE DESTRUCTIVE SAMPLES CONTRIBUTE
C     TO THE NEUTRON PROBE READING
        DO 40 I = 2,N-1
          Y1 = (Y(I-1)+Y(I))/2
          Y2 = (Y(I+1)+Y(I))/2

          IF(Y1.LE.XLOW .AND. Y2.GT.XLOW)THEN
           H = (Y2-XLOW)
           XMULT = ((1./3.)*3.1416*(H**2)*(3*R-H))/VOL
           XMOLD = XMULT
           TEMP=(XMULT)*DS(I)+TEMP

          ELSEIF(Y1.GE.XLOW .AND. Y2.LE.XTOP)THEN
           XMOLD = ((1./3)*3.1416*(H**2)*(3*R-H))/VOL
           H = H+(Y2-Y1)
           XMULT = ((1./3)*3.1416*(H**2)*(3*R-H))/VOL - XMOLD
           TEMP=(XMULT)*DS(I)+TEMP

          ELSEIF(Y1.LE.XTOP .AND. Y2.GT.XTOP)THEN
           XMOLD = ((1./3)*3.1416*(H**2)*(3*R-H))/VOL
           H = H+(XTOP-Y1)
           XMULT = ((1./3)*3.1416*(H**2)*(3*R-H))/VOL - XMOLD
           TEMP=(XMULT)*DS(I)+TEMP

          ENDIF
   40   CONTINUE

      PR(NP)=TEMP

C     THE NEW RADIUS OF INFLUENCE IS DETERMINED
C     AND THE MOISTURE CONTENT IS RECALCULATED.
      R = 10 - (6./32)*PR(NP)
      TEMP = 0.
      XLOW = NP - R  j^@^@^@^@^@     XTOP = NP + R
        HTOTAL = 0
        VOL = (4./3)*3.1416*(R**3)

        DO 60 I = 2,N-1
          Y1 = (Y(I-1)+Y(I))/2
```

```
          Y2 = (Y(I+1)+Y(I))/2

          IF(Y1.LE.XLOW .AND. Y2.GT.XLOW)THEN
           H = (Y2-XLOW)
           MULT = ((1./3)*3.1416*(H**2)*(3*R-H))/VOL
           MOLD = MULT
           TEMP=(MULT)*DS(I)+TEMP

          ELSEIF(Y1.GE.XLOW .AND. Y2.LE.XTOP)THEN
           MOLD = ((1./3)*3.1416*(H**2)*(3*R-H))/VOL
           H = H+(Y2-Y1)
           MULT = ((1./3)*3.1416*(H**2)*(3*R-H))/VOL - MOLD
           TEMP=(MULT)*DS(I)+TEMP

          ELSEIF(Y1.LE.XTOP .AND. Y2.GT.XTOP)THEN
           MOLD = ((1./3)*3.1416*(H**2)*(3*R-H))/VOL
           H = H+(XTOP-Y1)
           MULT = ((1./3)*3.1416*(H**2)*(3*R-H))/VOL - MOLD
           TEMP=(MULT)*DS(I)+TEMP

          ENDIF

   60   CONTINUE

C     THE NEW MOISTURE CONTENT IS OUTPUT TO THE SCREEN AND A
C     OUT PUT FILE.
      PR(NP) = TEMP
      PRINT*,NP,PR(NP),R
      WRITE(99,50)NP,PR(NP)
   50 FORMAT(4X,I5,4X,F6.2)

   30 CONTINUE

      END
```

Appendix J. Neutron Probe Calibration Data

CALIBRATION INFORMATION FOR OLD AND NEW NEUTRON PROBE CALIBR
DESTRUCTIVE SAMPLES OBTAINED FROM:
1. GOLF COURSE NEAR WATER HAZARD # 13 (SHELBE TUBES)
2. NEUTRON ACCESS TUBE INSTALLATION NEAR PIT (100 CC RINGS)
3. NEUTRON ACCESS TUBE INSTALLATION (SPLIT SPOON)

LOCATION		MOISTURE CONTENT				
		ADJUSTED DESTR. (CC/CC %)	HAND AUGERED (CC/CC %)	SPLIT SPOON (CC/CC %)	OLD PROBE (CC/CC %)	NEW PROBE (CC/CC %)
GC 1	9.0	28.68			30.71	29.38
	15.0	26.90			33.13	26.99
	21.0	24.63			32.92	26.60
	27.0	22.89			30.42	24.49
	33.0	20.85			29.92	25.18
	39.0	20.85			27.47	24.74
	45.0	24.10			28.39	24.15
	52.0	22.40			27.79	24.60
GC 2	10.0	11.68			13.49	11.60
	16.0	13.97			15.48	13.50
	22.0	15.80			16.67	14.57
	28.0	16.36			18.44	16.27
	34.0	14.09			17.37	15.38
	40.0	13.23			16.35	14.77
	46.0	14.97			15.53	13.58
	52.0	15.25			16.48	14.69
GC 3	9.0	15.04			12.95	14.27
	15.0	13.60			16.36	12.89
	21.0	11.33			16.07	12.29
	27.0	9.25			14.74	11.15
	33.0	6.91			14.02	10.57
	39.0	6.14			12.70	10.32
8-15	36.0		15.86			18.60
	48.0		29.44			18.00
	60.0		31.51			16.50
	72.0		20.49			14.80
	84.0		19.95			14.10
	96.0		13.67			14.80
	108.0		15.56			16.00
15-5	48.0		10.29			11.40
	60.0		8.15			9.30
25-25	2.5			11.20	11.85	
	3.5			6.80	9.70	
	6.0			6.50	10.20	
	7.5			9.00	10.15	
	11.5			3.60	11.80	
	12.0			13.10	12.10	
	13.0			6.70	9.70	
	15.5			3.90	14.20	
	17.5			5.40	7.35	
	4.5			7.70	9.40	
	5.0			8.60	9.30	
15-28	5.5			7.00	9.60	
	6.5			5.90	9.50	
	10.5			1.90	8.70	
15-22	5.5			8.70	10.10	
	6.5			7.80	9.40	
	11.5			2.20	9.10	
	14.5			2.90	7.15	
	15.5			2.90	7.20	
5-25	5.0			12.00	7.90	
	6.0			4.80	7.40	
	10.5			2.50	7.10	
	14.0			2.90	6.50	
	15.0			24.90	6.40	
2-15	5.0			10.90	9.80	
	6.0			9.00	8.30	
	10.5			3.00	8.35	
	15.0			2.00	8.40	
	16.0			2.00	7.00	

CALIBRATION INFORMATION FOR OLD AND NEW NEUTRON PROBE CALIBR
DESTRUCTIVE SAMPLES OBTAINED FROM:
1. GOLF COURSE NEAR WATER HAZARD # 13 (SHELBE TUBES)
2. NEUTRON ACCESS TUBE INSTALLATION NEAR PIT (100 CC RINGS)
3. NEUTRON ACCESS TUBE INSTALLATION (SPLIT SPOON)

LOCATION		MOISTURE CONTENT				
		ADJUSTED DESTR. (CC/CC %)	HAND AUGERED (CC/CC %)	SPLIT SPOON (CC/CC %)	OLD PROBE (CC/CC %)	NEW PROBE (CC/CC %)
8-15	5.5			21.60	17.55	
	6.5			9.10	14.85	
	10.5			4.60	9.80	
5-5	5.0			8.40	8.60	
	6.5			8.60	9.80	
	10.5			7.80	8.90	
	11.5			8.40	8.65	
	15.0			2.90	8.70	
	16.0			4.80	8.80	
22-15	7.0			9.10	22.50	
	11.5			13.10	17.85	
	12.0			36.30	18.90	
	13.0			26.80	15.10	
	16.0			5.20	11.20	
28-15	15.0			13.80	13.50	
	16.0			7.40	10.60	
28-15	3.5			12.00	12.70	
	10.5			16.40	16.00	
25-5	5.5			11.60	11.00	
	9.5			8.30	9.95	
	10.0			8.10	8.90	
15-2	3.1			5.90	17.00	
	13.3			5.90	10.50	
	17.7			2.50	8.00	
	18.7			2.50	7.80	
	22.6			41.20	8.40	
	23.8			2.60	7.00	
	5.7			11.50	16.10	
	7.1			15.20	16.50	
	8.4			17.40	16.00	
	9.0			10.50	15.00	
	9.5			12.30	14.30	
	10.7			9.80	13.40	
	2.6			11.60	12.10	
	3.4			4.00	10.20	
	7.5			5.30	8.50	
	8.5			6.80	8.70	
	12.9			3.90	8.50	
	18.1			2.80	6.90	
	23.1			2.00	6.20	
	4.9			4.70	9.20	
	6.2			5.30	9.00	
	9.8			6.50	8.10	
	10.8			4.50	8.00	

Appendix K. Laboratory Tensimeter Calibration

Three Tensimeters were calibrated in the laboratory, by twc different calibration experiments. The first experiment calibrated Tensimeter #773863 (Soil Measurement Systems Inc., Las Cruces, NM), which is commonly called the 'E&A' Tensimeter. A porous cup, on a tensiometer of similar construction to those installed in the field, was placed below the water surface in a sealed flask (Figure 5.4). The needle of the Tensimeter was inserted into the septum stopper of the tensiometer. The pressure in the flask was determined using a water manometer enabling simultaneous readings of the Tensimeter and the water manometer. A hand vacuum pump was used to incrementally decrease the pressure in the flask. The system was allowed tc equilibrate, then readings were taken. This procedure was continued to a negative pressure head of 147 cm of water. A total of 11 sets of readings were recorded (Table K.1). A linear regression analysis yielded a coefficient of determination (r^2) of 1.00, and the following calibration equation:

$$P = 2.35 + 1.06*TR \qquad (K.1)$$

where P, the pressure head (cm); and TR, the Tensimeter reading (mbar), are considered positive values.

The second calibration experiment calibrated Tensimeters #774309 and #8510007, commonly referred to as 'Jim's Tensimeter' and 'Warren's Tensimeter' respectively. Instead of using a tensiometer, as in the previous experiment, a septum stopper was fitted to a large

glass jar to enable the Tensimeter to read the pressure in the jar directly. The needles of both of the Tensimeters were permanently installed in the septum stopper through out the experiment. Water and mercury manometers were connected to the calibration jar to determine true jar pressure. A hand vacuum pump was used to decrease the pressure in the jar incrementally. The system was allowed to equilibrate, and readings were then taken of both Tensimeters, the water manometer and mercury manometer. When the jar pressures reached the limit of the water manometer it was disconnected and only the mercury manometer was used to determine the true jar pressure. Fifteen sets of data points were collected using the water manometer and an additional 19 sets with the mercury manometer. All data was corrected for temperature effects. Linear regressions for Jim's and Warren's tensiometers were determined on the data sets, both with an r^2 of 1.00 (Table K.2). The calibration equation for Jim's Tensimeter is:

$$P = 0.05 + 1.025*TR \qquad (K.2)$$

Warren's Tensimeter calibration equation is:

$$P = -1.0 + 1.02*TR \qquad (K.3)$$

where the pressure head and tensimeter readings are considered positive values.

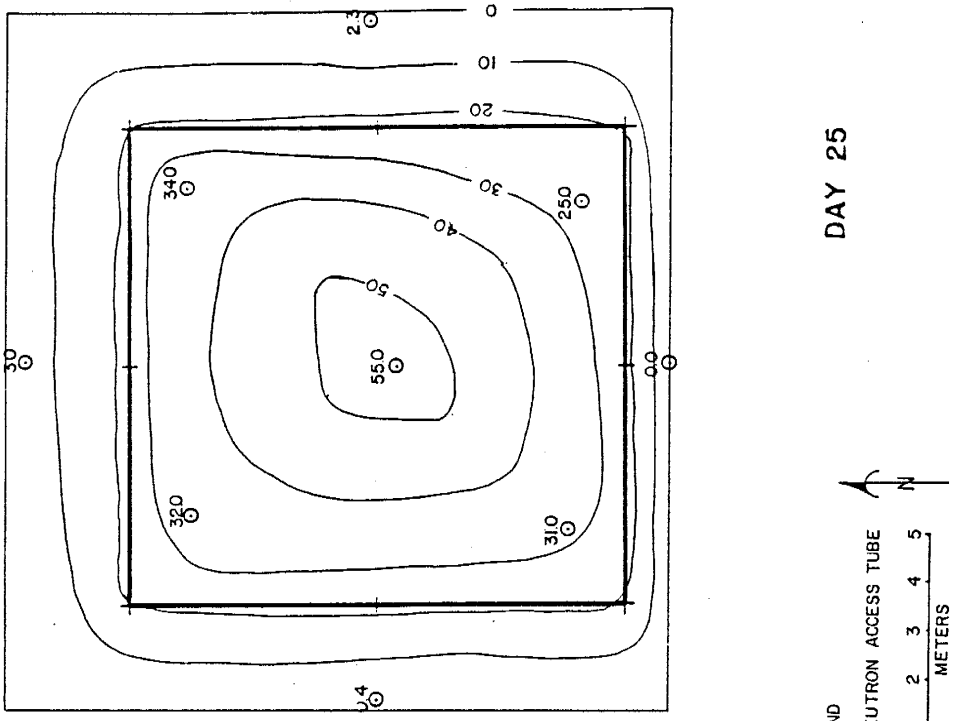
0
10
20
30
40
50
340
250
550
320
310
30
00
2.3
1.4

DAY 25

N
LEGEND
NEUTRON ACCESS TUBE
0 1 2 3 4 5
METERS

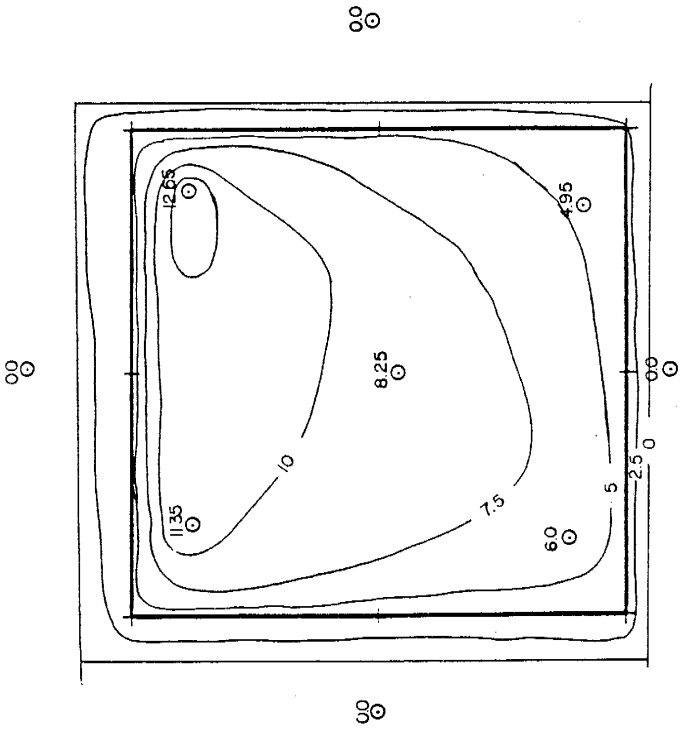
00
12.65
4.95
8.25
00
10
7.5
5
2.5
0
11.35
6.0
00

DAY 7

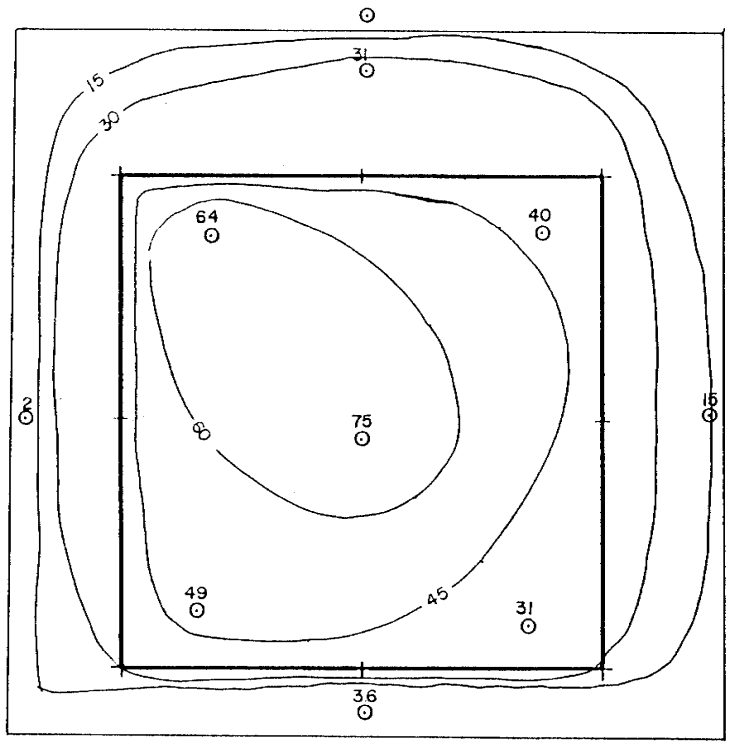

DAY 39

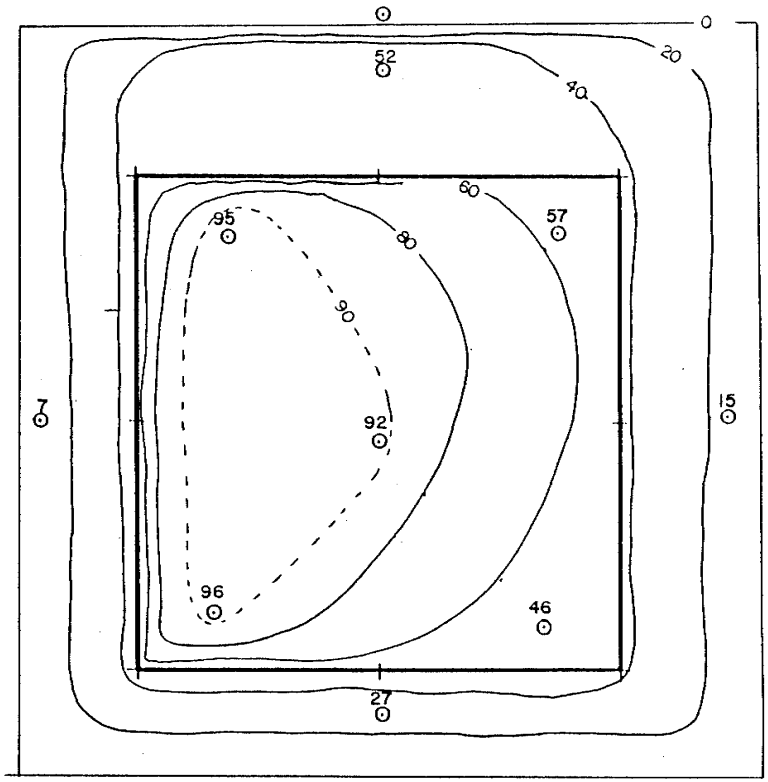

DAY 60

LEGEND

⊙ NEUTRON ACCESS TUBE

0 1 2 3 4 5

METERS

N

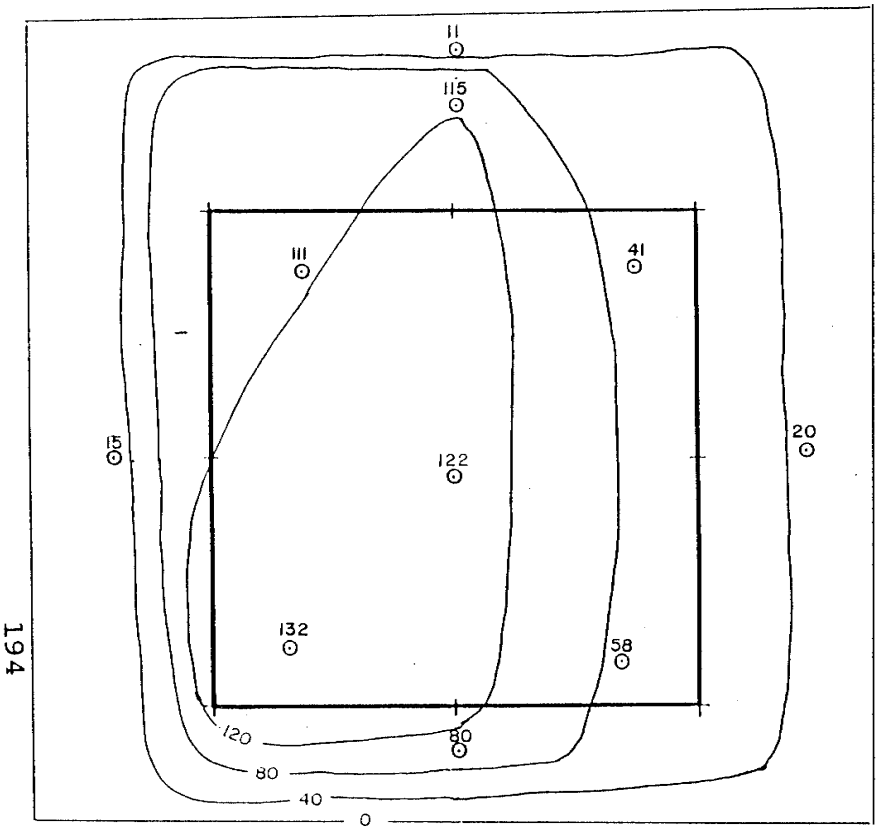

DAY 81

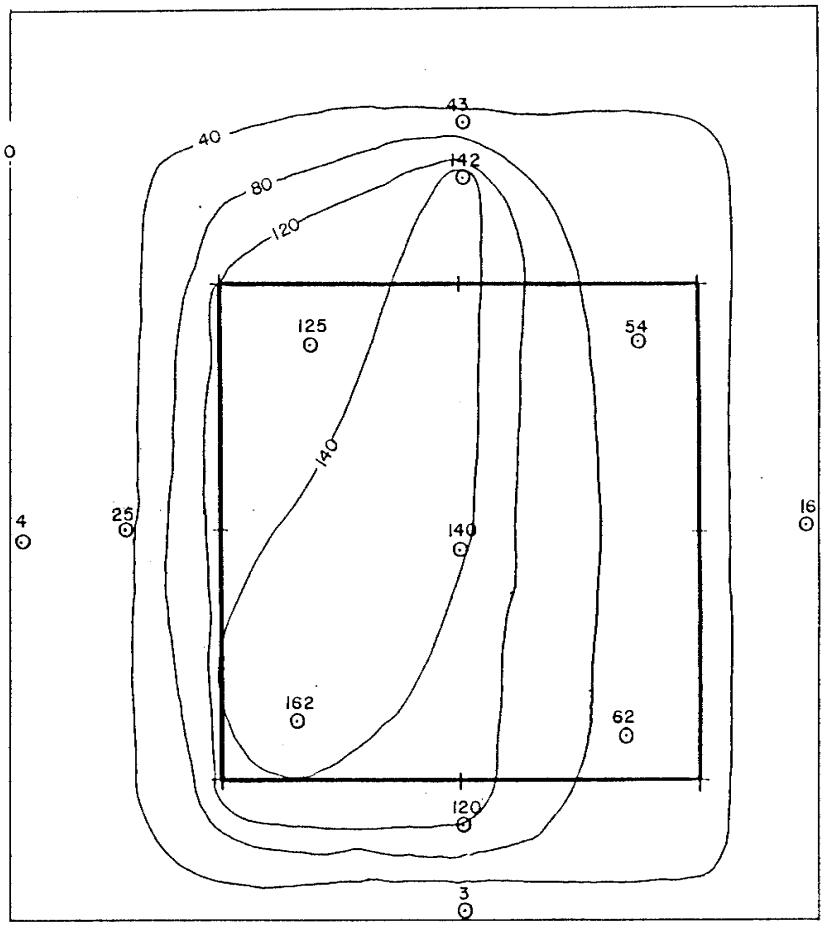

LEGEND

⊙ NEUTRON ACCESS TUBE

0 1 2 3 4 5

METERS

N

DAY 125

Appendix M. Moisture Content and Pressure Head Field Data

STATION 15-2 MOISTURE CONTENT

DATE	1/26/87	2/13/87	6/4/87	8/11/87
TIME	1500	1645	1000	1000
MCHI	0.94	1.02	0.97	0.89
EXP. DAYS		15.1	125.8	193.8
DBD (M)				
0.65	23.9	22.6	14.2	9.3
0.96	14.2	13.0	10.7	8.6
1.26	12.7	13.2	11.4	9.9
1.57	11.9	12.1	11.7	10.2
1.87	13.5	13.4	12.2	10.4
2.18	11.7	11.5	11.7	10.6
2.48	11.6	11.5	11.4	10.6
2.79	11.6	11.2	10.8	11.1
3.09	10.6	10.3	10.3	10.1
3.40	9.8	9.7	10.0	10.1
3.70	10.7	10.5	10.5	10.6
4.01	10.4	10.0	10.6	10.7
4.31	11.3	11.2	11.5	11.3
4.62	11.0	10.8	11.3	11.1
4.92	10.3	10.3	10.5	11.1
5.23	8.8	8.8	9.3	10.0
5.53	5.3	5.2	5.3	6.5
5.84	5.6	5.5	5.1	5.2
6.14	5.4	5.2	5.5	5.5
6.45	8.6	8.8	8.5	8.8
6.75	7.5	8.3	7.6	7.9
7.06	6.1	6.2	5.6	5.7
7.36	5.1	4.8	4.6	4.9
7.67	4.8	4.7	4.5	4.4
7.97	4.9	4.7	5.1	4.8
8.27	5.8	5.5	5.2	5.3
8.58	4.2	4.2	4.2	4.1
8.88	4.0	4.2	4.1	3.6

Appendix M. Moisture Content and Pressure Head Field Data

STATION 15-2 MOISTURE CONTENT

DATE	1/26/87	2/13/87	6/4/87	8/11/87
TIME	1500	1645	1000	1000
MCHI	0.94	1.02	0.97	0.89
EXP. DAYS		15.1	125.8	193.8
DBD (M)				
0.65	23.9	22.6	14.2	9.3
0.96	14.2	13.0	10.7	8.6
1.26	12.7	13.2	11.4	9.9
1.57	11.9	12.1	11.7	10.2
1.87	13.5	13.4	12.2	10.4
2.18	11.7	11.5	11.7	10.6
2.48	11.6	11.5	11.4	10.6
2.79	11.6	11.2	10.8	11.1
3.09	10.6	10.3	10.3	10.1
3.40	9.8	9.7	10.0	10.1
3.70	10.7	10.5	10.5	10.6
4.01	10.4	10.0	10.6	10.7
4.31	11.3	11.2	11.5	11.3
4.62	11.0	10.8	11.3	11.1
4.92	10.3	10.3	10.5	11.1
5.23	8.8	8.8	9.3	10.0
5.53	5.3	5.2	5.3	6.5
5.84	5.6	5.5	5.1	5.2
6.14	5.4	5.2	5.5	5.5
6.45	8.6	8.8	8.5	8.8
6.75	7.5	8.3	7.6	7.9
7.06	6.1	6.2	5.6	5.7
7.36	5.1	4.8	4.6	4.9
7.67	4.8	4.7	4.5	4.4
7.97	4.9	4.7	5.1	4.8
8.27	5.8	5.5	5.2	5.3
8.58	4.2	4.2	4.2	4.1
8.88	4.0	4.2	4.1	3.6

STATION 15-6 MOISTURE CONTENT

	4/20/87	7/1/87
DATE		
TIME	1415	1150
MCHI	1.08	0.99
STD. CNT.	8184	8325
EXP. DAYS	81.0	152.9

DBD (M)		
0.69		
0.85		
1.00		
1.15		
1.30	9.1	9.8
1.46	8.7	
1.61	8.1	8.1
1.76	7.2	
1.91	6.9	7.5
2.07	7.5	
2.22	8.1	6.9
2.37	7.2	
2.52	6.9	5.8
2.68	5.8	
2.83	5.8	6.1
2.98	6.0	
3.13	6.4	5.7
3.29	6.0	
3.44	5.9	6.0
3.59	5.9	
3.74	6.2	6.2
3.90	6.1	
4.05	6.1	6.0
4.20	6.0	
4.35	6.0	6.4
4.50	6.0	
4.66	6.0	6.6
4.81	5.8	
4.96	5.7	8.6
5.11	4.9	10.6
5.27	5.7	10.8
5.42	4.7	10.0
5.57	4.8	7.1
5.72	4.3	4.9
5.88	4.4	4.5
6.03	4.2	4.6
6.18	4.6	4.1
6.33	6.3	4.2
6.49	4.2	4.4
6.64	4.1	
6.79	4.4	3.8
6.94	4.9	
7.09	5.0	4.9
7.25	4.9	
7.40	4.1	3.9
7.55	3.7	
7.70	3.7	3.5
7.85	3.3	
8.01	3.5	3.7
8.16	4.5	
8.31		4.7

STATION 15-8 MOISTURE CONTENT

DATE	1/26/87	1/29/87	2/5/87	2/23/87	4/20/87	7/1/87
TIME	1520	1445	1550	1415	1420	1109
MCHI	0.94	1.02	1.09	0.86	1.08	
STD. CNT.		8407	8411	8356	8184	
EXP. DAYS		0.0	7.0	25.0	81.0	152.9
DPD (M)						
0.56	14.7	15.1	15.2			
0.87	10.7	10.3	10.5	11.1		
1.02	8.9	8.5	8.7	8.6		
1.17	8.1	8.1	7.9	8.1	8.3	
1.33	7.8	7.5	7.4	7.4	8.0	11.5
1.48	6.9	7.1	6.9	6.8	7.2	
1.63	6.5	6.5	6.6	6.6	6.8	10.3
1.78	6.5	6.2	6.2	6.2	9.2	11.6
1.94	6.5	6.0	6.3	6.5	13.5	14.6
2.09	6.8	6.5	6.4	6.6	16.3	15.6
2.24	6.3	6.3	6.0	6.4	14.6	16.2
2.39	5.8	5.8	5.6	5.5	12.6	13.5
2.55	6.1	6.1		6.0	14.1	13.2
2.70	6.3	6.3		6.2	12.8	14.4
2.85	6.3	6.3		6.1	9.4	13.2
3.00	5.9	5.9		6.1	7.5	12.5
3.16	5.7	5.7		5.8	7.8	12.2
3.31	5.5	5.5		5.7	7.5	12.3
3.46	5.8	5.8		5.7	8.8	11.8
3.61	6.0	6.0		5.7	10.8	
3.77	5.9	5.9		5.9	12.7	12.5
3.92	6.0	6.0		5.9	13.3	
4.07	6.0	6.0			14.3	14.2
4.22	6.2	6.2			15.0	
4.37	6.3	6.3			15.5	15.9
4.53	6.5	6.5			15.3	
4.68	6.4	6.4			15.2	16.0
4.83	6.3	6.3			14.0	
4.98	6.0	6.0			13.5	15.0
5.14	5.5	5.5			12.7	
5.29	5.2	5.2			11.9	13.5
5.44	5.0	5.0			9.3	
5.59	4.9	4.9			5.6	13.5
5.75	4.6	4.6			4.7	
5.90	4.6	4.6			4.7	12.1
6.05	4.6	4.6			4.5	
6.20	4.8	4.8			4.8	11.6
6.36	6.9	6.9				11.7
6.51	8.5	8.5				14.5
6.66	10.1	10.1				17.1
6.81	7.9	7.9				14.1
6.97	5.6	5.6				10.8
7.12	4.9	4.9				9.4
7.27	4.1	4.1				7.6
7.42	3.8	3.8				6.8
7.58	3.6	3.6				7.7
7.73						8.7
7.88	3.1					8.2
8.03						7.6
8.18	3.0					5.6
8.33						3.6
8.49	3.6					
8.79	4.2					3.7
9.10	5.1					4.5

STATION 15-15 MOISTURE CONTENT

DATE	1/23/87	1/29/87	2/5/87	2/23/87	4/20/87	7/1/87
TIME	1540.0	1510	1420	1530	1525	900.0
MCHI	0.9	1.02	1.09	0.86	1.08	0.99
STD. CNT.		8407	8411	5356	8184	8325
EXP.DAYS		0.0	7.0	25.0	81.0	152.7
DBD (M)						
0.55						
0.86	5.5	5.5	7.6			
1.01	18.9	18.3	23.2	19.0		
1.16	18.9	18.2	20.8	21.0	21.1	21.3
1.32	16.0	15.9	18.1	18.7		
1.47	14.3	14.0	15.3	15.7	16.3	
1.62	13.5	13.3	14.4	15.4		
1.77	13.5	13.2	15.2	15.7	16.6	16.1
1.93	14.2	14.4	15.4	16.8		
2.08	13.8	13.3	14.3	15.8	16.8	
2.23	13.1	13.1	13.5	15.6		
2.38	13.2	13.2	13.1	15.0	15.2	15.3
2.54	12.2	12.2		14.1		
2.69	12.5	12.5		13.7	13.9	
2.84	12.5	12.5		14.4		
2.99	13.3	13.3		16.5	16.7	16.9
3.15	13.7	13.7		17.3		
3.30	13.1	13.1		16.8	16.9	
3.45	12.5	12.5		16.2		
3.60	12.2	12.2		16.2	16.2	15.5
3.76	10.9	10.9		14.6		
3.91	9.8	9.8		14.6	15.2	
4.06	7.9	7.9		15.5		
4.21	6.0	6.0		15.3	16.1	15.5
4.36				14.5		
4.52	5.6	5.6		14.2	14.3	
4.67				13.5		
4.82	5.8	5.8		12.8	14.2	13.5
4.97				12.3		
5.13	5.6	5.6		12.0	13.4	
5.28				10.2		
5.43	5.2	5.2		7.2	13.2	13.1
5.58						
5.74	5.4	5.4			13.2	
5.89						
6.04	5.7	5.7			12.4	12.5
6.19					11.6	
6.35	5.2	5.2			10.8	
6.50					10.0	
6.65	4.1	4.1			9.4	9.2
6.80					8.8	
6.96	3.8	3.8			8.8	
7.11					9.0	
7.26	3.8	3.8			9.2	9.3
7.41					9.2	
7.57	4.1	4.1			10.2	
7.72					9.8	
7.87	3.4	3.4			7.6	9.9
8.02					5.1	
8.17	4.1	4.1			4.6	
8.33					4.5	
8.48	3.7	3.7			3.9	9.1
8.63					3.6	
8.78	3.8	3.8				
8.94						
9.09	4.3	4.3				

STATION 15-22 MOISTURE CONTENT

DATE	1/27/87	1/29/87	2/5/87	2/23/87	4/20/87	7/1/87
TIME	1615.0	1528	1650	1900	1510	1030
MCHI	1.0	1.02	1.09	0.86	1.08	
STD. CNT.		8407	8411	8386	8184	
EXP. DAYS		0.0	7.1	25.2	81.0	152.8
DBD (M)						
0.69	15.3	15.5	15.8			
0.85	11.8	11.8	11.4			
1.00	8.3	8.8	8.3	8.8		
1.15	7.9	7.7	7.7	8.2		
1.30	8.1	7.6	7.8	8.2	9.7	12.5
1.46	9.3	8.6	9.1	9.2	12.2	
1.61	11.3	10.5	10.7	11.2	15.3	16.5
1.76	11.3	11.0	10.4	11.6	15.7	
1.91	9.9	9.3	9.5	10.1	14.8	16.1
2.07	8.8	8.5	8.8	9.2	14.6	
2.22	8.4	8.3	8.6	8.7	14.4	14.5
2.37	8.8		9.0	10.3	13.2	
2.52	9.9		10.5	10.5	12.4	12.7
2.68	11.4			11.3	12.5	
2.83	11.8			11.6	13.1	13.6
2.98	12.5			12.8	14.4	
3.13	12.2			13.1	14.7	14.6
3.29	12.0			13.0	14.2	
3.44	12.3			14.6	15.6	15.7
3.59	12.3			13.2	16.0	
3.74	11.0			11.5	15.5	15.1
3.90	8.2			8.1	15.0	
4.05	6.2			5.7	14.2	14.8
4.20	5.6			5.1	14.4	
4.35	5.3			4.9	14.1	14.0
4.50	4.9			4.3	13.5	
4.66	4.3			4.6	12.6	13.2
4.81	4.6			5.1	12.5	
4.96	4.9			4.8	12.5	12.1
5.11	4.9			5.1	11.6	
5.27	4.9				11.7	12.7
5.42	5.1				12.3	
5.57	5.4				11.8	12.6
5.72	5.7				12.4	
5.88	5.9				13.5	14.1
6.03	5.9				13.4	
6.18	6.0				13.3	14.0
6.33	5.8				12.7	
6.49	5.5				12.4	12.7
6.64	5.2				11.4	
6.79	4.9				11.0	11.9
6.94	4.8				10.8	
7.10	4.6				10.7	11.7
7.25	5.5				10.7	
7.40	6.3				9.5	12.4
7.55	6.5				8.5	
7.71	6.7				6.5	10.8
7.86	6.6				6.7	
8.01	6.4				6.2	11.8
8.16	5.6				5.3	11.2
8.31	4.7				4.9	10.8
8.47	4.1				3.9	10.5
8.62	3.6				3.6	10.3
8.77						
8.92	3.3					9.8
9.08						
9.23	3.8					9.3

STATION 15-23 MOISTURE CONTENT

DATE		4/16/87	7/1/87
TIME		1520	1000
MCHI		1.07	0.99
STD.	CNT.	8284	8325
EXP.	DAYS	77.0	152.8

DBD (M)		
0.71		
0.87		
1.02		
1.17		
1.32	10.1	9.7
1.48	9.4	8.5
1.63	9.2	8.2
1.78	8.4	7.7
1.93	7.7	8.0
2.09	8.0	8.1
2.24	8.0	9.2
2.39	7.4	11.2
2.54	7.1	12.8
2.70	8.3	13.1
2.85	9.2	13.4
3.00	10.1	13.9
3.15	11.0	13.1
3.31	10.4	12.5
3.46	11.2	12.8
3.61	10.4	12.1
3.76	9.2	13.2
3.92	9.2	13.2
4.07	9.1	13.7
4.22	8.5	13.5
4.37	6.8	12.8
4.52	6.0	11.5
4.68	5.6	10.8
4.83	5.7	9.4
4.98	5.5	8.3
5.13	5.6	6.9
5.29	5.9	6.6
5.44	6.0	9.3
5.59	7.3	13.9
5.74	8.4	15.7
5.90	9.1	15.1
6.05	8.6	14.4
6.20	8.1	12.7
6.35		12.8
6.51		12.8
6.66		
6.81		8.8
6.96		
7.12		7.5
7.27		
7.42		9.3
7.57		
7.73		12.1
7.88		
8.03		8.8
8.18		
8.33		5.1
8.49		
8.64		4.4

STATION 15-28 MOISTURE CONTENT

DATE	1/27/87	6/4/87	7/2/87
TIME	1600	1000	1000
MCHI	1.01	0.97	0.81
EXP. DAYS		125.8	153.8
DBD (M)			
0.65	13.5	8.7	
0.96	7.3	7.2	
1.26	6.5	6.4	6.6
1.57	6.2	6.3	6.3
1.87	6.3	6.3	6.3
2.18	6.0	6.4	6.5
2.48	5.6	5.7	5.6
2.79	4.9	4.8	4.8
3.09	4.9	4.8	4.9
3.40	4.9	4.9	4.9
3.70	5.4	5.0	5.4
4.01	5.1	5.0	5.0
4.31	4.5	4.6	4.5
4.62	3.8	3.8	3.8
4.92	3.6	3.6	3.6
5.23	3.8	3.8	3.8
5.53	4.2	4.0	4.1
5.84	4.5	4.3	4.4
6.14	4.2	4.1	4.3
6.45	4.2	4.1	4.4
6.75	4.2	4.6	4.6
7.06	5.1	5.3	5.3
7.36	4.9	4.6	4.9
7.67	6.8	7.3	7.7
7.97	8.1	7.0	7.1
8.27	5.4	5.5	5.8
8.58	5.8	5.8	6.0
8.88	6.5	6.1	6.1

STATION 2-15 MOISTURE CONTENT

DATE	1/26/87	7/2/87
TIME	1615	1000
STD. CNT.	0.94	0.81
EXP. DAYS		153.8

DBD (M)		
0.57	16.2	6.7
0.88	9.5	7.6
1.18	7.1	6.7
1.49	8.3	5.4
1.79	7.1	5.5
2.10	5.8	5.5
2.40	5.6	5.4
2.71	5.7	5.6
3.01	5.3	6.0
3.32	5.5	5.9
3.62	6.0	5.2
3.93	5.8	4.8
4.23	5.6	5.3
4.54	5.2	4.2
4.84	5.5	4.3
5.15	4.1	4.3
5.45	4.3	4.5
5.76	4.2	5.4
6.06	4.0	4.9
6.37	5.5	4.7
6.67	5.0	6.0
6.98	4.6	8.8
7.28	5.4	6.2
7.59	9.0	4.9
7.89	7.3	4.9
8.19	5.0	4.6
8.50	4.9	
8.80	4.6	
9.11	6.2	

STATION 6-15 MOISTURE CONTENT

DATE	4/13/87	4/30/87	7/1/87
TIME	1600	1450	1100
MCHI	1.22	1.04	0.99
STD. CNT.	8358	8241	8325
EXP. DAYS	74.0	91.0	152.8
DBD (M)			
0.69			
0.85			
1.00			
1.15			
1.30	13.4	14.7	13.8
1.46	16.5	15.0	
1.61	14.5	16.0	14.6
1.76	14.8	14.5	
1.91	14.8	12.7	12.5
2.07	12.8	12.5	
2.22	11.9	12.3	13.0
2.37	12.0	12.0	
2.52	11.6	11.9	12.6
2.68	11.0	13.6	
2.83	12.0	13.9	13.7
2.98	13.0	12.6	
3.13	12.2	10.5	11.5
3.29	11.1	8.7	
3.44	8.8	8.4	10.6
3.59	8.5	8.3	9.1
3.74	8.8	7.4	7.5
3.90	7.7	7.1	6.4
4.05	7.3	5.9	5.8
4.20	6.3	5.6	5.7
4.35	6.0	5.4	5.7
4.50	6.0	5.6	5.1
4.66	5.3	4.9	4.5
4.81	4.8	4.4	4.0
4.96	4.4	4.0	3.9
5.11	4.1	4.1	
5.27	4.0	4.1	3.8
5.42	4.2		
5.57	4.1		4.0
5.72	4.1		
5.88	4.0		3.9
6.03	3.9		
6.18	3.9		4.1
6.33	3.9		
6.49	3.9		3.8
6.64	3.8		
6.79	3.8		3.8
6.94	3.8		
7.10	3.7		3.8
7.25	3.7		
7.40	4.2		4.9
7.55	5.6		
7.71	4.9		4.5
7.86	4.8		
8.01	4.7		5.0
8.16	4.9		
8.31	5.1		4.9
8.47	5.2		
8.62	4.8		
8.77	4.4		
8.92	4.5		

STATION 8-15 MOISTURE CONTENT

DATE	1/26/87	1/29/87	2/5/87	2/20/87	4/20/87	7/1/87
TIME	1555	1601	1635	1415	1510	1051
MCHI	0.94	1.02	1.09		1.08	0.99
STD. CNT.		8407	8411		8184	8344
EXP. DAYS		0.0	7.1	22.0	81.0	152.8
DBD (M)						
0.56	15.5	15.4	15.2			
0.72		15.9	15.7			
0.87	15.2	15.7	15.5	15.2		
1.02	15.3	15.6	15.7	15.4		
1.17	16.2	16.3	16.2	16.4	16.8	16.1
1.33	15.3	15.7	15.4	15.7	16.1	
1.48	15.0	14.6	14.6	14.8	15.7	15.5
1.63	15.1	14.6	14.4	14.9	15.7	
1.78	14.1	14.1	14.1	13.9	14.7	14.6
1.94	13.0	13.0	12.5	13.1	14.1	
2.09	12.0	11.8	11.4	12.2	12.6	12.7
2.24	11.2	10.9	10.9	10.9	11.7	11.5
2.39	11.2		11.2	11.4	12.1	12.0
2.55	11.4			11.5	12.1	11.7
2.70	11.2			11.1	12.6	12.6
2.85	12.6			12.4	13.5	12.7
3.00	12.5			12.5	13.5	13.7
3.16	11.9			11.8	13.4	12.0
3.31	11.0			10.7	13.3	13.2
3.46	9.2			9.6	13.0	10.4
3.61	7.5			7.6	12.6	13.2
3.77	7.1			7.1	11.2	7.1
3.92	7.2			7.0	8.1	13.3
4.07	7.2			7.2	7.1	13.9
4.22	7.3			6.9	7.1	13.0
4.37				6.6	6.6	12.3
4.53	6.4			6.6	6.5	11.5
4.68				6.5	6.7	9.0
4.83	6.5			6.3	6.5	7.0
4.98				5.9	6.2	7.1
5.14	6.5			6.0	6.2	6.9
5.29				6.0	6.0	6.1
5.44	6.0				6.3	5.9
5.59					6.0	
5.75	6.0				6.1	6.1
5.90					5.9	
6.05	5.1				5.2	5.1
6.20					4.9	
6.36	5.1					5.1
6.51						
6.66	4.8					4.9
6.81						
6.97	5.1					5.2
7.12						
7.27	7.0					6.9
7.42						
7.58	5.7					5.9
7.73						
7.88	9.7					10.2
8.03						
8.18	8.2					7.1
8.34						
8.49	5.6					5.6
8.64						
8.79	5.2					4.7

STATION 22-15 MOISTURE CONTENT

DATE	1/27/87	1/29/87	2/5/87	2/23/87	4/20/87	7/1/87
TIME	1525	1615	1615	1400	1420	1015
MCHI	1.01	1.02	1.09	0.86	1.08	0.99
STD. CNT.			8411	5356	8184	8325
EXP. DAYS		0.0	7.0	25.0	81.0	152.8
DBD (M)						
0.93		19.5	19.5			
1.09		22.8	22.3			
1.24	20.0	20.6	19.4			
1.39	16.5	15.8	15.9			
1.54	16.4	15.6	16.0	16.5	16.7	13.5
1.70	18.0	17.5	18.2	18.2	18.8	
1.85	18.6	18.1	18.9	18.9	19.4	17.3
2.00	18.5	18.3	18.0	18.6	19.3	
2.15	16.0	15.8	15.8	15.7	16.8	14.9
2.31	14.5	14.2	14.6	14.5	15.4	
2.46	14.4	13.9	14.0	14.5	14.9	13.9
2.61	12.8		12.7	12.6	13.6	
2.76	11.6		12.0	12.2	12.7	12.1
2.92	12.5			12.3	13.4	13.3
3.07	13.3			12.9	14.1	13.5
3.22	12.5			12.6	13.7	13.5
3.37	12.7			12.6	13.8	13.8
3.53	12.5			12.5	13.8	13.2
3.68	11.6			11.4	12.5	12.5
3.83	11.3			11.4	12.3	12.6
3.98	11.3			11.7	13.4	13.7
4.14	11.6			12.5	14.3	15.0
4.29	14.1			14.4	15.4	15.1
4.44	12.9			12.8	14.1	13.1
4.59	10.6			10.2	11.7	11.4
4.74				9.0	10.3	10.1
4.90	7.6			7.7	9.4	9.4
5.05				7.5	10.3	
5.20	7.5			7.3	9.4	9.2
5.35				7.4	9.7	
5.51	7.4			7.5	9.1	9.3
5.66				7.1	9.2	
5.81	7.1				8.7	9.2
5.96					8.6	
6.12	7.2				7.3	8.1
6.27					7.0	
6.42	6.0				6.1	7.0
6.57					6.0	
6.73	6.5				6.7	7.5
6.88					8.9	
7.03	8.7				8.7	7.8
7.18					5.9	
7.34	5.1				5.3	5.0
7.49					5.1	
7.64	4.7				4.5	4.7
7.79					3.8	
7.95	3.4					3.3
8.10						
8.25	3.8					4.1
8.40						
8.55	4.4					4.8
8.71						
8.86	4.4					4.1
9.01						
9.16	3.7					3.9

STATION 22-15 MOISTURE CONTENT

DATE	1/27/87	1/29/87	2/5/87	2/23/87	4/20/87	7/1/87
TIME	1525	1615	1615	1400	1420	1015
MCHI	1.01	1.02	1.09	0.86	1.08	0.99
STD. CNT.			8411	5356	8184	8325
EXP. DAYS		0.0	7.0	25.0	81.0	152.8
DBD (M)						
0.93		19.5	19.5			
1.09		22.8	22.3			
1.24	20.0	20.6	19.4			
1.39	16.5	15.8	15.9			
1.54	16.4	15.6	16.0	16.5	16.7	13.5
1.70	18.0	17.5	18.2	18.2	18.8	
1.85	18.6	18.1	18.9	18.9	19.4	17.3
2.00	18.5	18.3	18.0	18.6	19.3	
2.15	16.0	15.8	15.8	15.7	16.8	14.9
2.31	14.5	14.2	14.6	14.5	15.4	
2.46	14.4	13.9	14.0	14.5	14.9	13.9
2.61	12.8		12.7	12.6	13.6	
2.76	11.6		12.0	12.2	12.7	12.1
2.92	12.5			12.3	13.4	13.3
3.07	13.3			12.9	14.1	13.5
3.22	12.5			12.6	13.7	13.5
3.37	12.7			12.6	13.8	13.8
3.53	12.5			12.5	13.8	13.2
3.68	11.6			11.4	12.5	12.5
3.83	11.3			11.4	12.3	12.6
3.98	11.3			11.7	13.4	13.7
4.14	11.6			12.5	14.3	15.0
4.29	14.1			14.4	15.4	15.1
4.44	12.9			12.8	14.1	13.1
4.59	10.6			10.2	11.7	11.4
4.74				9.0	10.3	10.1
4.90	7.6			7.7	9.4	9.4
5.05				7.5	10.3	
5.20	7.5			7.3	9.4	9.2
5.35				7.4	9.7	
5.51	7.4			7.5	9.1	9.3
5.66				7.1	9.2	
5.81	7.1				8.7	9.2
5.96					8.6	
6.12	7.2				7.3	8.1
6.27					7.0	
6.42	6.0				6.1	7.0
6.57					6.0	
6.73	6.5				6.7	7.5
6.88					8.9	
7.03	8.7				8.7	7.8
7.18					5.9	
7.34	5.1				5.3	5.0
7.49					5.1	
7.64	4.7				4.5	4.7
7.79					3.8	
7.95	3.4					3.3
8.10						
8.25	3.8					4.1
8.40						
8.55	4.4					4.8
8.71						
8.86	4.4					4.1
9.01						
9.16	3.7					3.9

STATION 24-15 MOISTURE CONTENT

DATE	4/20/87	7/24/87
TIME	1420	1041
MCHI	1.08	1.02
STD. CNT.	8184	8249
EXP. DAYS	83.0	177.8

DBD (M)		
0.69		
0.85		
1.00		
1.15		
1.30	12.9	11.3
1.46	12.6	
1.61	12.3	12.0
1.76	11.7	
1.91	12.3	15.1
2.07	12.4	
2.22	11.5	13.6
2.37	10.9	
2.52	10.8	13.2
2.68	9.9	
2.83	9.9	11.5
2.98	10.3	12.5
3.13	10.5	13.0
3.29	10.9	12.5
3.44	11.5	12.7
3.59	11.0	12.2
3.74	10.2	10.5
3.90	11.3	11.1
4.05	11.9	12.4
4.20	13.0	13.3
4.35	12.4	12.2
4.50	10.5	11.0
4.66	9.6	10.3
4.81	10.1	10.7
4.96	11.0	12.0
5.11	12.0	
5.27	11.0	11.9
5.42	10.6	
5.57	10.5	10.5
5.72	9.3	
5.88		7.6

STATION 28-15
CORRECTED MOISTURE CONTENT

DATE			1/27/87	2/13/87	7/2/87
TIME			1000	1030	1000
MCHI			1.01	0.90	0.81
EXPERIMENTAL DAYS				14.8	153.8
ELEV. (M)	DPTH BELOW DATUM(CM)	DEPTH (FT)			
1416.4	1.01	1.0	17.1	17.8	
1416.1	1.32	2.0	11.9	12.7	
1415.8	1.62	3.0	10.3	10.2	9.6
1415.5	1.93	4.0	9.9	9.6	9.2
1415.2	2.23	5.0	10.0	10.0	9.2
1414.9	2.54	6.0	9.6	9.3	8.6
1414.6	2.84	7.0	10.0	9.8	9.2
1414.3	3.15	8.0	11.4	10.9	9.2
1414.0	3.45	9.0	11.8	11.8	9.2
1413.7	3.76	10.0	11.2	11.0	8.9
1413.4	4.06	11.0	10.7	10.4	9.0
1413.1	4.37	12.0	10.5	10.4	9.2
1412.8	4.67	13.0	10.1	9.5	9.1
1412.5	4.98	14.0	13.8	13.5	13.9
1412.3	5.13	14.5			12.7
1412.2	5.28	15.0	10.6	9.9	10.6
1412.0	5.43	15.5			10.0
1411.9	5.59	16.0	8.7	8.6	10.5
1411.6	5.89	17.0	6.9	7.0	9.2
1411.3	6.20	18.0	5.3	4.9	8.3
1410.9	6.50	19.0	4.6	4.3	6.7
1410.6	6.81	20.0	7.9	8.1	9.1
1410.3	7.11	21.0	8.9	8.7	8.0
1410.0	7.42	22.0	4.6	4.7	4.7
1409.7	7.72	23.0	5.8	5.9	6.2
1409.4	8.03	24.0	5.9	5.6	5.8
1409.1	8.33	25.0	5.0	5.2	4.9

STATION 15-2 PRESSURE HEAD (CM)

DATE	1/26/87	2/13/87	6/4/87	7/24/87
TIME	1500	1645	1200	1200
EXP. DAYS		15.1	125.9	175.9
DBD (M)	PSI (CM)	PSI (CM)	PSI (CM)	PSI (CM)
0.94	-18.1	-25.5	-88.0	-242.1
0.95	-13.5	-23.4	-272.6	-389.2
1.37	-14.7	-22.7	-62.6	0.0
1.44	-0.6	-11.1	-8.3	-26.2
1.93	-9.1	-21.9	-9.6	-70.9
2.24	-11.2	-26.9	-11.3	-85.9
2.94	-2.3	-15.4	-2.6	2.4
3.03	6.9	-27.2	-13.2	-8.2
3.55	11.4	-39.3	-21.0	-12.0
3.71	-7.0	-22.9	-3.7	4.3
4.00	-3.0	-42.1	-30.7	-12.2
4.54	-204.1	-185.3	-108.3	-73.8
5.12	-16.6	-55.0	-45.7	

15-8 PRESSURE HEAD (CM)

DATE	1/26/87	1/29/87	2/5/87	2/23/87	4/20/87	7/1/87
TIME	1520	1445	1550	1415	1515.0	815.0
EXP.DAYS		0.0	7.0	25.0	81.0	153.0
DBD (M)						
0.79	-381	-387	-379	-308	-501	-53
0.89	-289	-288	-278	-191	-502	-82
1.26	-4	-17	-80	-67	-475	-38
1.29	11	-516	-529	-399	-536	-27
1.71					-10	
2.31	-388	-431	-455	-464	-43	-34
3.36	-345	-345	-376		-38	-47
3.45	-382	-379	-394	-401	-58	-35
3.97	-272	-262	-274	-210	-36	-22
4.22	-256	-202	-265	-305	-17	14
4.70					10	22
5.24	-283			293	146	24
5.26	-203			-238	-96	6

15-15 PRESSURE HEAD (CM)

DATE	1/23/87	1/29/87	2/5/87	2/23/87	4/20/87	7/1/87
TIME	1540.0	1510	1420	1530	1525	900
EXP.DAYS		0.0	7.0	25.0	81.0	153.0
DBD (M)						
1.41	-32	-13	-5	-16	-9	16
1.48	-22	-18	-25	-45	-20	-9
1.88	-19		-6	-44	-13	8
1.88	-12	-11	-18	-38	-12	-10
2.62	-52	-42	-58	-68	-37	-38
2.82	-21	-8	-14	-36		4
3.41	-35	-21	-31	-57	-11	-31
3.53	-50	-38	-47	-50	3	
3.88	-71	-51	-67	-70	-35	-14
4.99	-103			-126	-18	-4
5.12	-124			-150	-26	-12

STATION 15-22 PRESSURE HEAD (CM)

DATE	1/27/87	1/29/87	2/5/87	2/23/87	4/20/87	7/1/87
TIME	1615.0	1528	1650	1900	1510	1030
EXP. DAYS		0.0	7.1	25.2	81.0	152.8
DBD (M)						
0.92	-249	-218	-249	-173	-89	-168
1.01	-139	-128	-157	-132	-102	-36
1.34	-61		-84	-81	-97	-56
1.51	-91	-74	-119	-117	-127	-46
2.44						
2.50	-31	-19	-44	-35	-95	-38
3.24	-74	-69	-107	-81	-55	-24
3.47						
3.77						
3.92	-127	-109	-130	-106	-14	5
3.95	-175			-145		8
4.90	106			120	246	134

STATION 15-28 PRESSURE HEAD (CM)

DATE	1/27/87	2/13/87	6/4/87	7/2/87
TIME	1600	1200	1200	1000
EXP. DAYS		14.9	125.9	153.8
DBD (M)				
0.91	-471	-275	-341	-428
0.95	-444	-415	-235	-287
1.40	-457	-469	-425	-402
1.43	-15	-33	-70	-124
1.86	-23	-46	-102	-70
1.90	-574	-522		
2.22	-463	-489	-493	
2.46	-413	-432		
2.64	-438	-456		
3.01	-65	-17		
3.14	19	5	48	-92
3.27	-271	-281	-187	
3.97	-190	-202	-95	-64
5.28	203	238	357	444
5.39	-140	-144		

STATION 2-15 PRESSURE HEAD (CM)

DATE	1/26/87	2/13/87	7/2/87
TIME	1615	1615	1000
EXP. DAYS		15.0	153.8
DBD (M)			
0.75	-26.4	-28.6	-482.8
0.79	-11.7	-22.8	
1.31	-3.1	-10.5	-68.0
1.32	-10.5	-19.5	
2.21	-147.1	-122.0	
2.51	-54.2	-87.6	-81.9
3.61	-152.4	-142.1	
3.62	-62.3	-66.8	-60.7
4.30	-173.2	-178.9	
4.47	-210.8	-217.1	
5.25	-74.7	-188.6	
5.33	-149.7	-141.7	-79.8

STATION 8-15 PRESSURE HEAD (CM)

DATE	1/26/87	1/29/87	2/5/87	2/23/87	4/20/87	7/1/87
TIME	1555	1601	1635	1700	1510	1050
EXP. DAYS		0.0	7.1	25.1	81.0	152.8
DBD (M)						
0.82			-16	-25	-11	-24
0.86	-18		-9	-19	-12	-33
1.28	-13		-25	-25	-11	19
1.35	-16	6	-4	-11		-2
2.19	-15		-27	107	-17	20
2.29	-19	-8	-6	-21	-38	2
2.78	1	27	-6	-21	-6	4
3.26	-23	-6	-37	-55	-36	-12
3.27	-43	-40	-41	234	-42	-13
3.31	-36	-33	-56	-61	-31	-7
3.77	-152			-112	-25	-12
3.80	-116			-115	-72	5
4.12	-136			-139	-97	-5
4.15	104			-65	-42	3
5.24	-29			-50	-38	12
5.29	-54			-73	-64	-36

STATION 22-15 PRESSURE HEAD (CM)

DATE	1/27/87	1/29/87	2/5/87	2/23/87	4/20/87	7/1/87
TIME	1525	1615	1615	1510	1420	1000
EXP. DAYS		0.0	7.0	25.0	81.0	152.8
DBD (M)						
1.03	2	13	-14	-19	-47	-8
1.08	-2	-26	2	-32	-11	-13
1.54	-10	22	-15	-23	-20	-4
1.56	-3	-25	-21	-31	-23	-4
1.98	-1	-13	-16	-29	-26	-2
2.04	-2	-26	2	-32	-11	-13
2.50	6	-17	-5	-27	-13	-5
2.60	11	5	-4	-21	-1	14
3.57	-9	-12	-20	-33	-32	-4
3.76	-242	-2	-39	-55	-39	-14
3.77	-7			-34	-39	-3
4.12	-22			-60	-34	-13
4.44	-40			-68	-44	-4
4.59	-16			-47	-24	-4
5.56	-15			-44	-24	11
5.61	-36			-75	-47	-8

STATION 28-15 PRESSURE HEAD (CM)

DATE	1/27/87	2/13/87	7/2/87
TIME	1200	1030	1200
EXP. DAYS		14.8	153.9
DBD (M)			
1.17	-63	-50	-88
1.28	-14	-31	-190
1.64	-43	-37	-31
1.72	-47	-41	-400
2.66			
2.66	-76	-75	-175
3.14	-46	-56	-51
3.62	-28	-10	
3.15			
3.71	-63	-69	-72
4.07	-32	-46	-43
4.20	-81	-85	-73
4.61	-33	-48	
5.16	-47	-51	
5.35	-102	-113	
5.60	-36	-66	